JPRS L/10390

16 March 1982

Translation

OCEAN RESEARCH ON

HYDROPHYSICAL FIELD VARIABILITY

Ed. by

R.V. Ozmidov

FBIS FOREIGN BROADCAST INFORMATION SERVICE

NOTE

JPRS publications contain information primarily from foreign newspapers, periodicals and books, but also from news agency transmissions and broadcasts. Materials from foreign-language sources are translated; those from English-language sources are transcribed or reprinted, with the original phrasing and other characteristics retained.

Headlines, editorial reports, and material enclosed in brackets [] are supplied by JPRS. Processing indicators such as [Text] or [Excerpt] in the first line of each item, or following the last line of a brief, indicate how the original information was processed. Where no processing indicator is given, the information was summarized or extracted.

Unfamiliar names rendered phonetically or transliterated are enclosed in parentheses. Words or names preceded by a question mark and enclosed in parentheses were not clear in the original but have been supplied as appropriate in context. Other unattributed parenthetical notes within the body of an item originate with the source. Times within items are as given by source.

The contents of this publication in no way represent the policies, views or attitudes of the U.S. Government.

APPROVED FOR RELEASE: 2007/02/09: CIA-RDP82-00850R000500040036-3

JPRS L/10390

16 March 1982

OCEAN RESEARCH ON HYDROPHYSICAL FIELD VARIABILITY

Moscow ISSLEDOVANIYE IZMENCHIVOSTI GIDROFIZICHESKIKH POLEY V OKEANE in Russian 1974 pp 2-31, 42-65, 83-98, 155-162, 208-211

[Excerpts from "Ocean Research on Hydrophysical Field Variability," edited by R. V. Ozmidov, doctor of physical and mathematical sciences, Izdatel'stvo "Nauka", 211 pages, number of copies unknown]

APPROVED FOR RELEASE: 2007/02/09: CIA-RDP82-00850R000500040036-3

[Text]

ANNOTATION

This collection of articles is about the results of experimental and theoretical investigations of the variability of hydrophysical fields in the ocean. Particular attention is devoted to the fine structure of fields and microscale oceanic turbulence, experimental data on which were obtained on specialized expeditions of the Institute of Oceanology imeni P.P. Shirshov using newly created towed and sounding measurement devices. The articles give the results of large-scale computations of the statistical characteristics of velocity and conductivity microfluctuations in sea water in different regions of the world ocean and also data on the statistical characteristics and parameters of macroscale variability of fields. A number of articlesgive the theoretical and experimental results of investigations of internal waves and the processes of diffusion of impurities in the ocean. Possible types of spectra of fluctuations of velocity, temperature and Reynolds stress in the stratified ocean are theoretically analyzed. Also examined are some methodological problems involved in the collection and processing of data on variability of hydrophysical fields in the ocean. Information is also given on new sensors and measurement systems for investigating fine structure in the ocean.

APPROVED FOR RELEASE: 2007/02/09: CIA-RDP82-00850R000500040036-3

INVESTIGATION OF VARIABILITY OF HYDROPHYSICAL FIELDS IN OCEANIC POLYGON

Moscow ISSLEDOVANIYE IZMENCHIVOSTI GIDROFIZICHESKIKH POLEY V OKEANE in Russian 1974 pp 3-31

[Article by R. V. Ozmidov, V. S. Belyayev, M. M. Lyubimtsev and V. T. Paka from monograph "Ocean Research on Hydrophysical Field Variability," edited by R. V. Ozmidov, doctor of physical and mathematical sciences, Izdatel'stvo "Nauka," 211 pages, number of copies printed unknown]

[Text] Spatial-temporal variability is a distinguishing characteristic of hydrophysical fields in the ocean. The scales of this variability have a wide range. Due to the turbulent character of movement of ocean waters fluctuations can exist in it whose minimum dimensions are determined by the effect of molecular forces. The dimensions L_{min} of such fluctuations in the velocity field can be evaluated using the formula for locally isotropic turbulence $L_{min} = \sqrt[4]{\nu^3/\varepsilon}$, where ν is the kinematic coefficient of molecular viscosity of sea water, being about 0.01 cm^2/sec; ε is the rate of dissipation of turbulent energy in the ocean. The ε parameter is extremely variable, but with its reasonable evaluations in the range 10^{-6}–10^{0} cm^2/sec^3 for L_{min} we obtain values 0.3 mm-1 cm. The minimum time scale T_{min} of the turbulent fluctuations of the velocity field can be evaluated using another formula for locally isotropic turbulence $T_{min} = \sqrt{\nu/\varepsilon}$, which with these same ε evaluations gives the order of magnitude T_{min} of 0.1–100 sec. The maximum spatial scale L_{max} of variability of hydrophysical fields in the ocean is evidently governed by the geometric dimensions of the ocean basins, that is, it can attain several thousand kilometers. However, the upper boundary T_{max} of temporal variability in general is difficult to indicate, since together with seasonal variations of the fields there are also year-to-year fluctuations and climatic variability.

In the experimental investigation of variability of hydrophysical fields it is first of all necessary to establish the limits of the scales of variability which must be investigated. The fact is that the total duration of the necessary observations, the position of the observation points and also the characteristics of the used instruments are related to these limits. In order to determine the statistical characteristics of field variability the duration of the measurements must be approximately an order of magnitude greater than the maximum investigated time scale of variability and the extent of the measurement runs (or the distances between the extreme points of placement of the instruments) must also exceed by an order of magnitude the maximum investigated spatial field inhomogeneities. The discreteness of the observations in this case should be at least less than half the period (or spatial scale) of the minimum investigated field variations and the time constant of the instrument (and the entire measurement-registry channel) is about

1/10 of this period. Due to these requirements it follows very clearly that it is virtually impossible to investigate any significant interval of scales of variability of this field in the ocean with instruments of a single type. In actuality, low-inertia instruments (such as thermoanemometers) are usually not capable of operating continuously in the ocean for a long time; more approximate instruments (of the hydrological current meters type) have large time constants and large measurement discreteness intervals. Accordingly, for this type of investigations it is necessary to have, in general, an entire "arsenal" of instruments with overlapping frequency characteristics. It is desirable that the researcher have instruments capable of registering the most small-scale field fluctuations. This is important because without information on such fluctuations the data from some instruments (such as BPV-2 current meters), operating with a great discreteness, can give erroneous ideas concerning the spectral structure of the process due to discretization noise. If there is also information concerning microscale fluctuations as well, such errors can be avoided [1].

If the macroscale limit of the investigated scales of fluctuations is determined, it is desirable that the subsequent observations be made in the following way. In the ocean one or more regions (polygons) with typical macroscale characteristics are selected. Among these characteristics it is necessary to include the mean vertical profiles of density (temperature and salinity) and current velocity, the characteristic horizontal current velocities, the direction of the heat flow through the ocean surface (heating, cooling), mean regime of wind and waves in the polygon. A number of such polygons with different sets of typical characteristics to a certain degree can also ensure investigation of the spatial variability of hydrophysical fields at the scale of the entire ocean. In actuality, the discreteness of the points of such observations can attain many tens or even hundreds of kilometers and therefore in principle it is possible to "cover" the entire ocean with this type of polygons. However, for an investigation of the long-period temporal variability of the fields it is necessary to carry out prolonged observations in a polygon with a temporal discreteness which is consistent with the investigated processes. For example, in an investigation of the statistical characteristics of variability up to an annual period observations must be carried out in the polygon for about 10 years, but their discreteness can be several days. The greatest attained duration of continuous observations in such a sort of polygon at the present time is equal to several months [2, 3].

The extent of the polygon can be different, but the desire to "overlap" all the spatial scales of variability, beginning with L_{min}, leads to a limitation of L_{max} to several tens or a few kilometers. In the ocean area of the polygon there should be buoy stations with approximate instruments operating for the entire period of observations in the polygon. However, the duration of operation of low-inertia instruments can be considerably less, but in this case there should be multiple repetition of such measurements with different values of macroscale factors. In each individual measurement low-inertia instruments cannot operate for a long time, for example, about 10 minutes, but the number of such measurements must be sufficiently great for a comparison of the characteristics of microscale processes with the meso- and macroscale factors varying in time and in space.

Investigation of this variability of fields in polygons with the use of low-inertia instruments was initiated in 1969 [4]. Thereafter several specialized runs were made by scientific research ships with work in polygons. The tracks of these vessels and

the location of the investigated polygons are given in [5]. In this article as an example we will make a detailed examination of the complex of measurements and give their results in one of the polygons of the seventh voyage of the scientific research ship "Dmitriy Mendeleyev" (1972).

The polygon was situated in the region of the sources of the Somali Current to the east of Socotra Island (Fig. 1). Work in the polygon was initiated from a hydrological section whose data were routinely processed on a shipboard electronic computer by the dynamic method. Sections of the fields of temperature, salinity and geostrophic current velocities (Figures 2-4) made it possible to determine the macroscale hydrological structure of the work region, define the contours of the branch of the Somali Current and thereby afforded a possibility for validly selecting the place for setting out a buoy station and carrying out measurements of microscale variability with low-inertia instruments. A buoy station with BPV-2 current meters and photothermographs was situated in the current and served as a reference point for other measurements*.

The macroscale thermal structure of waters in the polygon, according to data for hydrological stations 488-494 (Fig. 1), is shown in the sections in Fig. 2. These same data were also used in constructing the section of distribution of water salinity (Fig. 3). It can be seen from the temperature section that in the upper 400-m layer the depth of the isotherms decreases somewhat in a southeastern direction, which indicates an upwelling of waters in this part of the section. The advection of water masses from adjacent regions of the ocean can be seen from the positioning of the isohalines in the section in Fig. 3. The penetration of more saline and warmer waters of Red Sea origin determines the vertical structure of the upper layer of water in the northern part of the section; the existence of a salinity maximum at a depth of about 100 m is an indication that the Somali Current during winter carries waters forming in the Red Sea and Arabian Sea regions.

Thus, the development and maintenance of the vertical water density gradients in the polygon region exerts an influence on the horizontal transport of water masses which acquired their principal physical characteristics prior to arrival in the region of the Somali Current.

The hydrological structure of the waters in the neighborhood of station 490 was characterized by a relatively poorly expressed temperature jump layer (Fig. 5, Fig. 6). The mean temperature gradient in the upper 100-m layer is $\sim 0.02°/m$ and increases in the jump layer to $0.07°/m$, whereas in equatorial polygons, occupied on this same voyage in the Indian Ocean, the temperature gradient attained $0.25°/m$. Accordingly, density stratification in the polygon ensured a small vertical stability of the water mass in the upper layer of the ocean, including the temperature jump layer, which could facilitate the development of microscale turbulence in the upper layer of the ocean.

Figure 4 shows a vertical section of the current field in the polygon, constructed on the basis of data from computations by the dynamic method. The figure shows

---

* The hydrological work in the polygon was carried out under the direction of V. G. Neyman.

that in the region of hydrological stations 490 and 491 there is a clearly defined flow with a southwesterly current component whose maximum was situated in the upper 100-m water layer. To the southeast of station 490 and to the northwest of station 491 the current velocity changes sign, attaining values greater than 40 and 50 cm/sec. In the deep layers at the left edge of the section there was again a flow of southwesterly direction with a current velocity up to 20 cm/sec.

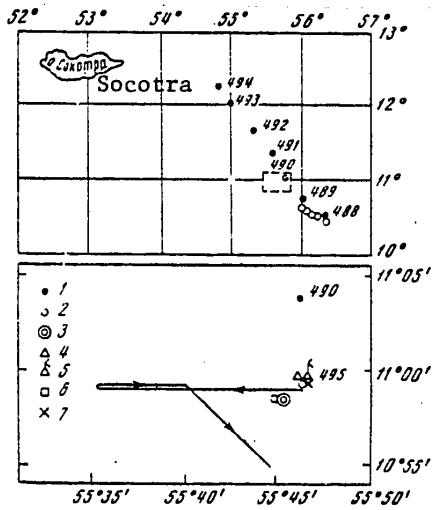

Fig. 1. Diagram of polygon for measuring oceanic turbulence and background conditions with indication of numbers of hydrological stations. 1) hydrological series, bathythermogram, sounding with AIST instrument and acoustic probe to ascertain current velocity; 2) sounding with AIST instrument and acoustic probe to ascertain current velocity; 3) multiple sounding with AIST; 4) anchored buoy station with current meters and photothermographs; 5) radio temperature buoy; 6) measurement with "Sigma" probe; 7) bathythermogram. The solid line with the arrows indicates the towing of turbulence meters. The rectangle enclosed in a dashed line is shown at a larger scale in the lower part of the figure.

As is well known, computations of currents by the dynamic method give only the pattern of the current field averaged over a great time interval, dependent at the same time on the choice of the reference (zero) surface. Accordingly, in the region of microscale measurements a buoy station with BPV current meters was set out; the current meters were at the horizons 15, 25, 50, 75, 100, 150, 200, 400, 600, 1,000 and 1,500 m. Figure 7 shows the vertical profiles of current components averaged for the entire period (63 hours) along the parallel (u) and meridian (v) and also the distribution of the mean current vectors with depth. The figure shows that in the layer from the ocean surface to a depth of 1,500 m during the period of observations there were two almost oppositely directed flows, which agrees with data from the dynamic section. The boundary between the flows was approximately at a depth of 400 m, but the transition zone from one flow to another is already traced from 200 m. In the upper layer the velocity vectors had a northwesterly direction with a modulus 15-20 cm/sec, whereas in the lower layer the current was close to easterly with velocities ~ 15 cm/sec (which deviates from the dynamic section data with respect to both modulus and direction). It can be seen from the distribution of the current vectors that in the layer 50-100 m the vertical current

gradients developed due to a simultaneous change of both current direction and velocity with depth; in the layer 100-200 m the vertical current gradients developed primarily exclusively due to a change in flow direction. Large gradients were observed in the layer from 200 to 600 m, where there is a marked change in both direction and modulus of current velocity. In the water layer deeper than 600 m the mean vertical current gradients become insignificant. The sharpest change in the meridional velocity component was observed, as indicated in the figure, in the uppermost layers of the ocean and the maximum v value was registered at the 200-m horizon. The latitudinal velocity component changes relatively smoothly from 18 cm/sec at the upper horizon to 15 cm/sec at the 600-m horizon, after which it remains virtually constant to the lowest observation horizon.

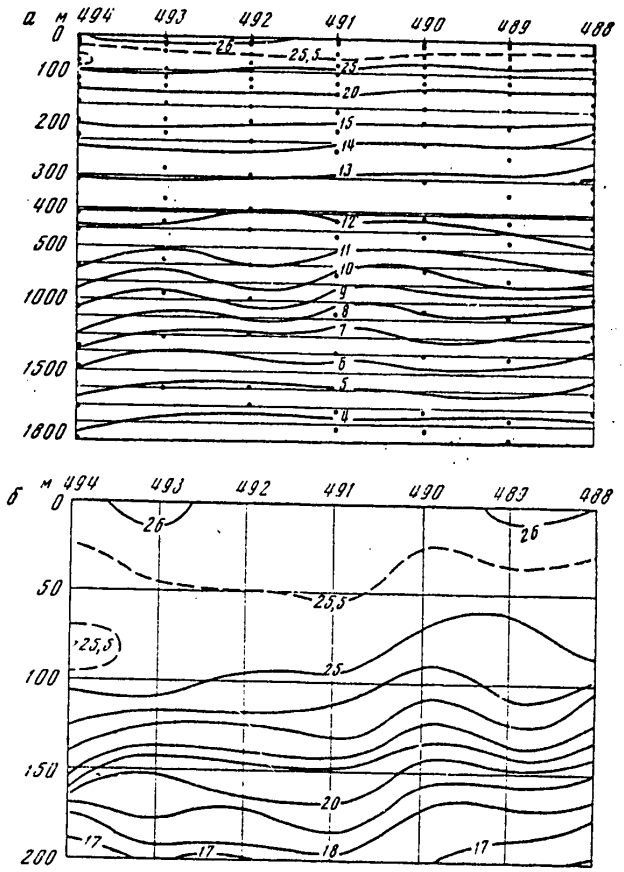

Fig. 2. Field of isotherms according to hydrological series (a) and bathythermograms (b) in hydrological section. The numbers of the stations are indicated along the horizontal scales. The temperature values are given in °C.

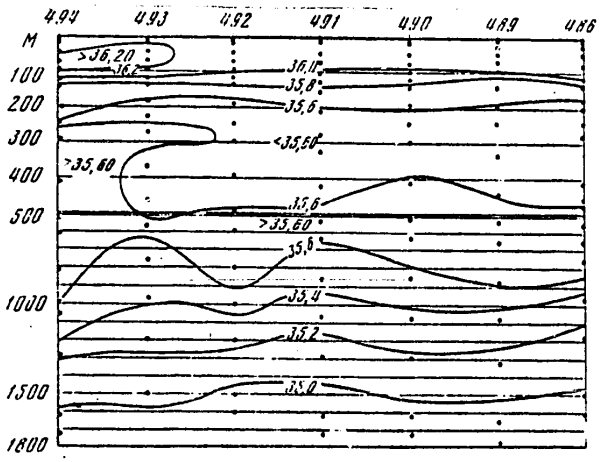

Fig. 3. Isolines of salinity (in °/oo) based on measurements in hydrological section. The numbers of the stations are indicated along the horizontal scale.

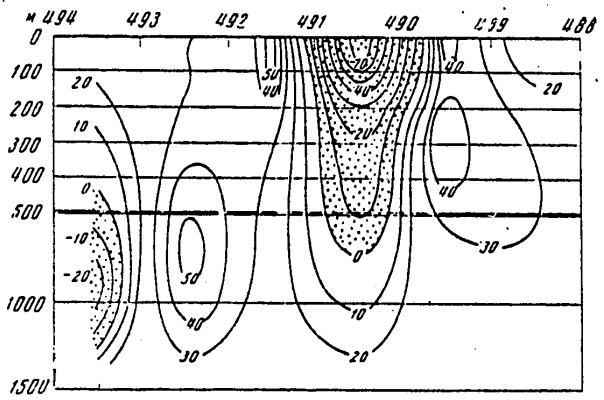

Fig. 4. Current velocity field computed by dynamic method (the positive values correspond to the current direction "in the figure").

Some idea concerning the macroscale variability of the velocity field in the polygon can be obtained from Fig. 8, which shows the curves of the half-sum of spectral densities of fluctuations of the horizontal velocity components on the basis of data from current meters at the seven upper horizons at the buoy station. Time series of the values of velocity components with a discreteness of 5 minutes were subjected to statistical processing. The spectral functions were scaled into spatial functions using the "frozen-in" hypothesis with use of the values of mean current velocities at each of the observation horizons. Due to the short duration of the series used for the computations the interval of wave numbers of the constructed spectral functions E(k) extends approximately only 1 1/2 orders of magnitude, whereas the E(k) values in this interval change approximately by four orders of magnitude. The spectral functions for all seven horizons have virtually

an identical level and in logarithmic coordinates are close to straight lines with a mean value of the tangent of slope of about 2.7. Such a rapid dropoff of the E(k) values with an increase in k is evidently evidence of a predominance in the considered range of wave numbers of well-developed two-dimensional turbulence, for whose spectral density the "-3 law" can be satisfied [6, 7]. It is also not precluded that in this k range an important role in the velocity field can be played by wave movements of different origin.

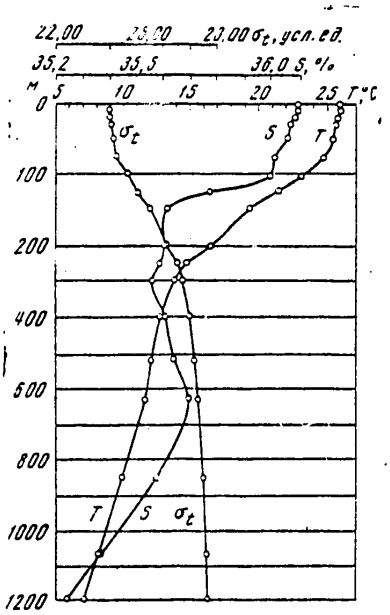

Fig. 5. Vertical profiles of temperature T, salinity S and conventional density σ_t according to measurements at station 490.

arbitrary units

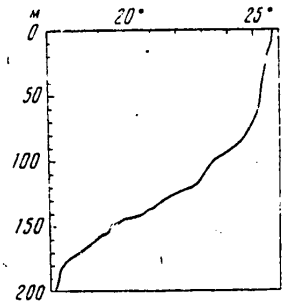

Fig. 6. Bathythermogram at station 490.

Due to the great spatial discreteness of observations of current velocities made using current meters information on the vertical structure of the flow (including on its vertical gradients) is quite approximate. A direct comparison of the data from individual measurements of microscale turbulent fluctuations (with scales from L_{min} to 1-2 m) with such macroscale characteristics evidently does not make it possible to discover any relationships between them [8]. The characteristics of microscale fluctuations must evidently be directly related to the finer (local) parameters of the oceanic velocity field. It was possible to obtain this sort of information on the vertical profiles of current direction and current velocity modulus in the polygon using a new acoustic sounding instrument developed at the Pacific Ocean Division of the Institute of Oceanology imeni P. P. Shirshov, USSR Academy of Sciences (now the Pacific Ocean Oceanological Institute, Far Eastern Center, USSR Academy of Sciences). The instrument registers the Doppler frequency shift of acoustic oscillations of a signal scattered on density inhomogeneities moving with the flow. The volume of fluid in which the scattering of ultrasound

occurs is about 1 cm^3 and is quite distant from the instrument housing. The probe does not require the calibration mandatory for current meters and thermoanemometers. The error in velocity measurements was about 1 cm/sec and is determined for the most part by the error in frequency measurement. The probe also has a meter for registering orientation relative to the magnetic meridian based on measurement of the signal phase induced in a wire loop during its rotation in the earth's magnetic field. Current direction is measured with an accuracy to 3^o.

Figure 9 shows examples of the vertical profiles of current velocity modulus and direction obtained using the new instrument. The measurements were made from a drifting ship, and as a result, the values for current velocity and direction are relative, at the same time that their gradients must coincide with the gradients of true current velocities in the ocean (during the time of sounding the ship's drift velocity must be considered constant). The curves show how more complex the vertical structure of the field of currents is in comparison with the pattern obtained using data from current meter observations at buoy stations. Using sounding data it is easy to see the fine vertical stratification of the current. The adjacent layers of fluid with a thickness of several meters move at different velocities differing by 5 and sometimes by 10 cm/sec. The direction of movement of the fluid in such layers can also differ appreciably. For example, the layers at depths of 175 and 185 m moved at an angle of 100^o to one another. The velocity gradients, computed on the basis of probe data, are considerably greater than the values obtained using current meter profiles in Fig. 7. Whereas in this figure the gradients were found to be no more than 0.1-0.3 cm/sec per meter, according to sounding data in individual cases they can attain several centimeters per second per meter. It is clear that such local characteristics of the velocity field must exert a definite influence on the microscale fluctuations of hydrophysical fields in the ocean.

Information on the macroscale variability of the temperature field in the polygon was obtained from photothermographs installed at a buoy station at the horizons 100, 150, 200 and 400 m. The discreteness of readings of temperature by the photothermographs was 5 minutes and the duration of observations was 63 hours. The resulting series of temperature values were used in computing the spectral density functions shown in Fig. 10. For the three upper observation horizons the spectral density functions E(k) for temperature fluctuations were virtually identical, but at a depth of 400 m the E(k) values were considerably less. The E(k) functions, computed using data from the photothermographs at the horizons 100, 150 and 200 m, fit well with the sectors of the spectral functions in Fig. 14 situated in the more high-frequency region (radio buoy data). Comparisons of Fig. 10 and Fig. 14 also make it possible to explain some decrease in the slope of the spectral curves in Fig. 10 with an increase in k. It is clearly associated with discretization noise, since in the interval of wave numbers greater than 10^{-3} the spectral density function, although it decreases rapidly, is nevertheless different from zero. The tangent of the angles of slope of the spectral density functions in the zone of wave numbers where the influence of discretization noise is not expressed is close to 2.5.

More detailed information on the vertical structure of the fields of temperature, salinity (conductivity) and density in the polygon were obtained using the AIST sounding instrument. This instrument makes it possible to determine the vertical

profiles of temperature and salinity to a depth of 1,000 m and with an accuracy to 0.02-0.03°C and 0.03-0.04°/oo respectively. Such an accuracy is provided by a carefully calibrated thermoresistor and induction-type conductometer. The vertical resolution of the instrument for ordinary sounding rates is about 1 m. Analog signals from the sensors are coded and registered on a punched tape and at the same time on an automatic recorder. After processing of the punched tape on an electronic computer the profiles of temperature, conductivity, salinity and density are fed out and the latter two parameters are determined by computations.

Examples of the vertical profiles of temperature, salinity and density obtained using the AIST instrument in the polygon are shown in Fig. 11. It can be seen easily from the figure how much more complex these profiles are with the high resolution of the instrument in comparison with the "smooth" curves in Fig. 5, constructed using the infrequent points of the bathometric series*. The AIST data reveal individual layers with an approximately constant temperature which are separated by interlayers of water with great t gradients. The vertical dimensions of such "steps" are not constant; the temperature drops from layer to layer are also variable. It is entirely obvious that such a fine structure of the oceanological fields can exert a definite influence on the still finer field characteristics. For example, microscale turbulence (with characteristic dimensions from L_{min} to 1 m) must "react" very sensitively to the stepped field structure. In actuality, the density gradient is one of the most important parameters for turbulence; it determines the expenditure of turbulent energy on work against Archimedes forces (in the case of a stable stratification) and thereby the form of the spectrum and other statistical characteristics of turbulence. A confirmation of this will be presented below in an analysis of the data obtained using low-inertia instruments. However, an attempt to relate the characteristics of microscale turbulence directly to the mean hydrological conditions in the polygon did not lead to an unambiguous answer [8]. This example graphically illustrates the thought expressed earlier that it is undesirable to have "breaks" in the spatial-temporal scale in an experimental investigation of hydrophysical fields in the ocean. In the case of such a break it becomes difficult, and frequently impossible, to establish cause-and-effect relationships between the studied processes.

The mesoscale vertical structure of the fields registered with the AIST probe is extremely variable in both time and in horizontal directions. Such a variability can be investigated by means of multiple soundings carried out from an anchored or drifting ship. It is true that it is extremely difficult to determine what causes the observed variability -- nonuniformity of the vertical structure of the field in a horizontal direction or its nonstationary character. In actuality, the drifting ship moves relative to the water mass under the influence of the wind, but in the case of an anchored vessel the fluid is transported relative to it by the current. Accordingly, each subsequent sounding in general brings information concerning the vertical structure of the field at different moments and at different points in the water mass. In order to investigate the spatial variability of structure it is necessary to carry out synchronous soundings at a number of points in the ocean (for example, from several ships at the same time).

---

* We note that the zigzaging nature of the density profile in Fig. 11 is related to errors in computing σ_t on the basis of measurements of the temperature and conductivity values.

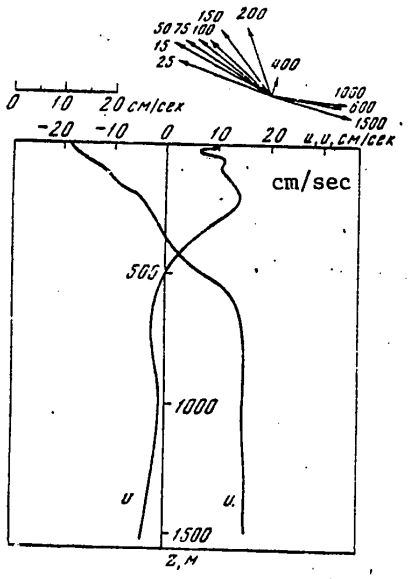

Fig. 7. Diagram of current velocity vectors and depth distribution of zonal u and meridional v components according to data from anchored buoy station. The numbers alongside the vectors denote depths in m.

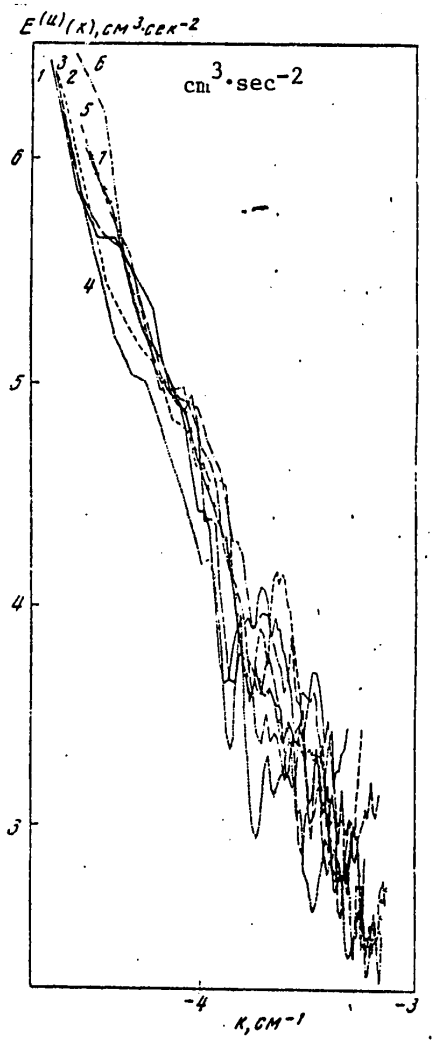

Fig. 8. Spectral densities of fluctuations of current velocity according to data from anchored buoy station at horizons 15 (1), 25 (2), 50 (3), 75 (4), 100 (5), 150 (6) and 200 m (7).

Figure 12 shows an example of the processing of six successive soundings (with intervals of about 1 hour) by the AIST instrument in the polygon. The thick curve represents the averaged temperature profile for all soundings. The profile became considerably "smoother," but there are individual "steps," interlayers with a virtually constant temperature, zones of increased gradients and a region of temperature inversions. The extreme curves in the figure show the value of the standard deviations of temperature values at the horizon according to data from individual soundings from its mean value. These deviations do not exceed fractions of a degree in the upper 85-m layer and then increase to 1.5-1.6°C in layers with large temperature gradients. Such a temperature variability at this horizon can be caused by both the spatial-temporal variations of mesostructure of the temperature field and by vertical movements of this entire structure under the influence of internal waves.

Interesting information on the characteristics and variability of temperature field mesostructure in the polygon were obtained using a radio buoy. The instrument temperature sensors were situated in the layer of greatest temperature gradients at the horizons 103, 115, 126, 138, 150, 170, 212 and 232 m. The discreteness

of interrogation of the sensors was 12 sec. The information received by ship via the radio channel was registered with digital magnetic recorders or on punched tapes, after which it could be introduced into an electronic computer. The program for processing on an electronic computer included one-point statistical analysis, construction of the field of isotherms and the field of spectral density of temperature fluctuations. Figure 13 shows an example of construction of the field (section) of isotherms on the basis of data for a 3.5-hour radio buoy operating interval. The total number of temperature readings used in constructing a section, as is easily computed, was approximately 8,000. From the macroscale characteristics of the field of isotherms in Fig. 13 it is possible to note a general tendency to a deepening of the isotherms during the observation period. Such a phenomenon can be caused, for example, by tidal internal waves of a semidiurnal or diurnal period. The figure also shows more high-frequency temperature fluctuations with periods of about 5-10 minutes which can be interpreted as internal gravitational waves. It is interesting to note that such internal waves did not exist during the entire period of observations, but only during definite time intervals, disappearing and arising anew. They sometimes occupied virtually the entire considered layer of the ocean and sometimes were observed only at a few horizons.

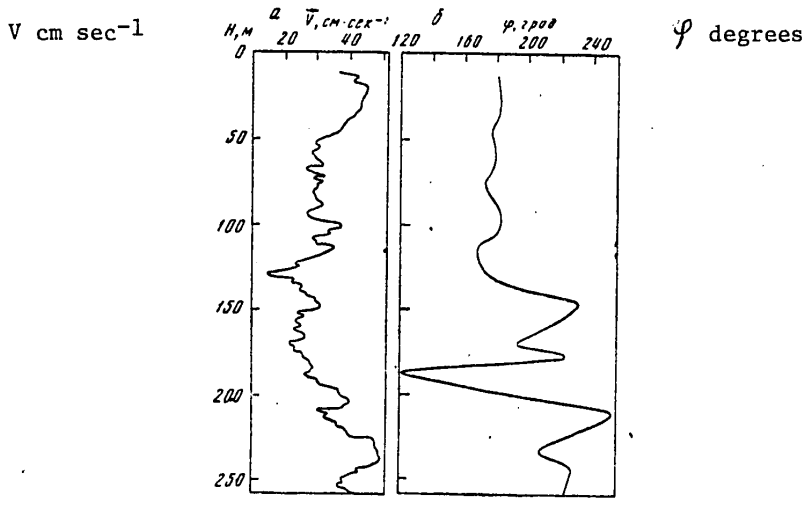

Fig. 9. Vertical profiles of intensity (a) and direction (b) of current velocity according to data from acoustic probe.

From the statistical characteristics computed on the basis of radio buoy data we will cite two families of spectral density curves E(k) for temperature fluctuations at each of the eight observation horizons (Fig. 14). In computing the first family of curves we used a four-hour record with the number of temperature readings at each horizon equal to 1,200, and for computing the second family -- a 3.5-hour record (of 1,032 terms), following the first record approximately after a 1.5-hour interval. The figures in the diagrams denote the observation horizons in the sequence of an increase in depth. The spectral densities were computed by the Tukey method (Fourier transform of correlation functions) with a maximum shift

in computing the correlation functions equal to 0.1 the total length of each series and when using a high-frequency cosine filter with a parameter equal to 0.2 the length of the series. On the x-axis in Fig. 14 we have plotted the values of the wave numbers k, scaled from the values of the frequencies f of oscillations using the "frozen-in" hypothesis with a mean velocity of the transport current V = 10 cm/sec.

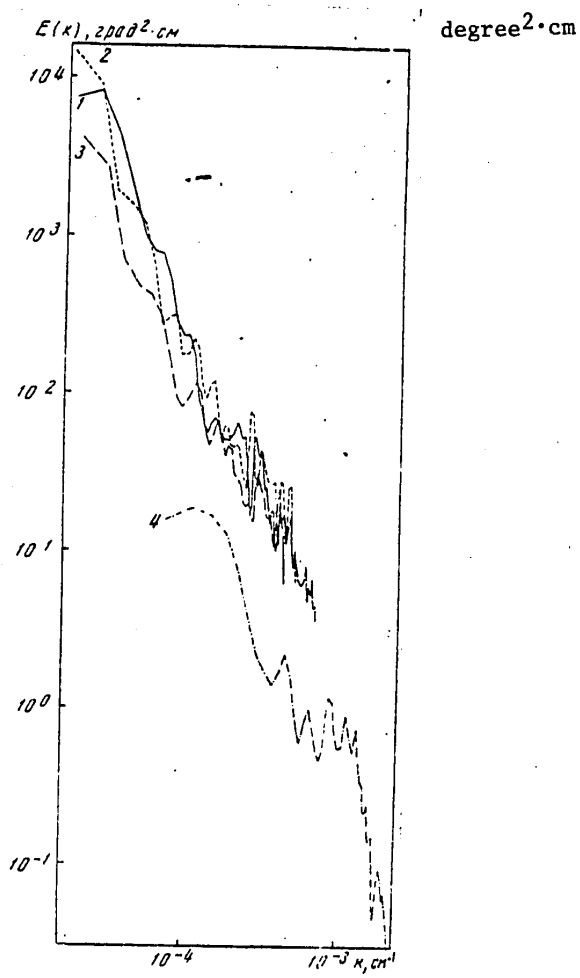

Fig. 10. Spectral densities of temperature fluctuations according to data from photothermographs at horizons 100 (1), 150 (2), 200 (3) and 400 m (4).

The principal characteristic of the spectral density curves in Fig. 14 is their rapid dropoff with k values greater than 10^{-3} cm^{-1}. The tangent of the slope of curves in this region, that is, the exponent in the power-law approximation of the curves, exceeds -3, gradually decreasing toward the right end of the graph. The decrease in the slope of these curves in the most microscale part of the spectrum

can be influenced by discretization noise because the energy of the higher-frequency temperature fluctuations, as we will see below, is quite high. The maxima on the curves in the region $k = 10^{-3}$ cm^{-1} are evidently caused by gravitational internal waves of the above-mentioned period. However, as can be seen from the spectral density curves, in the polygon during the observation period there were not only these waves, but an entire spectrum of higher-frequency temperature fluctuations. The energy of these fluctuations does not regularly change with depth; the curves for different horizons are intertwined with one another. A comparison

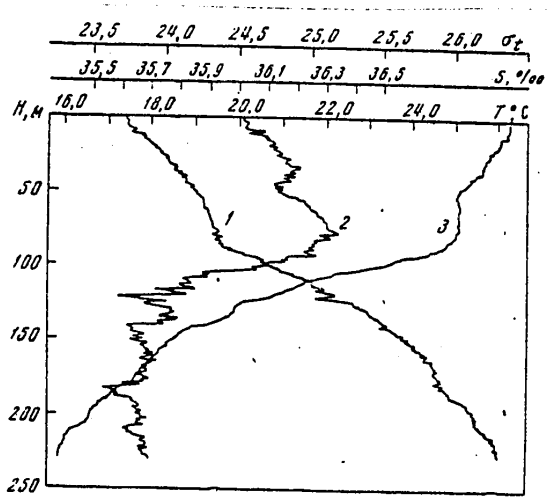

Fig. 11. Vertical profiles of conventional density (1), salinity (2) and temperature (3) according to AIST data.

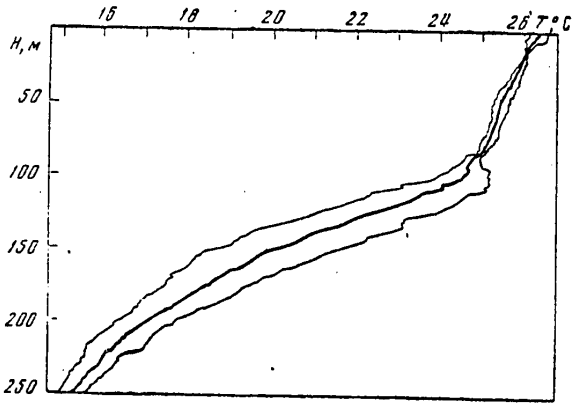

Fig. 12. Averaged vertical temperature profile (thick curve) according to data from multiple sounding with AIST instrument. The thin curves represent the mean square temperature scatter of individual soundings from mean value.

of the families of curves obtained for different parts of the record reveals some nonstationary nature of the process. In actuality, in Fig. 14,b the spectral curves on the average lie somewhat higher than in Fig. 14,a. Individual curves also do not maintain their shape and their relative position: they are somewhat modified and are displaced relative to one another.

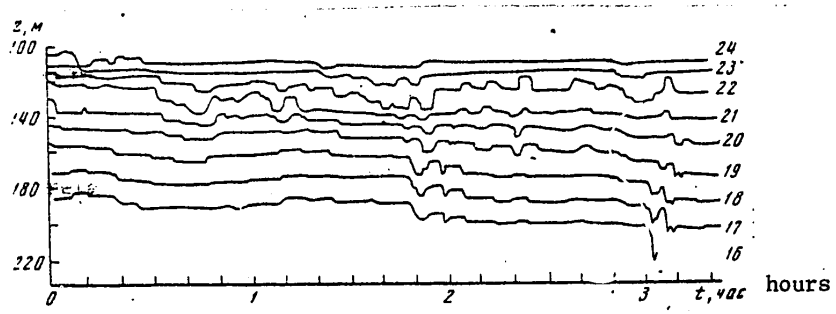

Fig. 13. Field of isotherms (in °C) using data from radio temperature buoy.

The distribution of the energy of temperature fluctuations by wave numbers and by depth h is graphically illustrated in Fig. 15. The isolines of spectral density are given in E(f) units; for scaling them into E(k) units it is necessary that the figures indicated on the isolines be multiplied by $V/2\pi = 1.59$. The figure shows that in the h, k sections of spectral energy density for temperature fluctuations there are individual maxima, where it is necessary to anticipate the generation of energy and from whence it can be propagated into the h, k region with small E(k) values. In our case the principal zone of energy concentration is the horizon 140 m and a wave number close to 10^{-3} cm^{-1}. It is interesting to note that at this same depth there is a density gradient maximum. The position and intensity of the energy density maximum vary very little from one period to the next (Fig. 15), whereas all the remaining field of E(k) isolines experiences appreciable variations. Thus, during the second period of observations there is a secondary maximum with h, k coordinates (220 m, 10^{-3} cm^{-1}), and the maximum with the coordinates 110 m, $8 \cdot 10^{-4}$ cm^{-1} is somewhat displaced and decreased. The configuration of the isolines in the upper right part of the section also was considerably changed.

The still finer structure of the temperature field in the polygon was obtained using a group of thermistors mounted on a special trawl. This special trawl, constructed at the Atlantic Division of the Institute of Oceanology, is a towed apparatus with a system of sensors for the mean and fluctuating values of velocity, temperature and conductivity of sea water. The optimum rate of towing of this trawl is 4-6 knots with a deepening up to 200 m. The number and makeup of the sensors on the trawl can vary depending on the situation and the purposes of the experiment. In measurements in the considered polygon the trawl carried a system of ten temperature sensors spaced 70 cm apart and two conductivity sensors separated by the same interval. In addition, there was also a sensor of velocity fluctuations and the mean velocity of movement of the trawl relative to the surrounding medium and a sensor for depth of submergence of the trawl. The conductivity and fluctuations

of velocity sensors were situated in a two-hull container (catamaran) oriented along the flow. The container also held a depth sensor. Oscillations of the container (course angle, banking, fore-to-aft fluctuations) were monitored by angular velocity sensors, which made it possible to avoid signal distortions due to instability of carrier movement. The measurements were made only in a case when the velocities of the oscillations did not exceed 1 degree/sec. Such conditions were ensured virtually constantly due to the system for suspending the container under a deepener with a great mass preventing the imparting of vibrations from the towing line to the container with the instrumentation.

Thermoresistors with a time constant of about 1.5 sec and a response of 0.05°C were used for measuring temperature. Conductivity was measured by capacitive sensors designed at the Leningrad Mechanical Institute. The sensing element of this sensor is a pair of electrodes covered with condenser ceramic, cut into a high-frequency circuit whose quality varies in dependence on the change in conductivity of sea water. With respect to operating principle the sensor is inertialess, but it averages the conductivity spatially with a radius of about 1 cm. The signal contains both constant and fluctuating components which are separated during the registry process by means of electric filters. With a constant salinity of about 35°/oo the sensor reacts to temperature fluctuations with an amplitude of 10^{-4}°C with a signal-to-noise ratio equal to unity.

In measuring velocity fluctuations use was made of a thermoanemometric sensor designed by V. V. Stolypin, whose sensing element is a conductivity sensor with a microelectrode near which, due to the release of Joule heat, there is a heating of the ambient conductive medium. An ordinary thermoanemometric effect arises during movement of the medium. This is called a hydroresistor thermoanemometer. In contrast to the film thermoanemometers used in study of turbulent flows the hydroresistor thermoanemometer has considerably greater mechanical reliability. Its inertial properties are determined for the most part by spatial averaging with a radius dependent on the dimensions of the electrode. In our case this radius did not exceed 3.5 mm. The sensor noise level was tenths of a millimeter per second.

The mean rate of towing at the observation horizon was measured by an electric current meter. This instrument has a rotor and frame from a standard current meter and in order to obtain an electric signal near the rotor there is a conductivity sensor producing pulses with each revolution of the rotor. The refashioning of the current meter did not worsen its metrological characteristics and therefore the error in measuring mean flow velocity did not exceed 3-5 cm/sec.

The depth of submergence was measured using a sensor of the vibrotron type with a range 0-50 atm and a measurement error of 1.25 m.

The recording devices of this special trawl included four-channel analog magnetic recorders suitable for the registry of constant and variable signals with a frequency up to 1 KHz. These magnetic recorders were used in registering fluctuations and the mean velocity and conductivity values. At the same time these same signals were visualized using a low-inertia three-pen automatic recorder and on oscilloscope screens.

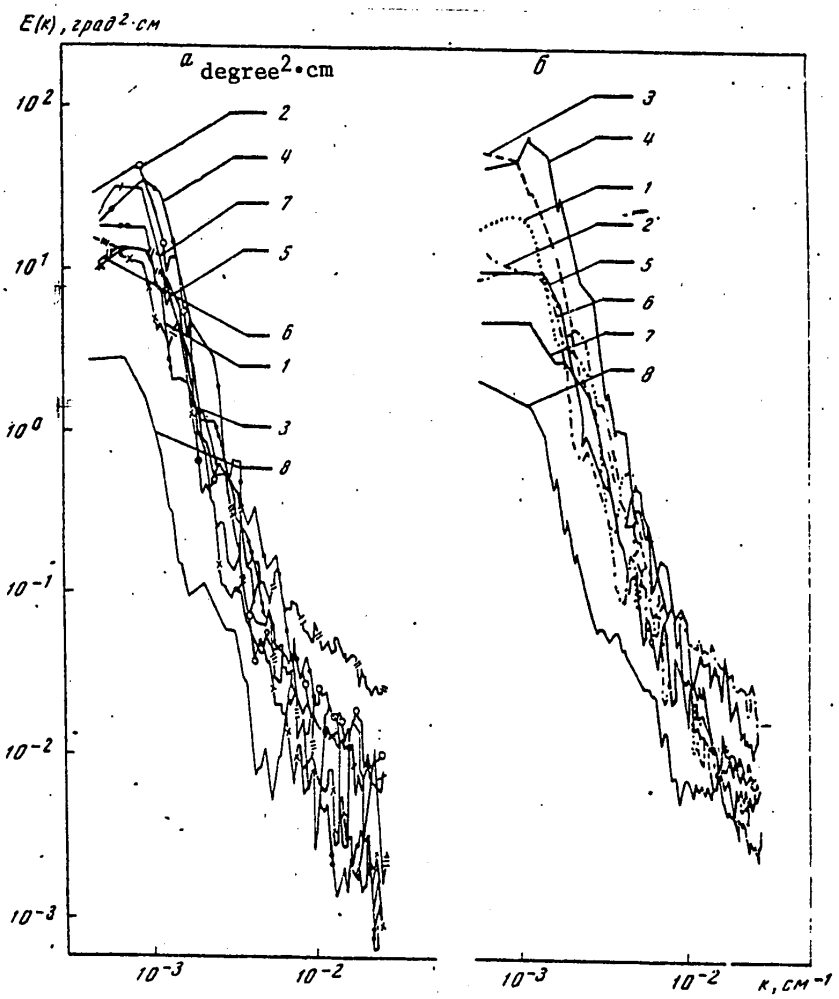

Fig. 14. Spectral densities of temperature fluctuations according to data from radio temperature buoy at horizons 103 (1), 115 (2), 126 (3), 138 (4), 150 (5), 170 (6), 212 (7) and 232 m (8) for two segments of records with a duration of 4 (a) and 3.5 hours (6).

The temperature signals were registered simultaneously in digital and analog forms on a digital magnetic recorder and by automatic recorders. The period of interrogation of the sensors did not exceed 2-3 sec. The frequency signals of the wave recorder and the vibrotone were monitored from the dials of electronic frequency meters and in case of necessity could be registered in digital form on a second digital magnetic recorder. In addition, the pulsed signal of the wave meter was registered on an analog magnetic recorder so as to ensure the transformation of the time scales of the investigated fluctuations into space coordinates.

Figure 16 shows the vertical spatial sections of the temperature field constructed using data for ten thermistors during the towing of the special trawl. The first section was computed on an electronic computer using temperature readings with a

discreteness at each horizon of 3 sec. The isotherms were drawn each 0.1°C with a total length of each of the series of 131 points. In order to construct the second section (Fig. 16,b) we used data on temperature with a sample of 6 sec with corresponding smoothing and a length of 227 points in each series. The isotherms were also drawn each 0.1°C. The first section clearly shows a localized layer with great vertical temperature gradients in which there are high-frequency temperature fluctuations against a background of a slower "variation" of isotherms with wavelengths of approximately 300 and 700 m. In the second section such a layer is absent and due to the smaller scale along the horizontal axis the isotherms frequently are very steep. The left part of the section is characterized by a relatively quiet temperature field. Then the field becomes more complex, the isotherms come closer together, and finally, the field acquires a calmer character. The vertical temperature drops in the zone of clustering of isotherms attain 0.2 and even 0.3°C per meter, whereas in quiet zones the temperature difference of 0.1°C can be attained at distances of several meters vertically.

The dependence of the characteristics of microscale fluctuations of hydrophysical fields on local field characteristics is illustrated well in Fig. 17, which shows synchronous records of high- (1) and low-frequency (2) fluctuations of conductivity, obtained using the special trawl, at two horizons with a vertical spacing of 70 cm. Curves 1a and 2a correspond to the lower, and curves 1b and 2b to the upper measurement horizon. In the registry of the high-frequency signals the amplification factor for the upper horizon was several times less than for the lower horizon. Curves 1 and 2 (a,b) are somewhat displaced relative to one another in the horizontal direction (approximately by 3 sec) due to design peculiarities of the automatic recorder. The records of the signals illustrated in Fig. 17 were obtained during the towing of the sensors at a depth of 94 m (lower measurement horizon).

The changes in conductivity (curves 2a and 2b) with a period of about 8-10 sec are related to the influence of rolling of the ship and indicate the existence of a local vertical gradient of mean conductivity (temperature) $d\bar{\sigma}/dz$. On the basis of the amplitude of change in conductivity with the mentioned period it is possible to judge qualitatively also about the $d\bar{\sigma}/dz$ value, which with a constant amplitude of the vertical displacements of the sensor must be directly proportional to the amplitude of the curves 2a and 2b with a period of 8-10 sec.

In Fig. 17 it is possible to define the following regions arbitrarily: during the course of the first 4 minutes the measurements were made in a layer with a relatively small vertical conductivity gradient, then for a period of 1 minute -- in a layer with a large conductivity gradient, in the next 0.5-1 minute -- again with a relatively small $d\bar{\sigma}/dz$ value and then with $d\bar{\sigma}/dz \approx 0$. The upper sensor entered the homogeneous layer ($d\bar{\sigma}/dz \approx 0$) sooner than the lower sensor by approximately 1 minute. The level of high-frequency conductivity fluctuations with relatively small $d\sigma/dz$ values is appreciably higher than with $d\bar{\sigma}/dz \approx 0$ and in the layer with a greater conductivity gradient. If it is assumed that $\sigma' \sim d\bar{\sigma}/dz w$, where σ' and w are the mean square values of microscale fluctuations of conductivity and the vertical component of current velocity respectively, then with $d\bar{\sigma}/dz \approx 0$ with any real w values the conductivity fluctuations will be small. With identical w values the σ' values must be greater in the layer with greater $d\bar{\sigma}/dz$ values, but with an increase in the vertical conductivity (temperature) gradient it is necessary to anticipate a considerable decrease in w and as a result this can lead to a decrease

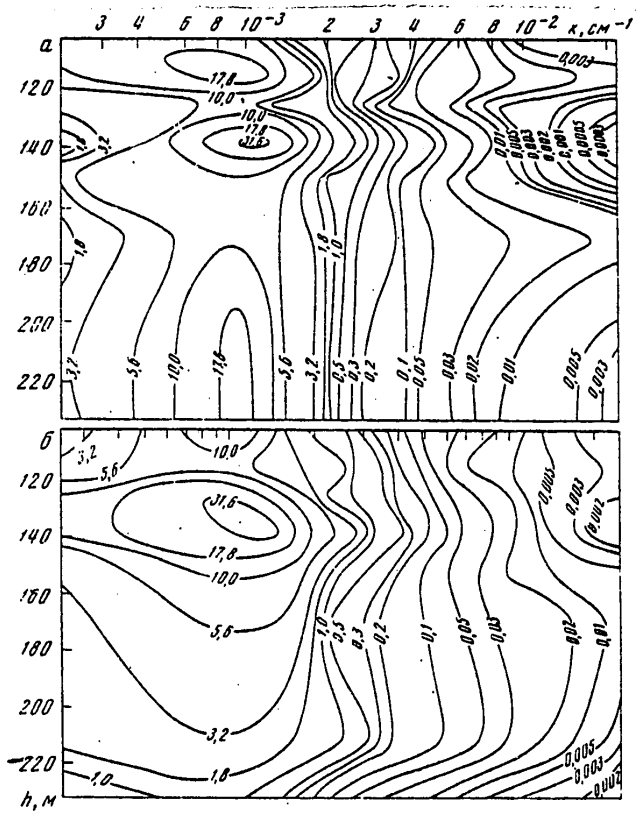

Fig. 15. Isolines of spectral density of temperature fluctuations (in degrees^2. sec) according to records of radio temperature buoy with a duration of 4 (a) and 3.5 hours (b).

in σ. Thus, the change in the level of high-frequency conductivity fluctuations in actuality is related to variations in the local background conditions (in actuality, variations of the vertical conductivity gradient).

Measurements of microscale fluctuations of the fields of current velocity and conductivity were made in a polygon at a number of depths in the layer from 20 to 213 m. The spectral densities of the high-frequency signals were were computed on an electronic computer by the fast Fourier transform method by segments of the record with a duration from 40 to 80 sec with a time discreteness of 1/260 sec. Figure 18 shows the spectra of fluctuations of current velocity in the range of scales from approximately 1 cm to 1 m. The level of fluctuations of current velocity was maximum at a depth of 195 m; its change with depth is nonmonotonic. At the very same depth the level of current velocity fluctuations can vary considerably (compare curves 13a and 13b in Fig. 18), which should be related to the difference in local background conditions. In the case of a linear (at a logarithmic scale) continuation of the high-frequency spectra into the region of lower frequencies their level is higher than the level of the spectra of macroscale

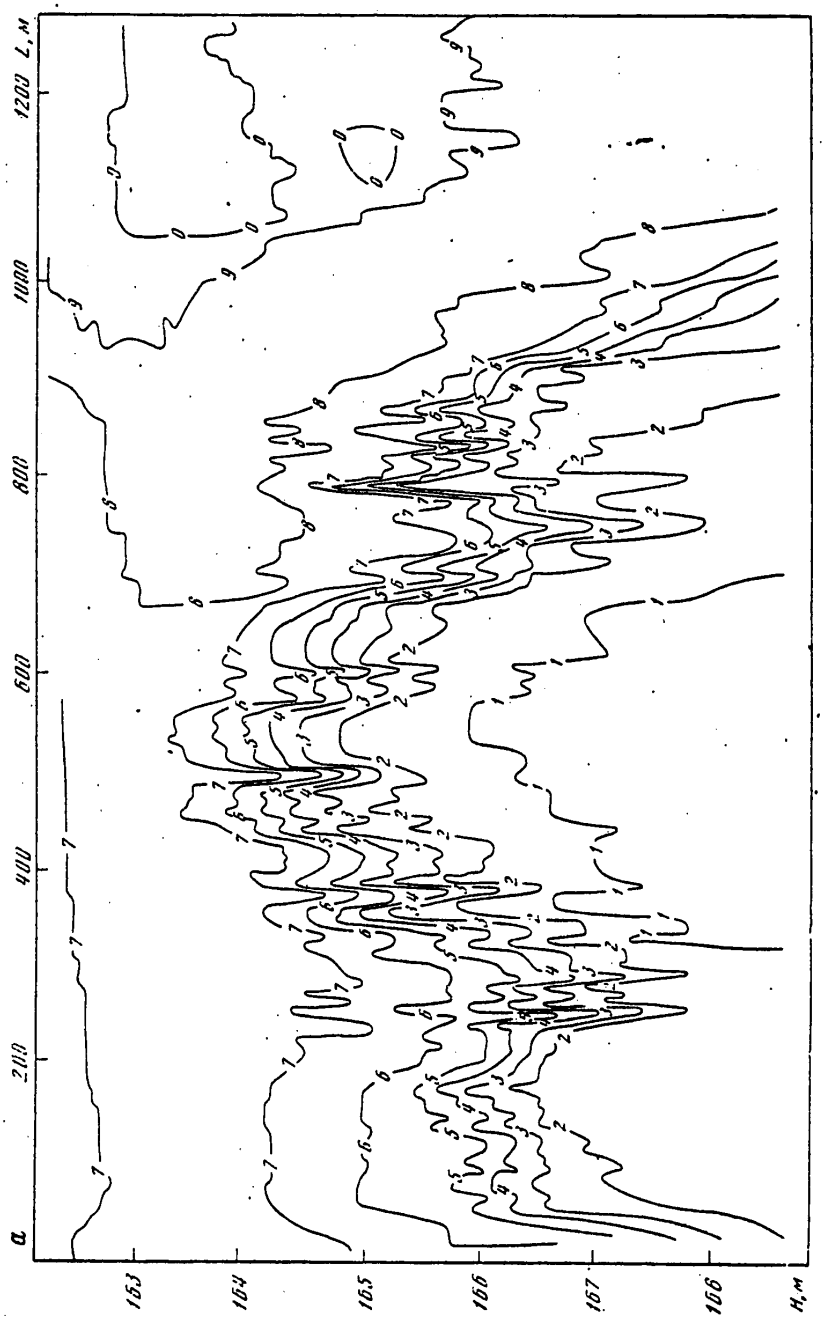

Fig. 16 (continued on next page).

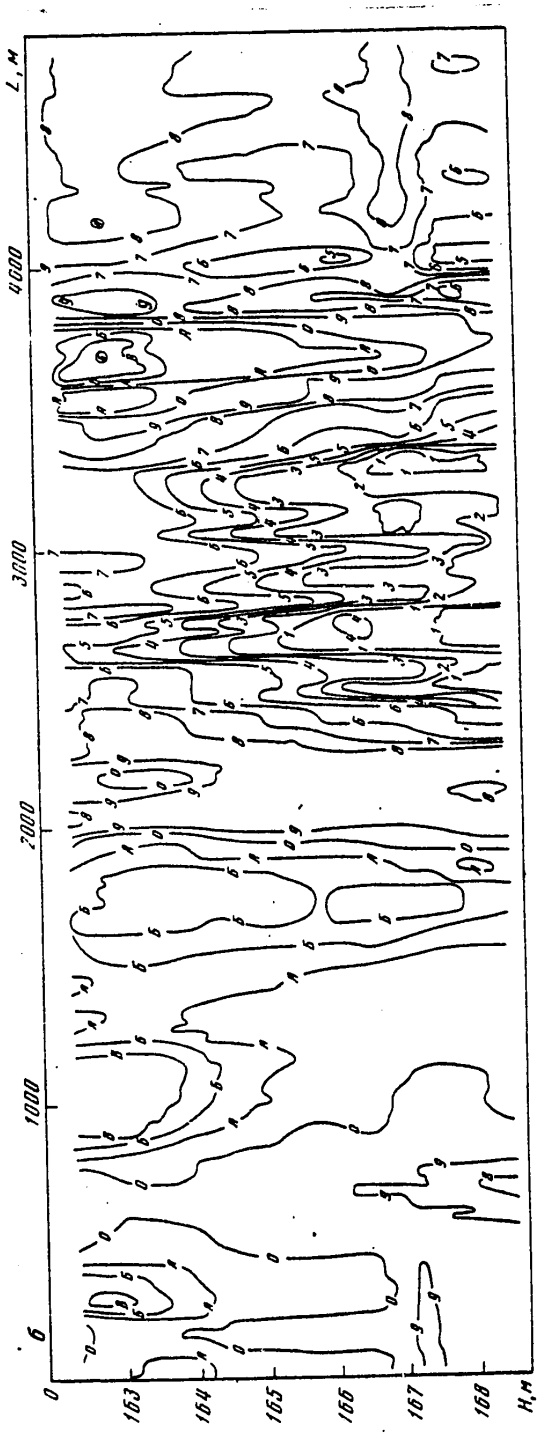

Fig. 16. Spatial sections of temperature field according to data from special trawl for two sectors of record (a, b). 1) 18.2; 2) 18.3; 3) 18.4; 4) 18.5; 5) 18.6; 6) 18.7; 7) 18.8; 8) 18.9; 9) 19.0; 0) 19.1; A) 19.2; Б) 19.3; В) 19.4.

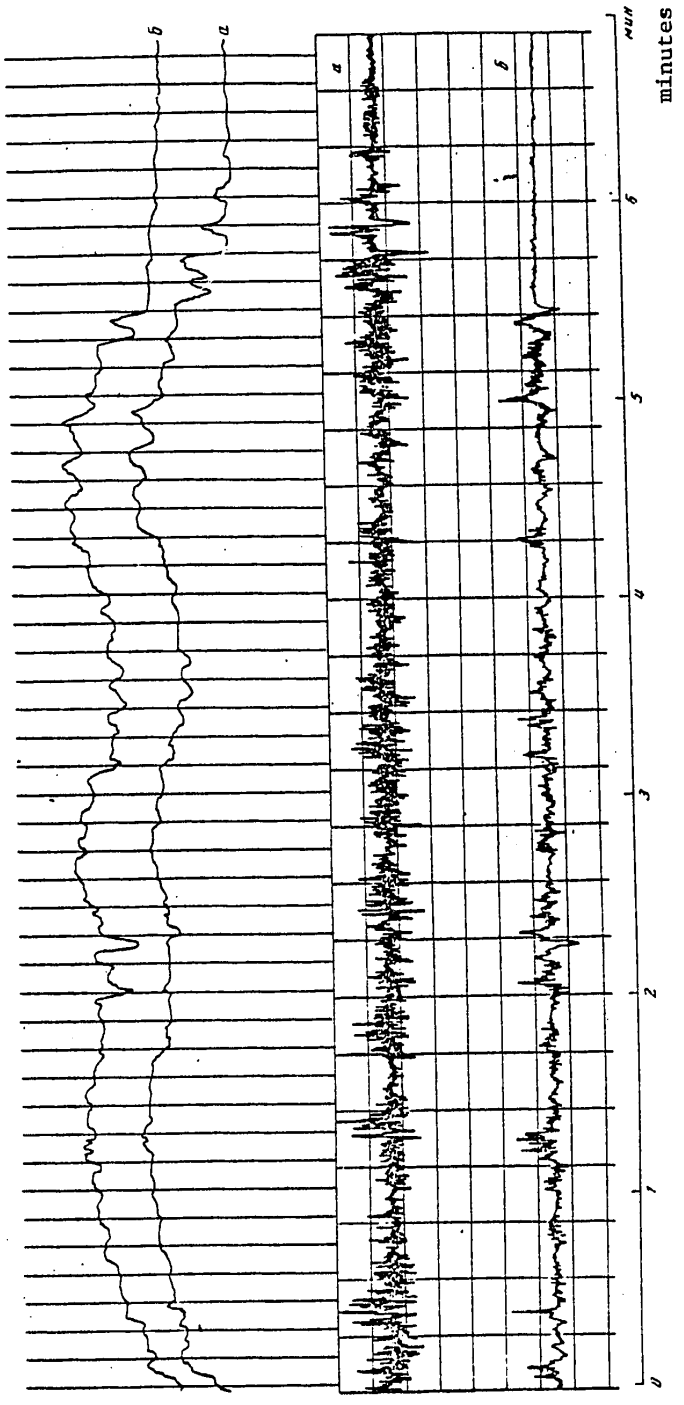

Fig. 17. Example of synchronous records of high- and low-frequency fluctuations of conductivity at two horizons with vertical spacing of 70 cm. a) lower sensor; b) upper sensor.

fluctuations of current velocity according to data from the anchored buoy station (see Fig. 8). This can be caused, in particular, by the influx of energy into the region of scales of about 10 m. The distribution of intensity of fluctuations of current velocity in the spectrum of wave numbers is shown in Fig. 19,a,b. In the investigated range of scales the contribution to the dispersion of current velocity fluctuations in general increases regularly with a decrease in wave numbers (with an increase in the scales of inhomogeneities), and accordingly, the microscale range does not determine the total dispersion of fluctuations of current velocity in the ocean. Figure 20,a,b gives the $k^2E_1(k)$ curves characterizing the spectral distribution of the dissipation of turbulent energy. The scatter of the curves here is considerable, since in the $k^2E_1(k)$ spectra there is a clearer manifestation of different types of interference. However, it can be seen in Fig. 20,b that the $k^2E_1(k)$ curves increase with an increase in k, but do not attain maxima in the investigated range of scales.

If the spectral curves in Fig. 18 are approximated by straight lines with the slope -5/3, it is found that the empirical curves deviate systematically from the approximating straight lines in the low-frequency region and have a steeper (close to -11/5) slope to the x-axis. This suggests a possible influence of buoyancy forces on turbulent fluctuations of the current velocity field. Adhering to [9], it is possible to obtain the universal spectral function $f_1(x)$ of longitudinal fluctuations of current velocity in a stratified medium for comparison with the experimental curves. Matching of the empirical spectra with the universal curve is accomplished in the following way. The experimental curve at a logarithmic scale is approximated in the high-frequency region by a straight line with the slope -5/3. A transparent sheet on which the universal spectrum is plotted is superposed on the empirical graph in such a way that the segment of the universal curve with the slope -5/3 coincides with the approximating straight line and then the sheet is moved along the approximating straight line until the best (visual) coincidence is attained between the experimental and theoretical curves. The result of such an operation with the spectra in Fig. 18 is shown in Fig. 21. The figure shows that the experimental curves fall well on the model spectrum (in Fig. 21 the longitudinal spectrum of current velocity fluctuations in the model [9] is shown as a thick curve).

The rate of dissipation of turbulent energy ε is easily computed from the inertial segment of the spectrum with the slope -5/3, and the matching of the empirical curves with the model spectrum makes it possible to determine the value of the buoyancy scale L_* (with an accuracy to the constant factor $4\alpha_0^{-3/4}\gamma^{-1/2}$, where α_0 is the ratio of the coefficients of turbulent thermal conductivity and viscosity, γ is a proportionality factor in the Heisenberg hypothesis on the form of the spectral coefficient of turbulent viscosity). Using an expression for the buoyancy scale in a stratified fluid [10]

$$L_* = \frac{\varepsilon^{1/4}}{N^{3/4}(g\alpha)^{1/4}},$$

where g is the acceleration of free falling, α is the coefficient of thermal expansion of the medium, it is possible to compute the rates of evening-out of temperature inhomogeneities N. The ε and N values, according to the data in Fig. 21, on the average are close to 10^{-2} cm^2/sec^{-3} and 10^{-3}-10^{-4} $degree^2/sec$, and the L_*

value has the order of the dimensions of "steps" of the fine structure of the density field in the polygon.

The measurements of the high-frequency fluctuations of conductivity in the polygon were carried out synchronously using two sensors which were spaced 70 cm apart vertically. The spectra of conductivity fluctuations at both measurement horizons are usually close, but in three cases they are somewhat different from one another with respect to form and level, which confirms the hypothesis expressed above concerning the dependence of turbulence characteristics on local background conditions. Figure 22 shows the spectral densities of conductivity fluctuations on the basis of measurements with one of the sensors. The spectral curve 2a falls considerably below all the other curves, forming a relatively dense group. We note that the spectrum 2b was obtained by measurements at the same depth of 138 m as in 2a. In the buoyancy interval, according to the model in [9], the spectral density of the conductivity (temperature) fluctuations has a power-law dependence with the exponent -7/5. In Fig. 22 the spectral density curves in most cases can actually be approximated in the low-frequency region by straight lines with the slope -7/5. Thus, the effect of Archimedes forces is manifested in the flow both in the current velocity field and in the conductivity field. Figure 23 shows the distribution of the intensity of conductivity fluctuations in the spectrum of wave numbers, and Fig. 24 shows the "dissipative" $k^2E_1(k)$ spectra. In their character they are similar to the corresponding curves for current velocity fluctuations.

In the polygon measurements of microscale conductivity fluctuations at great depths (to 1,200 m) were also made for the first time. The measurements were made using the "Sigma" turbulence probe, constructed from elements of the special trawl.

The number of sensors on the probe was reduced to the minimum adequate for determining the characteristics of the microstructure of the conductivity field against the background of the characteristics of field stratification. The probe had channels for the mean and fluctuating conductivity values, mean velocity of movement (current meter) and depth of submergence (vibrotron). The probe was placed at the end of a three-strand supporting and electrical cable with a fish-shaped deepening weight of 250 kg weight. Measurements with the probe could be made both in a vertical sounding regime and in a towing regime with constant or variable deepening, which was attained by a change in the rate of the ship's movement and the length of the supporting and electrical cable.

In the polygon the "Sigma" probe was used in carrying out vertical soundings and seven horizontal "sections" of the conductivity field were obtained in the range of depths from 40 to 845 m. The registry of the conductivity signal was simultaneous in the two magnetic recorder channels: in one channel the full (unfiltered) signal was registered, and in the other (with a greater amplification) -- the signal filtered from the low-frequency component. Such reception was caused by limitation on the dynamic range of the recording apparatus, not making it possible with adequate resolution to register the signal in a broad frequency range. The statistical characteristics of variability of the conductivity field were then computed for two frequency ranges and then "spliced." The computations were made using records with a duration of about 10 minutes.

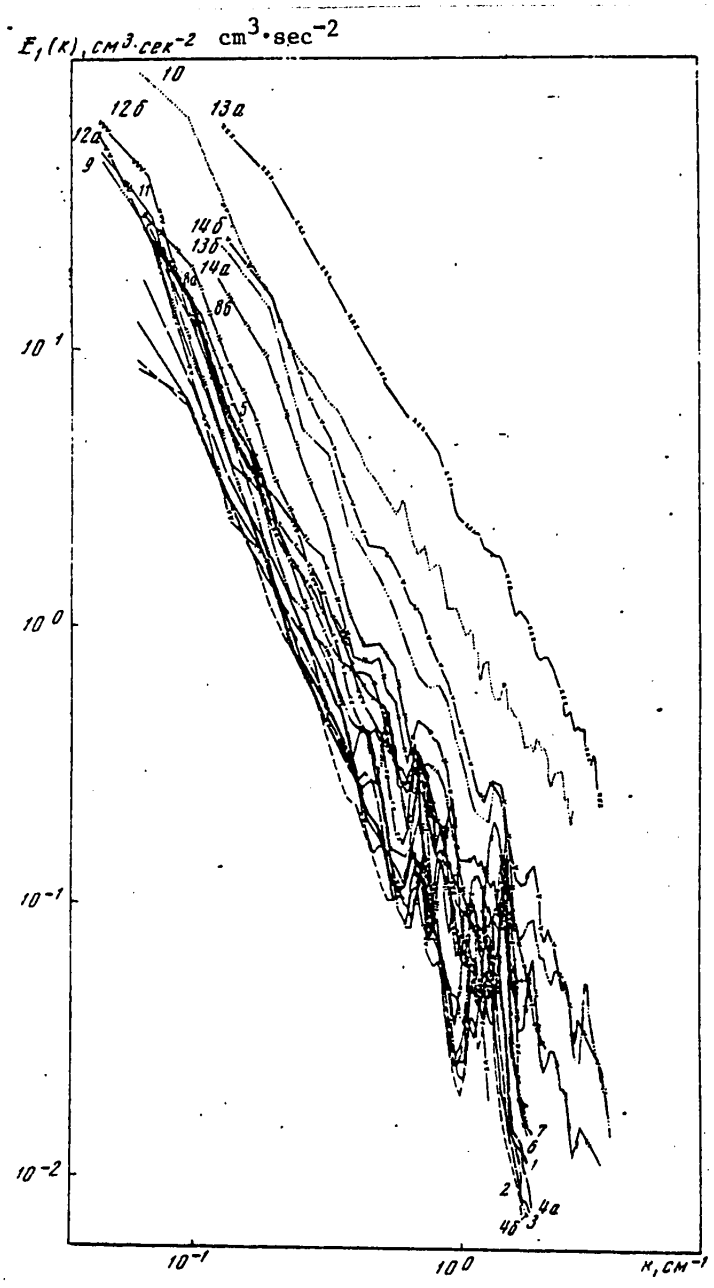

Fig. 18. Spectral densities of microscale current velocity fluctuations (according to hydrotrawl data) at horizons 20 (1), 33 (2), 55 (3), 77 (4a, 4b), 94 (5), 103 (6), 121 (7), 138 (8a, 8b), 141 (9), 157 (10), 160 (11), 168 (12a, 12b), 195 (13a, 13b) and 213 m (14a, 14b).

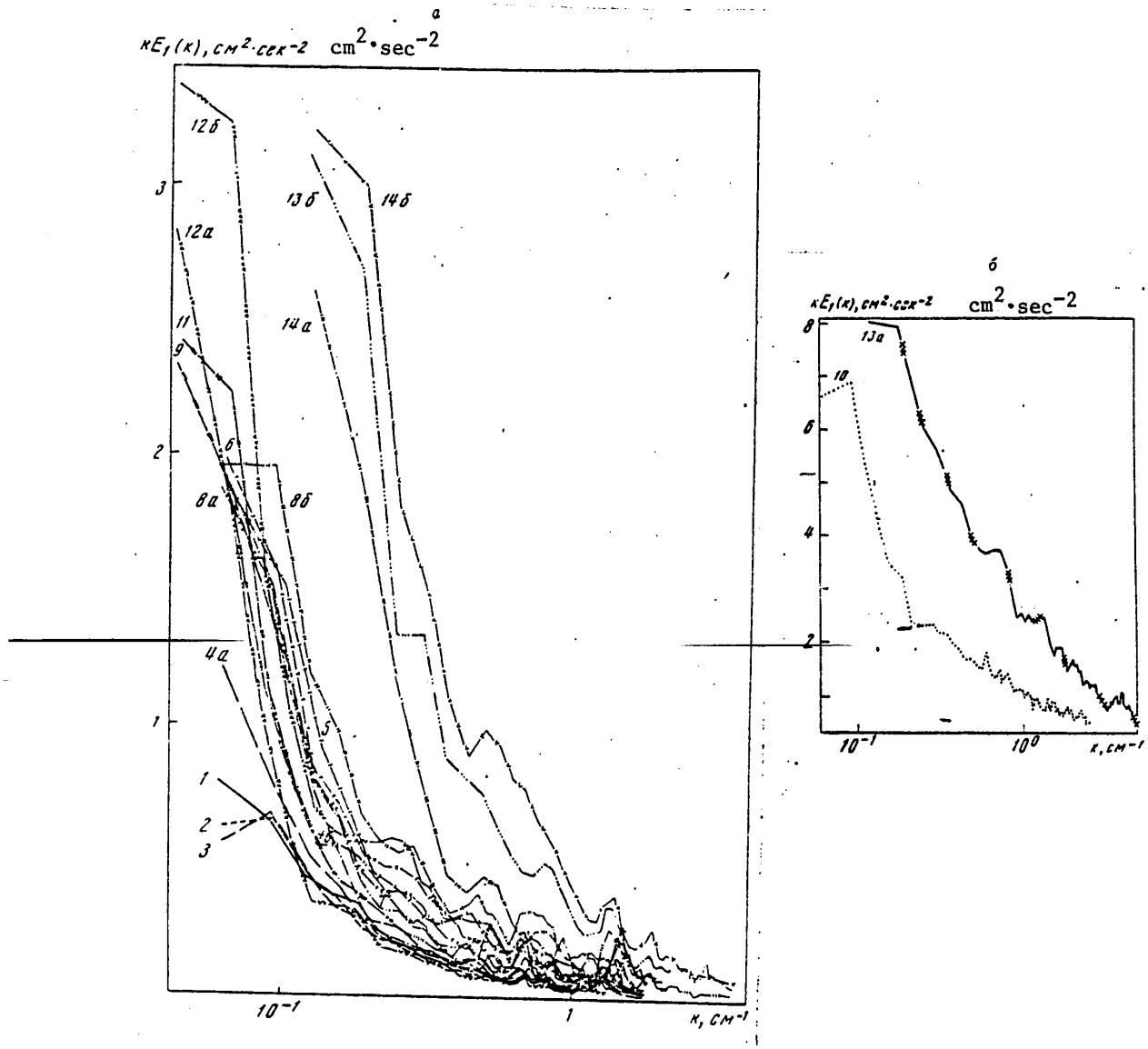

Fig. 19. Distribution of intensity of microscale fluctuations of current velocity in spectrum of wave numbers according to data from hydrotrawl. Notations are the same as in Fig. 18.

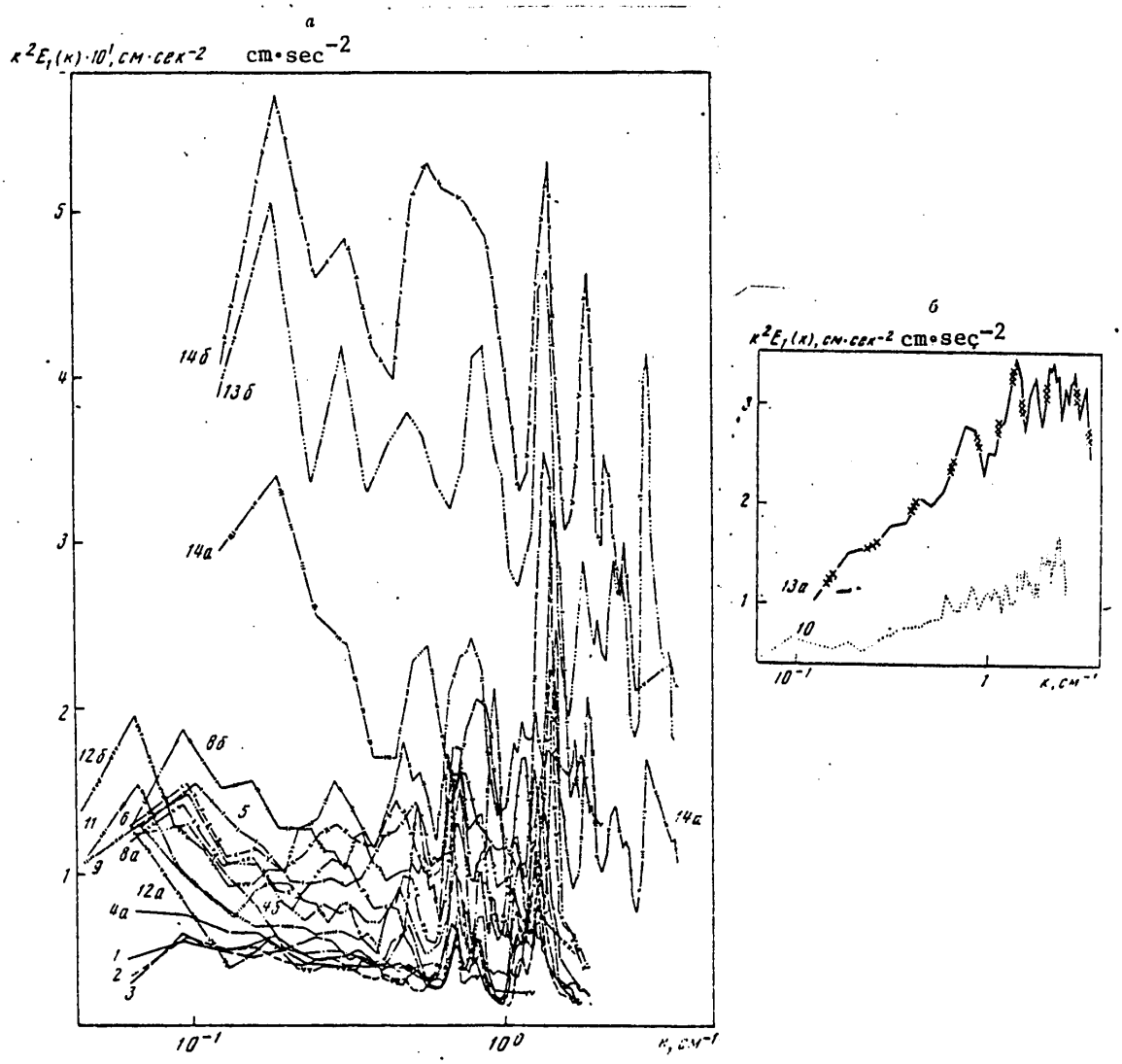

Fig. 20. Spectra of dissipation of current velocity fluctuations according to data from hydrotrawl. Notations are the same as in Fig. 18.

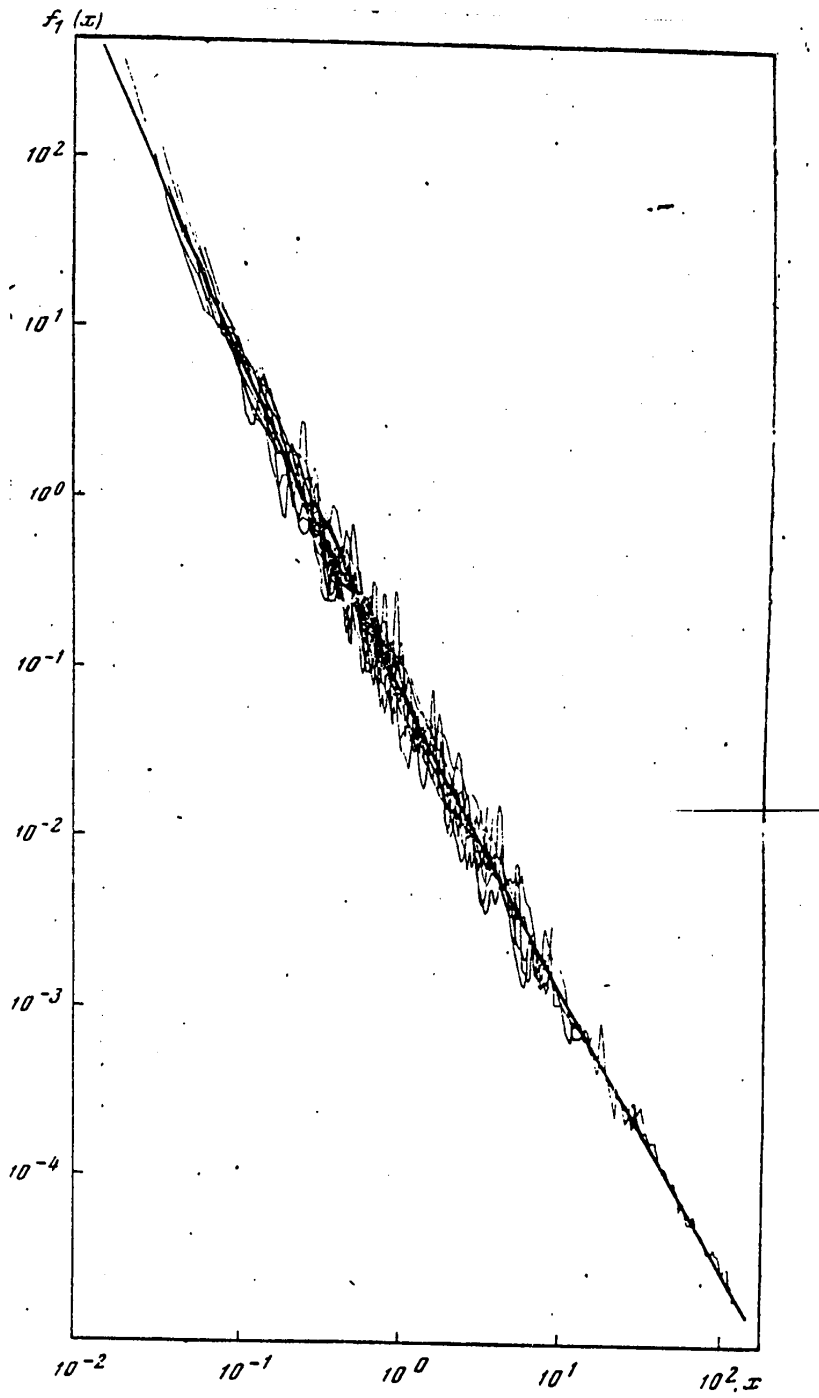

Fig. 21. Matching of spectral functions in Fig. 18 with Monin model curve [9].

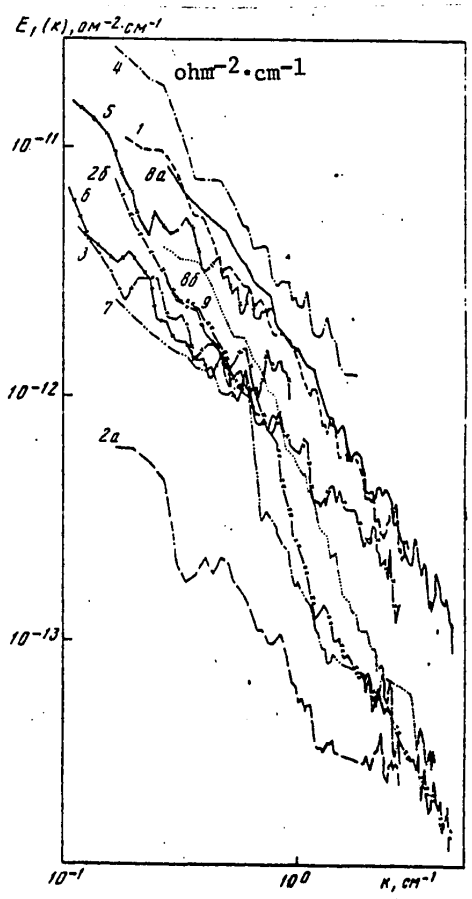

Fig. 22. Spectral densities of conductivity fluctuations (according to data from special trawl) at horizons 94 (1), 138 (2a, 2b), 141 (3), 157 (4), 160 (5), 168 (6), 174 (7), 195 (8a, 8b) and 213 m (9).

As an example, Fig. 25 shows the "spliced" spectral density functions for fluctuations of conductivity for records at depths of 645 and 720 m. The mean vertical conductivity profile, obtained by means of the probe, is shown in Fig. 26 in relative units. The depth scale on the profile is nonlinear; the depth marks are indicated on the profile itself. The figure clearly shows the fine layered structure of the conductivity field in the entire investigated ocean layer. As indicated in Fig. 25, the levels of the high-frequency conductivity fluctuations at great depths are comparable in order of magnitude with the levels of such fluctuations in the surface layer of the ocean (Fig. 22). The distribution of intensity of conductivity fluctuations by wave numbers for these same records is shown in Fig. 27. In the investigated range of wave numbers (scales) the contribution to the dispersion of conductivity fluctuations increases, as we see, almost monotonically with a decrease in wave numbers, that is, with an increase in the scales of the inhomogeneities. The maximum with $k = 0.01$ cm^{-1} on curve 2 is not reliable because

it falls in the limits of the 95% confidence intervals for evaluation of the kE(k) values. Thus, the investigated range of scales (from 4 cm to 12 m) does still not completely determine the dispersion of the fluctuations of conductivity and accordingly, in the considered case in the conductivity field there were inhomogeneities with horizontal dimensions greater than 12 m. The "dissipative" conductivity spectra $k^2E(k)$ (Fig. 28) have maxima in the field of scales from approximately 9 to 16 cm and slowly drop off with an increase and decrease in k.

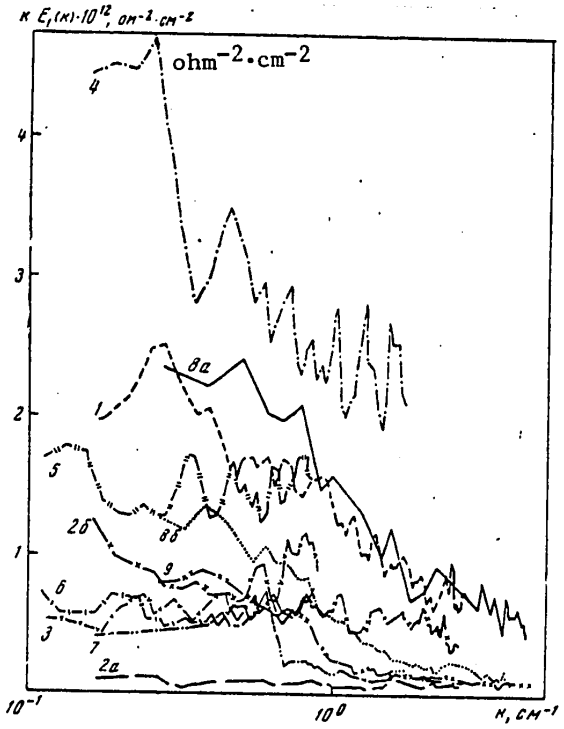

Fig. 23. Distribution of intensity of conductivity fluctuations in spectrum of wave numbers according to data from special trawl. The notations are the same as in Fig. 22.

Now we will summarize some of the general results. The illustrations cited above graphically show how complex and variable are the hydrophysical fields in the ocean. Against the background of the mean climatic macroscale structures there are mesoscale processes associated with weather effects and tidal forces. In turn, internal gravitational waves are superposed on these and these interact with the stepped structure of the vertical profiles. Finally, sensitively reacting to local background conditions, there are microscale fluctuations having a turbulent character. All these processes interact with one another, frequently in a definite way determining one another, frequently being related indirectly or stochastically. For example, macroscale density stratification determines the limiting frequency

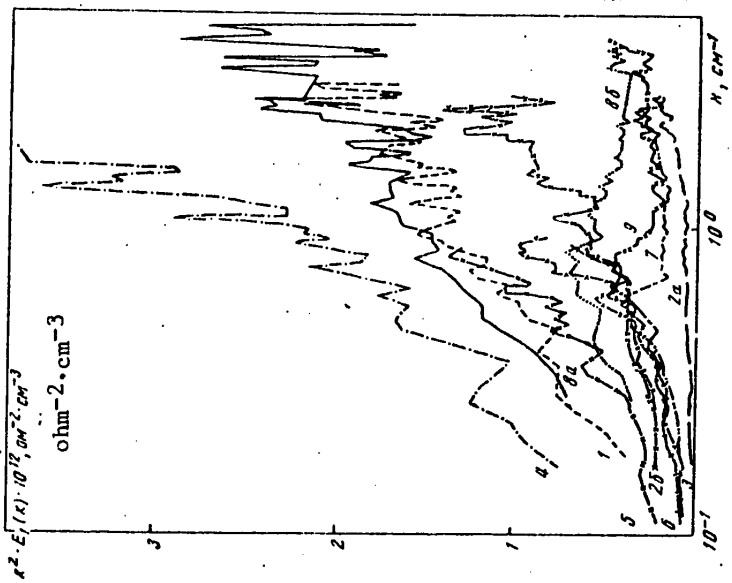

Fig. 24. Spectra $k^2E_1(k)$ for observed fluctuations of conductivity according to data from special trawl. Notations are the same as in Fig. 22.

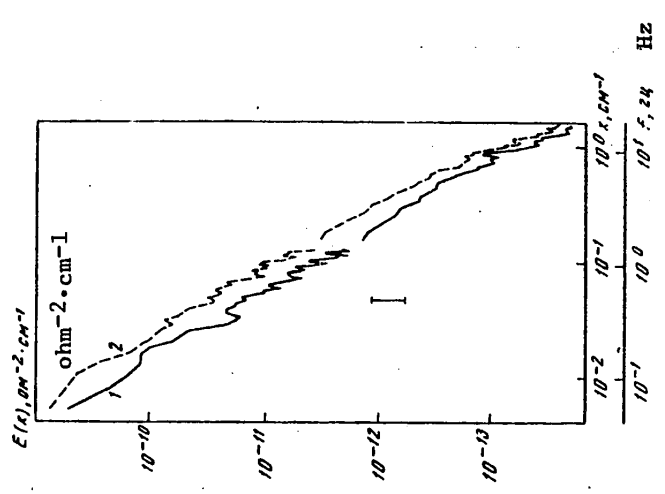

Fig. 25. Spectral densities of conductivity fluctuations at great depths according to data from "Sigma" probe. 1) at depth of 645 m; 2) at depth of 720 m. The vertical line indicates the 95% confidence intervals for evaluations of spectral density (in the low-frequency range).

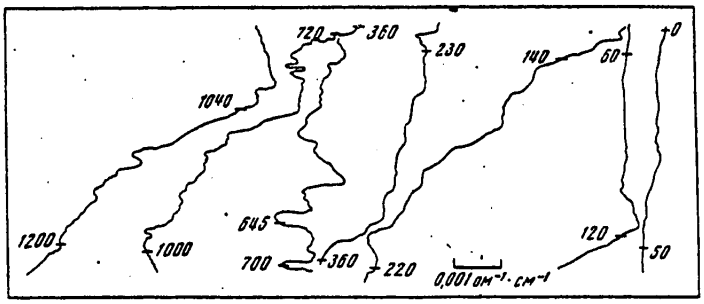

ohm^{-1}·cm^{-1}

Fig. 26. Example of record of mean conductivity obtained with "Sigma" probe. The numbers alongside the curves represent depth in m.

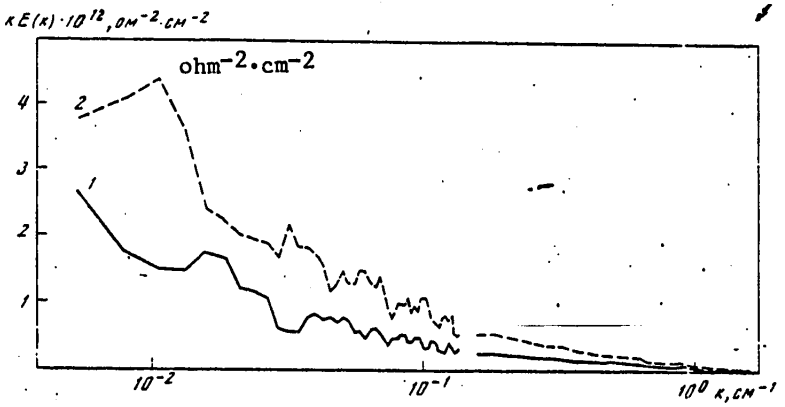

Fig. 27. Distribution of intensity of conductivity fluctuations in spectrum of wave numbers according to data from "Sigma" probe. Notations are the same as in Fig. 25.

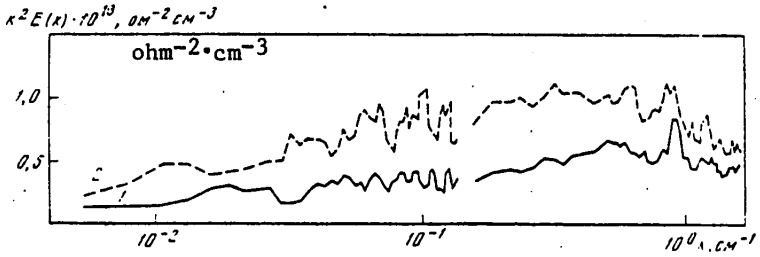

Fig. 28. Spectra of "dissipation" of conductivity fluctuations according to data from "Sigma" probe. Notations are the same as in Fig. 25.

of gravitational internal waves, which, overturning, create spots of highly turbulent fluid and "steps" on the vertical profiles of hydrophysical elements. In turn, microscale turbulence tends to mix the surrounding layers of fluid, leading them to a more homogeneous state. An intensification of turbulent exchange is favored by velocity gradients arising in currents of drift or geostrophic origin, and also in surface and internal waves. On the other hand, a stable density stratification suppresses turbulence, thereby reducing the intensity of mixing. With the cooling or salinization of the upper layers of fluid an unstable stratification of waters can arise which generates convective movements, frequently leading to the appearance of water layers close to homogeneous. Nonlinear interactions of surface and internal waves with one another and with the mean currents and turbulence can generate movements of different scales and intensities, lead to the localization of kinetic and potential energy and individual spatial-temporal zones in the ocean. However, dissipative molecular processes tend to level out existing gradients and bring the ocean into a state of thermodynamic equilibrium. But this process cannot go far due to the constant new receipts of energy in the considered volume of the ocean through its boundaries. In order to establish qualitative and quantitative cause-and-effect relationships among all these diverse processes in the ocean it is necessary to make measurements in a broad spatial-temporal range of scales. An example of such measurements can be the already described complex of observations in the oceanic polygon. We hope to carry out a more detailed quantitative analysis of the relationships among individual processes in the polygon in the immediate future.

In conclusion we take the opportunity to express appreciation to E. I. Karabasheva for assistance in carrying out the computations.

BIBLIOGRAPHY

1. Ozmidov, R. V., GORIZONTAL'NAYA TURBULENTNOST' I TURBULENTNYY OBMEN V OKEANE (Horizontal Turbulence and Turbulent Exchange in the Ocean), Moscow, "Nauka," 1968.

2. Shtokman, V. B., Koshlyakov, M. N., Ozmidov, R. V., Fomin, L. M. and Yampol'skiy, A. D., "Prolonged Measurements of the Variability of Physical Fields in Ocean Polygons as a New Stage in Investigation of the Ocean," DOKLADY AN SSSR (Reports of the USSR Academy of Sciences), 186, No 5, 1969.

3. Brekhovskikh, L. M., Ivanov-Frantskevich, G. I., Koshlyakov, M. N., Fedorov, K. N., Fomin, L. M. and Yampol'skiy, A. D., "Some Results of a Hydrophysical Experiment in a Polygon in the Tropical Atlantic," IZV. AN SSSR: FIZIKA ATMOSFERY I OKEANA (News of the USSR Academy of Sciences: Physics of the Atmosphere and Ocean), 7, No 5, 1971.

4. Ozmidov, R. V., "Second Voyage of the Scientific Research Ship 'Dmitriy Mendeleyev'," OKEANOLOGIYA (Oceanology), 11, No 1, 1971.

5. Ozmidov, R. V., "Experimental Investigations of Microscale Ocean Turbulence at the Institute of Oceanology imeni P. P. Shirshov USSR Academy of Sciences," ISSLEDOVANIYE OKEANICHESKIY TURBULENTNOSTI (Investigation of Ocean Turbulence), Moscow, "Nauka," 1973.

6. Kraichnan, R. H., "Inertial Ranges in Two-Dimensional Turbulence," PHYS. FLUIDS, 10, No 4, 1967.

7. Batchelor, G. K., "Computation of the Energy Spectrum in Homogeneous Two-Dimensional Turbulence," PHYS. FLUIDS, Suppl. II, 12, No 12, 1969.

8. Belyayev, V. S., Gezentsvey, A. N., Lyubimtsev, M. M., Ozmidov, R. V., Paka, V. T. and Pozdynin, V. D., "Some Results of an Experimental Investigation of Fluctuations of Hydrophysical Fields in the Upper Layer of the Ocean," ISSLEDOVANIYE OKEANICHESKOY TURBULENTNOSTI, Moscow, "Nauka," 1973.

9. Monin, A. S., "Spectrum of Turbulence in a Temperature-Inhomogeneous Atmosphere," IZV. AN SSSR: SERIYA GEOFIZ. (News of the USSR Academy of Sciences: Geophysical Series), No 3, 1962.

10. Obukhov, A. M., "Influence of Archimedes Forces on the Structure of the Temperature Field in a Turbulent Flow," DOKL. AN SSSR, 125, No 6, 1959.

5303
CSO: 8144/1839

SPECTRAL CHARACTERISTICS OF CONDUCTIVITY FLUCTUATION FIELD IN OCEAN

Moscow ISSLEDOVANIYE IZMENCHIVOSTI GIDROFIZICHESKIKH POLEY V OKEANE in Russian 1974 pp 42-49

[Article by V. S. Belyayev, A. N. Gezentsvey and R. V. Ozmidov from monograph "Ocean Research on Hydrophysical Field Variability," edited by R. V. Ozmidov, doctor of physical and matnematical sciences, Izdatel'stvo "Nauka", 211 pages, number of copies printed unknown]

[Text] On the 7th voyage of the "Dmitriy Mendeleyev" specialists carried out numerous measurements of high-frequency fluctuations of the conductivity field in the upper 200-m layer in a number of polygons in the Indian Ocean (the location of the polygons was given in [1]). Data on microfluctuations of conductivity were obtained using low-inertia hydroresistor sensors with a radius of spatial averaging of about 1 mm. The sensors were placed ~~on a special~~ towed line whose description was given in [2].

On the voyage use was made of three sets of a towed measurement system which differ somewhat in design. Using one of the towed lines the measurements were made in polygons 2, 4, 6 and 8; the second towed line was used in polygons 3 and 5; and the third was employed in repeated measurements in polygon 6.

The high-frequency signals were registered on analog magnetic recorders. The signals were visualized on photopaper and after inspection of the records segments with a duration of about 1 minute were selected for processing on an electronic computer. With the input of analog signals into the electronic computer use was made of an analog-code converter which made the signals discrete in time and quantized them in amplitude. First the signals were passed through low-frequency filters with different cutoff frequencies for the purpose of decreasing the effect of discretization noise. The discretization frequency exceeded the filter cutoff frequency by a factor of approximately 3. In computing the spectral density E(f), where f is frequency, use was made of a fast Fourier transform program prepared at the Atlantic Division of the Institute of Oceanology. The program provided for the breakdown of the initial series into individual "pieces," the Fourier coefficients are computed for each of them, and the spectral densities are averaged for the entire length of the series (for n_1 "pieces") and for a stipulated frequency band (for n_2 points on the frequency axis). In the computations the equivalent number of degrees of freedom ν, evaluated using the formula $\nu \approx 2n_1n_2$, was not less than 100. This ensured a high statistical significance of the resulting spectral density evaluations.

Figures 1-7, at a bilogarithmic scale, represent the one-dimensional spectral densities of conductivity fluctuations in the 2d-6th and 8th polygons of the 7th voyage of the scientific research ship "Dmitriy Mendeleyev." The spectral curves in each figure are numbered in the order of an increase in the depth of measurement. The spectra for different nonoverlapping segments of the record at one and the same measurement horizon are noted by differer · letters. The conversion from the frequencies f to the wave numbers k was accomplished on the assumption of the correctness of the hypothesis of "frozen-in turbulence" using the formula $k = 2\pi f/V$, where V is the velocity of motion of the sensor relative to the medium at the measurement horizon. Accordingly, for scaling the function E(f) into the spectral density $E_1(k)$ use was made of the formula $E_1(k) = V/\pi E(f)$.

The range of wave numbers when computing $E_1(k)$ extended from $6.3 \cdot 10^{-2}$ to 6.7 cm^{-1}, which corresponds to the change in scales of inhomogeneities of the conductivity field from 0.9 cm to 1 m. The figures show that the spectral density values vary in a wide range. In the low-frequency region the $E_1(k)$ values in each of Figures 1-7 vary in the range from one to more than two orders of magnitude.

Measurements of conductivity fluctuations by means of a towed line of the first type in polygons 2, 4, 6 and 8 were carried out under different hydrological conditions and this evidently explains the difference in the levels and diversity of the shapes of the spectral curves in Figures 1-4. The values of the $E_1(k)$ spectra with $k = 10^0$ cm^{-1} vary by almost three orders of magnitude (from $\sim 2 \cdot 10^{-14}$ $ohm^{-2} \cdot cm^{-1}$ to $\sim 10^{-11}$ $ohm^{-2} \cdot cm^{-1}$). The straight lines approximating the $E_1(k)$ functions at a bilogarithmic scale have a different slope to the x-axis (the tangent of the curve slope varies in the range from -1.4 to -3).

Figure 1 shows the spectral curves (polygon 2) based on measurements in stratified layers with the values of the vertical gradient of current velocity (about 1.5 cm/sec/m) maximum for this polygon. The lower group of curves is approximated well by a straight line with the slope -5/3 and the upper curves 1b and 2a have a steeper dropoff with an increase in the wave numbers. It should be noted that the spectral curves for one and the same measurement horizon can differ appreciably from one another with respect to both level and shape, which can be related to a difference in local background conditions (processes determining the generation and attenuation of microscale turbulence).

The spectra of conductivity fluctuations in Fig. 2 (polygon 4) were obtained from measurements in a layer with a constant density gradient (curves 1-7) and in the quasihomogeneous layer (curves 8, 9). The current velocity vector in polygon 4 with an increase in depth (in the investigated layer of the ocean) rotates in a counterclockwise direction and decreases in value from 45 cm/sec at a depth of 50 cm to 20-30 cm/sec at a depth of 100-125 m. At depths of 50 and 125 m the current velocity vectors are directed in the opposite direction. The current velocity gradient in the polygon is governed for the most part by a change not in the modulus but the direction of the current velocity with depth. The $E_1(k)$ values in polygon 4 change in the widest limits (in comparison with polygons 2, 6, 8). With an increase in the level of the $E_1(k)$ curves the dropoff of the spectral functions with an increase in k on the average becomes steeper and the slope of the approximating straight lines increases from -5/3 (for curve 9a) to -3 (for curves 2c and

3). The spectral curves 8 and 9a, 9b fall in the lower part of the bundle of curves: this is evidently attributable to the fact that measurements 8 and 9 fall in the quasihomogeneous layer. The bundles of curves in Figures 1 and 2 when matched virtually fall on one another.

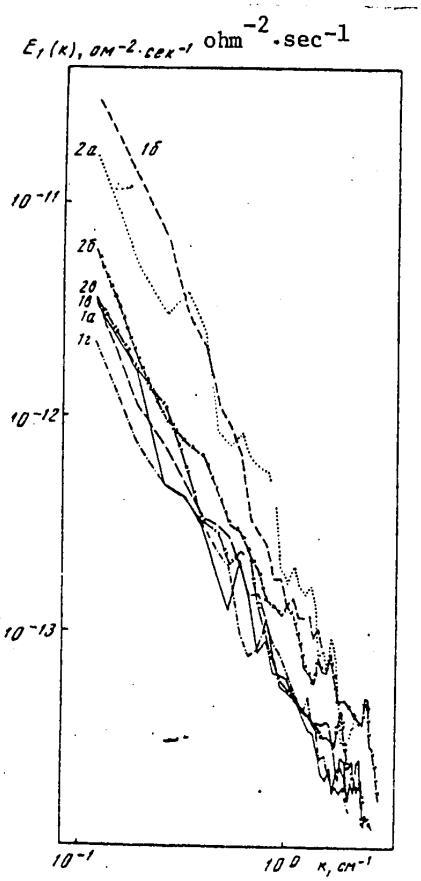

Fig. 1. Spectral densities of conductivity fluctuations in second polygon. Measurement horizons: 77 m (1a,b,c,d), 120 m (2a,b,c).

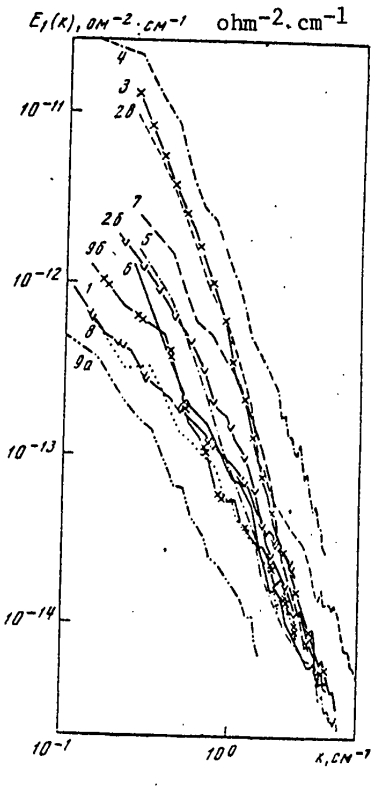

Fig. 2. Spectral densities of conductivity fluctuations in fourth polygon for horizons 49 (1), 60 (2b,2c), 65 (3), 67 (4), 70 (5), 75 (6), 80 (7), 103 (8), 120 m (9a, 9b).

In polygon 6 the measurements were made in the layer with a constant density gradient (curves 2-5) and at the upper (curve 1) and lower (curve 6) boundaries of this layer situated between the quasihomogeneous layers. The current velocity field has a complex vertical structure. The current velocity vector in the upper 75-m layer of the ocean rotates in a counterclockwise direction by the angle 3/4 and decreases in value from 95 cm/sec at a depth of 13 m to 35-40 cm/sec at a depth of 50-75 m and in the layer from 75 to 100 m rotates in a clockwise direction and decreases in value to 15 cm/sec. In the layer from 100 to 125 m there is a change in current direction to the opposite direction and at a depth of

125 m the velocity was close to 30 cm/sec. At a depth of 200 m the current velocity decreases to 10 cm/sec. The spectral curves in Fig. 3 form a dense group and fall somewhat above the curves in Figures 1 and 2. The $E_1(k)$ curves in Fig. 3 (except for 3, 4 and 5a) can be approximated by straight lines with a slope -5/3 and curves 3, 4 and 5a -- by straight lines with slopes -2 and -7/5. The good approximation of the curves 4 and 5a by straight lines with a slope -7/5 makes it possible to postulate a substantial influence of buoyancy forces on microscale turbulence in the ocean in a number of cases [3, 4].

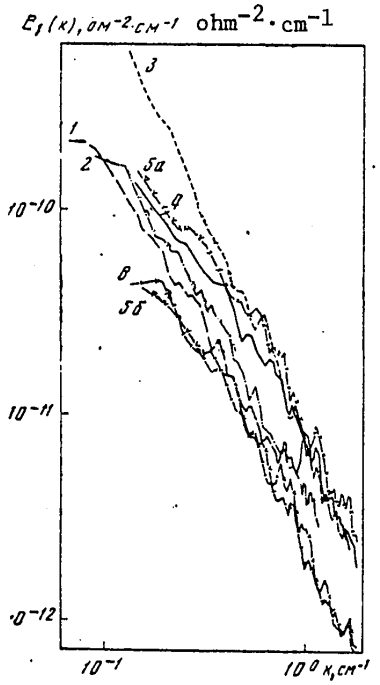

Fig. 3. Spectral densities of fluctuations of conductivity in sixth polygon for horizons 10 (1), 14 (2), 54 (3), 60 (4), 68 (5a, 5b), 89 m (6).

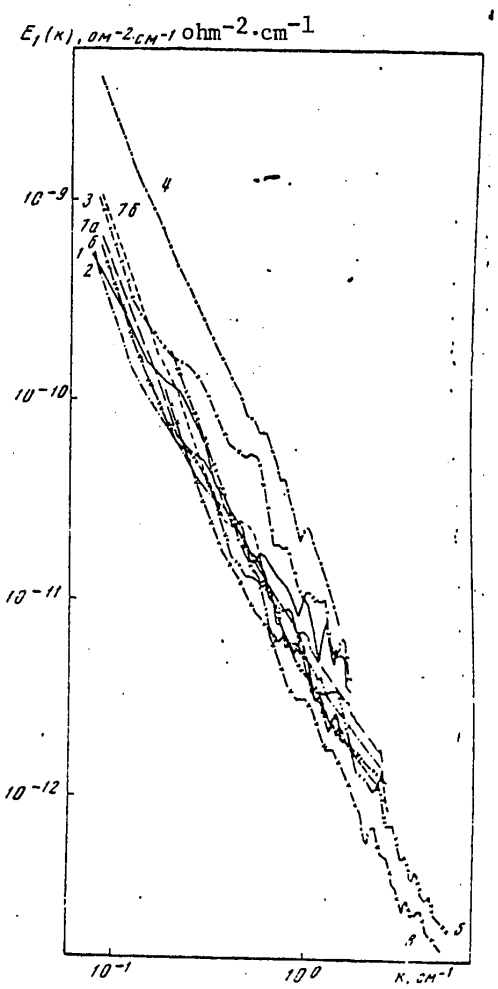

Fig. 4. Spectral densities of fluctuations of conductivity in eighth polygon for horizons 55 (1), 95 (2), 110 (3), 141 (4), 145 (5), 161 (6), 170 (7a, 7b), 175 m (8).

Figure 4 shows the spectral densities of conductivity fluctuations in polygon 8. The measurements were made in layers with different (different from zero) values of the density gradient (the maximum density gradient is at horizon 3). The measurements 4, 5 were made in the layer with a marked change in curvature

of the density profile. In the layer from 50 to 200 m in polygon 8 the direction of the flow changes by the angle $\sim\pi/4$; the current velocity vector below 75 m rotates is a clockwise direction, remaining unchanged in the layer 50-100 m ($\sim$55 cm/sec) and decreasing to 25 and 35 cm/sec respectively at depths of 125 and 200 m. The spectral curves in Fig. 4 form a relatively dense bundle and can be approximated at a bilogarithmic scale by straight lines with a slope close to -2. The bundles of $E_1(k)$ curves in Figures 4 and 3 are matched well with one another, except for curve 4 in Fig. 4.

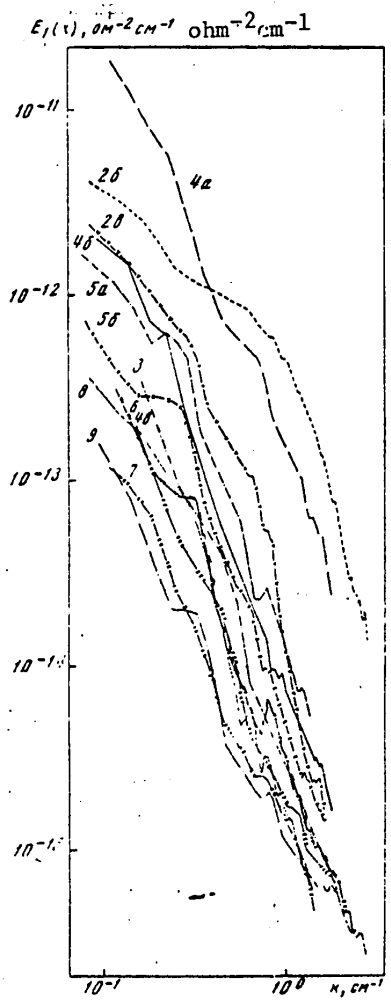

Fig. 5. Spectral densities of conductivity fluctuations in third polygon for horizons 35 (2b, 2c), 52 (3), 70 (4a,b,c), 72 (5a, 5b), 91 (6), 103 (7), 118 (8), 127 m (9).

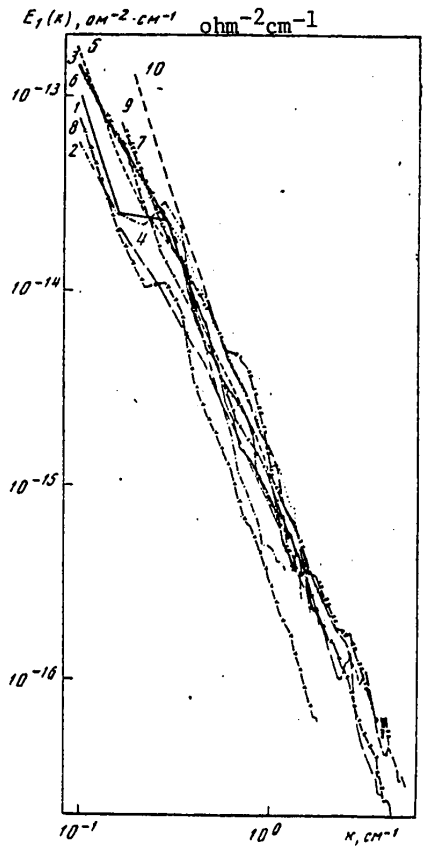

Fig. 6. Spectral densities of conductivity fluctuations in fifth polygon for horizons 55 (1), 80 (2), 90 (3), 100 (4), 105 (5), 115 (6), 120 (7), 129 (8), 150 (9), 187 m (10).

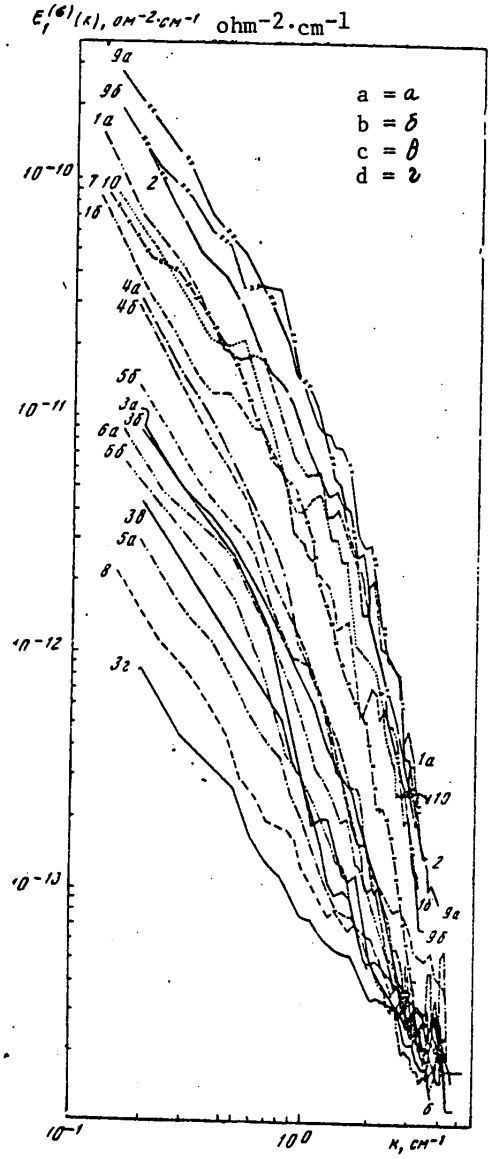

Fig. 7. Spectral densities of conductivity fluctuations according to repeated measurements in sixth polygon for horizons 23 (1a, 1b), 45 (2), 71 (3a,b,c,d), 75 (4a, 4b), 106 (5a, 5b), 125 (6a, 6b), 132 (7), 146 (8), 149 (9a, 9b), 217 m (10).

In polygon 3 the measurements were made by the second towed line in the layer from 35 to 127 m with a variable (nonzero) value of the density gradient. The current velocity vector in the upper 150-m layer has a value 20-25 cm/sec and varies in direction. The level of the $E_1(k)$ spectral curves in polygon 3 (Fig. 5) varies in a very broad range (by almost three orders of magnitude with $k = 10^0$ cm^{-1}). Some of the curves in Fig. 5 can be approximated in the entire investigated range of scales by straight lines (with a slope -2 for curves 7, 9 and with a slope for the other curves somewhat greater in absolute value). However, most of the curves in Fig. 5 are approximated by straight lines only in individual small segments; with an increase in k the slope of the $E_1(k)$ curves increases.

In polygon 5 the measurements were made in the layer from 55 to 187 m with different values of the density gradient (measurements 3-8 were made in a clearly expressed density jump layer and measurements 9, 10 in the quasihomogeneous layer). The current velocity field in the considered layer has a relatively complex vertical structure: the current velocity vector changes in value from 40 to 10 cm/sec with a change of direction within the limits of the angle 3/4 π. The $E_1(k)$ spectral curves in polygon 5 (Fig. 6) form a dense bundle which lies below the bundle of curves in Fig. 5. All the curves in Fig. 6 can be approximated by straight lines with slopes in absolute value somewhat greater than 2 (only the straight line approximating curve 10 has a greater slope, close to -3).

The measurements of high-frequency conductivity fluctuations in polygon 6 were made using towed lines of two types and an interval between measurements of 1 day. Repeated measurements were made in the layer from 23 to 217 m with different

density gradient values. The complex vertical structure of the velocity field in the polygon was described above. The "fan" of curves in Fig. 7 graphically illustrates the possibility of a great variability of the characteristics of microscale fluctuations of conductivity in the upper layer of the ocean. The spectral density of conductivity fluctuations $E_1(k)$ with some values of the wave numbers varies in polygon 6 by more than three orders of magnitude. The spectral curves in Fig. 7 in the low-frequency region can be approximated by straight lines with the slope -7/5 (for the lower curves) and -5/3 (for the upper curves). The spectral curves in Figures 3 and 5 agree quite well with one another, which makes it possible to consider the results of the measurements using different towed lines to be representative.

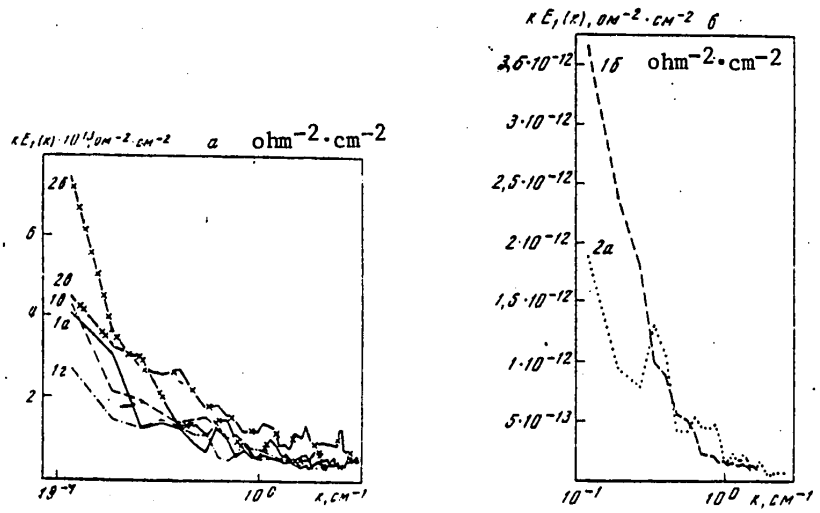

Fig. 8. Distribution of intensity of conductivity fluctuations in wave number spectrum in second polygon. Notations are the same as in Fig. 1.

Using the records of conductivity fluctuations obtained in the polygons we also computed the $kE_1(k)$ and $k^2E_1(k)$ functions. The $kE_1(k)$ curves at a semilogarithmic scale graphically show the distribution of the intensity of conductivity fluctuations in the wave number spectrum. The rate of evening-out of inhomogeneities in the conductivity field in an isotropic case is proportional to the area under the $k^2E_1(k)$ curve (in ordinary coordinates) and therefore the $k^2E_1(k)$ spectra can be arbitrarily called "dissipation" spectra.

As an example, Figures 8-11 show the spectral functions $kE_1(k)$ and the dissipation spectra for the conductivity field $k^2E_1(k)$ for polygons 2 and 6. In most cases the $kE_1(k)$ curves in all the polygons almost monotonically increase with a decrease in the wave numbers k (with an increase in the scales of the inhomogeneities). At individual horizons the $kE_1(k)$ curves with a decrease in k attain a maximum (for example, curves 1, 2, 5b, 6 in Fig. 10) and it can be assumed that in these cases there are processes of generation of inhomogeneities in the conductivity field with scales of several tens of centimeters. The "dissipation" spectra are very jagged and as a rule do not attain maxima in the investigated wave number range. An exception are the $k^2E_1(k)$ spectra for polygon 6 (according to

repeated measurements), most of which have maxima in the range of scales from 5 to 15 cm.

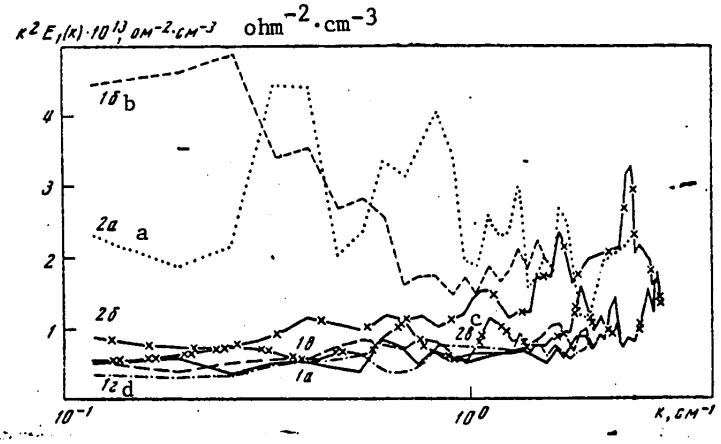

Fig. 9. "Dissipation" spectra of conductivity fluctuations in second polygon. The notations are the same as in Fig. 1.

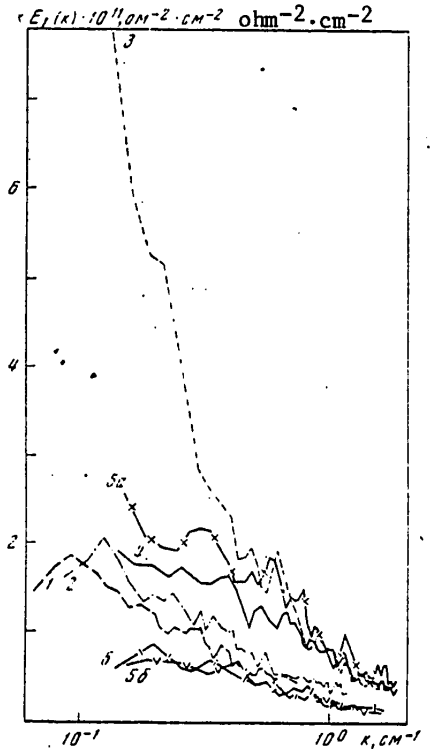

Fig. 10. Distribution of intensity of conductivity fluctuations in wave number spectrum in sixth polygon. Notations are the same as in Fig. 3.

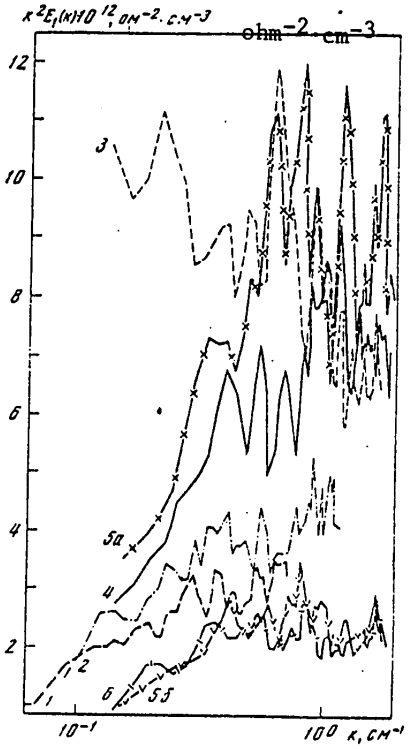

Fig. 11. "Dissipation" spectra of conductivity fluctuations in sixth polygon. Notations are the same as in Fig. 3.

Thus, the spectral characteristics of conductivity fluctuations in the upper layer of the ocean were extremely variable not only with substantially different macroscale hydrological conditions (in the case of interpolygon comparison), but also in the case of measurements at one and the same depth (or near depths) within the limits of an individual polygon, where the macroscale "background" conditions must be considered identical. In the generation of microscale turbulence an important role should evidently be played by mesoscale processes (with scales up to several meters). Accordingly, measurements of microfluctuations of hydrophysical fields must be accompanied by the registry of local background conditions (local mesostructure of hydrophysical fields). The spectral characteristics of microfluctuations of conductivity (level of the spectral curves and their shape) do not reveal a monotonic change with depth in any of the polygons. The $k^2E_1(k)$ dissipation spectra in the range of scales from 0.9 cm to 1 m do not have maxima. Evidently, the diversity of forms and levels of the spectral functions of conductivity fluctuations in the ocean indicates the existence of different mechanisms of their generation and attenuation. Among such mechanisms a major role can be played by buoyancy forces, local current velocity gradients, caused, for example, by high-frequency internal waves. The steep slopes of the $E_1(k)$ functions which we observed in some cases are also possibly attributable to the latter.

BIBLIOGRAPHY

1. Ozmidov, R. V., "Experimental Investigations of Microscale Oceanic Turbulence at the Institute of Oceanology imeni P. P. Shirshov USSR Academy of Sciences," ISSLEDOVANIYE OKEANICHESKOY TURBULENTNOSTI (Investigation of Oceanic Turbulence), Moscow, "Nauka," 1973.

2. Paka, V. T., "Complex Measurements of Physical Fields in the Ocean in a Towing Regime," AVTOMATIZATSIYA NAUCHNYKH ISSLEDOVANIY MOREY I OKEANOV (Automation of Scientific Investigations of Seas and Oceans), Part I, Sevastopol', Izd. MGI AN Ukrainian SSR, 1972.

3. Bolgiano, R., "Turbulent Spectra in a Stably Stratified Atmosphere," J. GEOPHYS. RES., 64, No 12, 1959.

4. Monin, A. S., "On the Turbulence Spectrum in a Temperature Inhomogeneous Atmosphere," IZV. AN SSSR: SERIYA GEOFIZ. (News of the USSR Academy of Sciences: Geophysical Series), No 3, 1962.

5303
CSO: 8144/1839

STATISTICAL EVALUATIONS OF PARAMETERS OF SMALL-SCALE TURBULENCE

Moscow ISSLEDOVANIYE IZMENCHIVOSTI GIDROFIZICHESKIKH POLEY V OKEANE in Russian 1974 pp 50-60

[Article by V. D. Pozdynin from monograph "Ocean Research on Hydrophysical Field Variability," edited by R. V. Ozmidov, doctor of physical and mathematical sciences, Izdatel'stvo "Nauka", 211 pages, number of copies unknown]

[Text] The expeditionary investigations of microscale turbulence undertaken during 1969-1972 by the Institute of Oceanology imeni P. P. Shirshov USSR Academy of Sciences yielded a considerable volume of empirical data making it possible to employ different mathematical processing methods for its study. In particular, the purpose of this study was obtaining a series of statistical evaluations of some parameters of microscale turbulence and also the degree of their variability in a horizontal direction and with depth.

Measurements of microscale turbulence carried out on the 9th voyage of the "Akademik Kurchatov" (1970-1971) in the Atlantic Ocean made it possible to give statisistical evaluations of its external and internal horizontal scales, energy level, rate of energy dissipation, coefficient of relative variability and other parameters.

The measurement method also provided means for collecting data which would be suitable for clarifications of the statistical uniformity of evaluations of the measured characteristics at one and the same depth and at different depths. For this purpose the unit for measuring turbulence was towed behind the ship in different directions or was lowered on a single run to a limiting depth of submergence with holding each 10-15 m for making turbulence measurements.

Interest in the statistical uniformity of empirical evaluations of different turbulence parameters was dictated by the following considerations. The diversity of the possible mechanisms of generation of microscale turbulence in a general case should give rise to some aging and spatial diversity of their evaluations, and in

particular, statistically significant differences between them. The detection of the latter at some measurement horizon could serve as an indication of the depths and water layers where investigations of differences in the mechanisms of generation of turbulence would be most successful. On the other hand, the absence of statistically significant differences in evaluations of turbulence parameters at a number of depths would indicate a statistical uniformity of the vertical structure of turbulence in the investigated water layer.

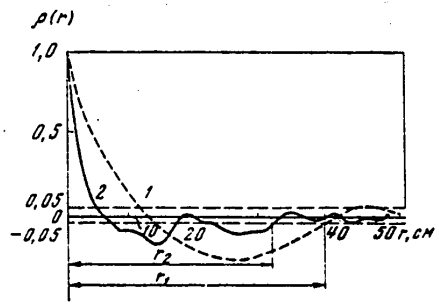

Fig. 1. Determination of limiting correlation radius $r_{0.05}$; r_1, r_2 correspond to the correlation functions 1, 2.

Measurements of fluctuations of current velocity were subjected to statistical processing. These measurements were made in three polygons on the 9th voyage of the scientific research ship "Akademik Kurchatov" situated in ocean regions with the coordinates 29°30'S, 46°W -- fifth polygon, 23°0'S, 36°0'W -- sixth polygon and 0°0'S, 24°0'W -- seventh polygon.

We note at once that all the procedures for the statistical processing of data are based on assumptions concerning the adequacy of microscale oceanic turbulence to the normal random process and the possibility of use of some formulas of isotropic turbulence for carrying out the necessary computations. In order to simplify the processing of the mass of measurement data the computation of the external turbulence scale was replaced by a determination of the limiting correlation radius; by the latter is meant the distance in which the correlation between the two ordinates of the process does not exceed 0.05. A graphic method for determining the limiting correlation radius from the graph of the normalized correlation function is shown in Fig. 1. From the limiting correlation radius we found the number of independent measurements in the record

$$n = T/r_{0.05}, \qquad (1)$$

where T is the length of the record, n is the number of independent measurements, $r_{0.05}$ is the limiting correlation radius.

The n value makes it possible to use different statistical criteria and evaluations in an investigation of the parameters of ocean turbulence. The computation of the mean values, dispersions and other statistical characteristics was carried out using known formulas and in accordance with the recommendations set forth in [1]. In Tables 1, 3, 5 and 6 cited below the first column gives the depth at which

turbulence was measured; the second column gives the number of independent measurements n: for some parameters this is the number of records, for others it is the number of independent measurements in the record multiplied by the number of records; the third and fourth columns give sample evaluations of the mean values of the parameter ($\bar{X}$) and their standard deviations ($S_{\bar{X}}$); the fifth column gives the standard deviation of an individual measurement (S); the sixth column gives the 95% confidence intervals for $\bar{X}$ and S (in Table 5 there is no second confidence interval); the seventh column gives the coefficient of relative variability computed using the formula $q = S/\bar{X}^*$.

Table 1 gives the results of statistical processing of material characterizing the limiting horizontal correlation radius $r_{0.05}$ of microscale turbulence in the polygons. The table shows that the evaluations of the mean limiting correlation radii have appreciable differences. The statistical significance of these differences was investigated using dispersion analysis [1]. In the fifth and sixth polygons these differences at the 0.05 level were insignificant. In the seventh, at the two lower horizons $r_{0.05}$ had statistically significant differences from $r_{0.05}$ at the above-lying horizons.

Table 1

Statistical Characteristics of Limiting Correlation Radius $r_{0.05}$

Depth, m	n	$\bar{r}_{0,05}$, cm	$S_{\bar{r}}$, cm	S, cm	95% confidence interval for $\bar{r}_{0.05}$	95% confidence interval for S	q
			Fifth polygon				
30	5	69	11	25	38—100	15—72	0,36
40	9	57	4	11	48—66	7—21	0,19
50	3	36	5	9	15—58	5—56	0,25
60	5	55	8	18	33—77	11—52	0,33
70	5	39	4	9	30—50	5—26	0,22
80	5	50	14	30	11—89	18—86	0,61
87	5	43	6	13	26—60	8—37	0,31
			Sixth polygon				
30	10	35	2	7	31—40	5—13	0,20
40	14	41	3	11	35—48	8—17	0,27
50	16	41	2	6	37—45	4—9	0,15
60	12	39	2	6	35—43	4—11	0,17
77	8	37	2	5	32—42	3—10	0,14
			Seventh polygon				
36	5	41	1	2	38—44	1—6	0,04
52	5	35	1	6	32—38	4—17	0,17
73	6	40	2	5	37—43	3—12	0,14
90	6	36	2	6	33—39	4—15	0,16
110	6	33	2	4	30—36	2—10	0,11
140	3	51	1	2	47—55	1—12	0,05

* In Tables 1, 2, 3 and 5 $\bar{X}$ and S are given rounded-off and therefore the q values computed from them can differ somewhat from the values given in the seventh column of these tables.

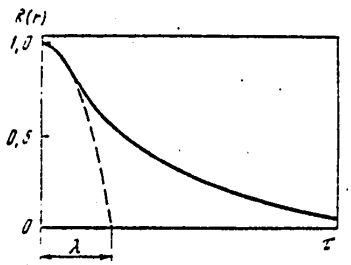

Fig. 2. Determination of turbulence microscale λ.

Thus, in each polygon in the water layer from 30 to 80-90 m depth at the limiting horizontal dimensions of the turbulent disturbances there was a statistically homogeneous structure with depth; for these layers we obtained the following mean values of the limiting correlation radii: 50 cm in the fifth polygon, 39 cm in the sixth polygon and 38 cm in the seventh polygon. We note that the same uniformity in depth was also characteristic of the temperature field.

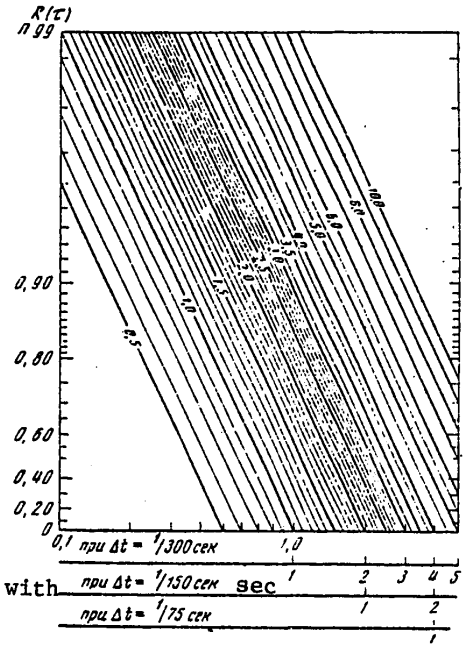

Fig. 3. Nomogram for determining microscale by graphic method.

The processing of synchronous measurements of temperature fluctuations, carried out at the same point with measurements of velocity fluctuations in the sixth polygon, revealed a surprising uniformity of the mean $r_{0.05}$ values at all measurement horizons:

Depth, m	30	40	50	60	77
$r_{0.05}$, cm	73	75	72	74	74

Table 2

Results of Dispersion Analysis of Variability of Limiting Correlation Radius

Variability $r_{0.05}$, cm	Depth of upper and lower boundaries of statistically homogeneous layer, m		
	30-87[1*]	30-77[2*]	36-90[3*]
At one depth	18	8	6
Between depths	8	1	2

1* Fifth polygon. 2* Sixth polygon. 3* Seventh polygon.

It is interesting to note that the limiting horizontal radius of the temperature inhomogeneities in this polygon was almost twice as great as the radius in the field of velocity fluctuations.

In the table the variability is represented by evaluations of the standard deviations of individual values of the correlation radius from their mean values.

The data in the table show that in all the polygons the horizontal variability exceeded the variability with depth; the variability in the fifth polygon was appreciably greater than in the other two, where it can be considered identical.

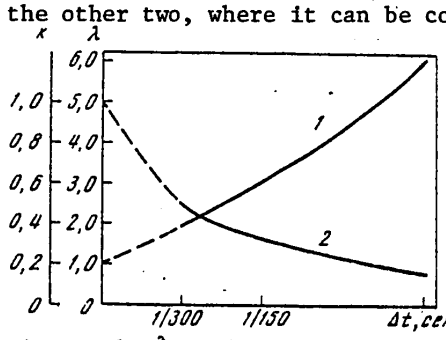

sec

Fig. 4. Dependence of microscale λ and coefficient k on discreteness of measurements.

As a result of statistical processing we determined the internal scale of turbulence λ or the Taylor microscale. It was also determined by a graphic method whose essence is the construction of a parabola conjugate with the correlation function curve (Fig. 2) [3].

In the mass processing of material it is more convenient to couple the correlation function with the parabola. For this it is necessary to construct the nomogram illustrated in Fig. 3, which represents the set of necessary parabolas. On the vertical axis of the nomogram we have plotted the y-scale of the normalized correlation function, and on the horizontal scale the scale of distances covered by the turbulence measuring instrument relative to the water. The family of parabolas is marked with the corresponding microscale values in centimeters. For determining the microscale the initial points of the correlation function curve are plotted on the nomogram and are joined by a smooth line to its juncture with the corresponding parabola.

The influence exerted on the microscale of inaccuracies in joining of the correlation function curve with the parabola, associated with the relatively great discreteness of data taken for computing the correlation function, was excluded by means of the following procedure. On the basis of the correlation functions, computed using one and the same record, but with a discreteness of the readings of 1/300, 1/150 and 1/75 sec, we determined the corresponding values of the microscales. The averaged data from these computations were used in constructing curve 1 in Fig. 4. The left end of the curve, represented by a dashed line, is the result of extrapolation of the resulting dependence for a discreteness of readings of less than 1/300 sec. The equivalence of microscales for a discreteness of initial data of 1/300, 1/150 and 1/75 sec was attained by scaling using the formula

$$\lambda_0 = k\lambda,$$

where k is the proportionality factor; λ is a microscale determined with the discreteness Δt; λ_0 is the value of the microscale corresponding to the continuous registry of initial data used as the final result of processing. The dependence of the k coefficient on the discreteness of readings is illustrated by curve 2 in Fig. 4. This curve was constructed using the very same data as curve 1.

Table 3

Statistical Characteristics of Internal Turbulence Scale (Taylor Microscale) λ_0

Depth m	n	$\bar{\lambda}_0$, cm	$\sigma_{\bar{\lambda}}$, cm	S, cm	95% confidence interval for $\bar{\lambda}_0$	95% confidence interval for S	q
Fifth polygon							
30	10	1,8	0,1	0,4	1,5—2,1	0,28—0,73	0,22
40	17	1,1	0,1	0,4	0,9—1,3	0,30—0,59	0,36
50	8	1,1	0,1	0,2	0,9—1,3	0,13—0,41	0,18
60	12	1,9	0,1	0,4	1,6—2,2	0,28—0,72	0,21
70	7	1,0	0,0	0,1	0,9—1,1	0,06—0,22	0,10
80	8	1,1	0,1	0,2	0,9—1,2	0,13—0,41	0,18
87	11	1,3	0,2	0,5	1,0—1,6	0,34—0,91	0,38
Sixth polygon							
30	10	0,8	0,02	0,08	0,8—0,9	0,05—0,14	0,10
40	16	0,8	0,04	0,15	0,8—0,9	0,11—0,24	0,20
50	10	1,0	0,05	0,16	0,9—1,1	0,11—0,29	0,17
60	10	1,4	0,10	0,32	1,2—1,6	0,22—0,58	0,23
77	8	1,2	0,02	0,05	1,1—1,2	0,03—0,10	0,04
Seventh polygon							
36	7	1,0	0,0	0,1	0,8—1,1	0,06—0,22	0,14
52	7	0,8	0,1	0,2	0,7—1,0	0,13—0,44	0,17
73	8	0,9	0,0	0,2	0,8—1,0	0,13—0,41	0,15
90	10	0,8	0,0	0,1	0,7—0,9	0,07—0,18	0,10
110	8	0,9	0,0	0,1	0,8—0,9	0,06—0,20	0,08
140	4	1,6	0,1	0,2	1,2—2,0	0,11—0,74	0,15

Table 3 gives the results of statistical processing of measurements in polygons characterizing the internal scale of oceanic turbulence.

The statistical significance of the differences in evaluations of the mean values of the microscales at different depths was checked using dispersion analysis. The analysis indicated that with a significance level 0.05 in the fifth polygon there were two statistically significant microscales: 1.8 cm at depths of 30 and 60 m and 1.1 cm in the layer 40-90 m (excluding a depth of 60 m); in the sixth polygon there were also two: 0.8 cm in the layer 30-50 m depth and 1.3 cm in the layer 60-77 m. In the seventh polygon the statistical uniformity of the microscale was noted in the layer from 30 to 110 m with a mean value 0.9 cm; at a depth of 140 m the microscale differed significantly from this value and was equal to 1.6 cm.

According to data from dispersion analysis, the variability of the microscale at one and the same depth and between depths (in the evaluations of the standard deviations) is characterized by the figures cited in Table 4.

The results of the statistical processing show that the internal scale of oceanic turbulence can retain statistical uniformity in depth over the extent of several tens of meters.

The processing of data on the energy level of microscale turbulence in the polygons was also carried out with computation of the information not only on the mean and extremal values of this parameter, but also on the degree of statistical uniformity of its empirical evaluations at the same depth and between depths.

Table 4

Results of Dispersion Analysis of Variability of Taylor Microscale

Polygon	In entire investigated water layer, cm		In layer with statistically homogeneous evaluations in depth, cm
	at one depth	between depths	between depths
5	0.35	0.36	0.00
6	0.14	0.07	0.03
7	0.14	0.24	0.06

Table 5

Statistical Characteristics of Energy Level for Microscale Turbulence

Depth m	n	$\overline{u'^2}$, cm^2/sec^2	S, cm^2/sec^2	*	q
			Fifth polygon		
30	80	1,01	0,41	0,79—1,49	0,41
40	160	0,67	0,26	0,55—0,88	0,39
50	72	0,49	0,20	0,37—0,66	0,41
	72	13,43	9,74	9,73—19,18	0,67
60	80	7,16	2,8	5,38—10,05	0,39
70	115	18,72	8,9	14,67—25,50	0,48
80	80	7,13	3,6	5,24— 9,86	0,50
87	105	22,0	8,76	17,05—29,48	0,40
			Sixth polygon		
30	280	5,80	1,79	4,75—7,07	0,31
40	288	0,80	0,26	0,66—0,98	0,32
	120	3,41	1,22	2,66—4,16	0,36
50	360	1,37	0,54	1,14—1,72	0,31
	48	4,25	1,36	2,96—6,55	0,32
60	208	0,69	0,30	0,58—0,85	0,43
	52	2,24	0,93	1,54—3,42	0,41
77	216	0,97	0,28	0,79—1,16	0,29
			Seventh polygon		
36	245	1,34	0,32	1,08—1,59	0,24
52	285	1,86	0,42	1,56—2,31	0,23
73	250	0,61	0,37	0,50—0,74	0,61
90	336	1,49	0,40	1,23—1,82	0,27
110	336	1,31	0,33	1,08—1,59	0,25
140	78	0,62	0,22	0,46—0,86	0,35

*95% confidence interval for mean energy level, cm^2/sec^2

The evaluations of the mean squares of the amplitudes of current velocity obtained at a single depth were subjected to checking for statistical homogeneity using the Cochran tests [1]. A detailed exposition of the procedure for applying the Cochran tests, and also some of the results of the processing are given in [2]. More complete results of the processing are given in Table 5.

In particular, in the sixth polygon more detailed data were obtained on statistically significant differences in the turbulence levels at depths from 40 to 60 m. On the basis of the results of measurements at three horizons, 40, 50, 60 m, using the Cochrane test, it was possible to discriminate two statistically significant turbulence levels (this was also recorded at a depth of 50 m in the fifth polygon). The differences in the levels were reflected in a similar way in the values of their mean square fluctuation amplitudes.

With all the diversity of evaluations of the mean turbulence levels indicated in Table 5 it is nevertheless possible to see a definite tendency to their changes with depth: in the fifth polygon the level increased with depth, in the sixth polygon it decreased, in the seventh it varied around some mean value. The statistical significance of changes in level with depth was investigated using the Bartlett test [1], which was usually employed in checking the hypothesis of an equality of the series of sample dispersions with unequal numbers of measurements in the samples.

If the empirical value of the test with a significance level 0.05 was less than its tabulated value, the assumption of an equality of the energy levels at comparable depths was regarded as noncontradicting the measurement data; the turbulence level at these depths was considered identical and its value was computed as the mean of the compared levels. However, if the empirical value of the test exceeded the tabulated value, this gave basis for assuming a nonrandom nature of the differences between the compared levels. Such a result of this checking was of great importance for a subsequent analysis of the material: precisely in these cases it was necessary to carry out a comparison of the different levels with the hydrological conditions corresponding to them or the values of individual hydrological factors. Otherwise the established dependences between the hydrological factors and the turbulence level could be random and would not be confirmed in subsequent measurements. In the light of the results obtained using the Bartlett test the vertical energy structure of turbulence in the polygons is represented in the following form.

Fifth polygon. At a depth of 30 m turbulence had the level 1.01 cm^2/sec^2. Then, in the range of depths 40-50 m the level was 0.61 cm^2/sec^2. However, at a depth of 50 m there was turbulence of a greater intensity -- 18.59 $cm^2 \cdot sec^2$. This same level was observed at depths of 70 and 87 m. The turbulence level at depths of 60 and 80 m was 7.14 cm^2/sec^2.

Thus, in the fifth polygon there was a total of four statistically significant turbulence levels. Their depth positioning was governed by the well-expressed stratification of the energy structure of turbulence. Accordingly, layers were determined which should be used in comparing hydrological factors with evaluations of the turbulence level in the search for relationships between them.

Sixth polygon. In this polygon there were four statistically significant levels: 5.80 cm^2/sec^2 at a depth of 30 m, 3.21 cm^2/sec^2 at depths of 40, 50 and 60 m, 1.37 cm^2/sec^2 at a depth of 50 m and 0.82 cm^2/sec^2 at depths of 40, 60 and 77 m. Of the two levels existing at the horizons 40, 50 and 60 m the higher was characteristic for the entire layer from 40 to 60 m, whereas the second, lower level, was observed only at depths of 40 and 60 m and then was repeated at a depth of 77 m.

Seventh polygon. The vertical energy structure of turbulence in this polygon was characterized by three statistically significant levels. In the upper homogeneous layer of the ocean, at a depth of 36 m, and also in the water temperature and density jump layer, at depths 90 and 110 m, the turbulence level was identical -- 1.38 cm^2/sec^2. The highest level 1.86 cm^2/sec^2 related to the depth 52 m; the lowest -- 0.62 cm^2/sec^2 -- was at the depths 73 and 140 m.

The evaluations of the mean square of the amplitudes of current velocity fluctuations $\overline{u'^2}$ and the internal turbulence scale λ_0 were used in computing the rate of dissipation of turbulent energy ε using the formula

$$\varepsilon = 15\nu \frac{\overline{u'^2}}{\lambda_0^2}, \tag{2}$$

where ν is water viscosity [3]

The determination of ε using this formula requires a high accuracy in measuring the initial data, as is easily confirmed, inspecting formula (3), which is used in computing the relative mean square error in the rate of dissipation δ_ε :

$$\delta_\varepsilon \doteq 2\sqrt{\delta_u^2 + \delta_\lambda^2 + \frac{1}{4}\delta_\nu^2}, \tag{3}$$

where δ_u, δ_λ and δ_ν are the relative mean square errors in the amplitudes of velocity fluctuations, turbulence microscale and water viscosity respectively.

With existing measurement techniques, even under the most favorable conditions the error in determining ε using formula (2) will nevertheless be about 20%. Accordingly, it was of definite interest, prior to proceeding to large-scale computations on the basis of formula (2), to compare the results of computations using this formula with the results of determination of ε by other methods. Such a possibility appeared due to the computations of ε made by V. S. Belyayev, M. M. Lyubimtsev and R. V. Ozmidov [4] on the basis of measurements made in the seventh polygon. The rate of dissipation of turbulent energy was computed by these authors using the formula

$$\varepsilon = \frac{15\nu}{V^2}\overline{\left[\frac{\partial u'}{\partial t}\right]^2}, \tag{4}$$

where V is the rate of towing of the instrument relative to the water, and using the universal curve for the spectral density of the energy of velocity fluctuations [5].

The results of determination of ε by the three indicated methods are shown graphically in Fig. 5. Curve 1 corresponds to computations of ε using formula (2), curve 2 corresponds to computations made employing the universal curve and curve 3

corresponds to computations using formula (4). When using formula (2) the dissipation rates were maximum and when using formula (4) they were minimum. The shape of the curves based on formula (2) and the universal curve agrees well, which, in particular, is determined by the insignificance of the fluctuations of the differences between the dissipation rates computed by these two methods. However, the discrepancies with the results of computations using formula (4) are unstable in value and vary in a considerable range. With an unknown absolute accuracy in determining ε by the considered methods the first two seem of equal value, and indeed, preferable. Accordingly, at the present time the carrying out of large-scale computations on the basis of formula (2) seems entirely feasible.

Table 6

Statistical Characteristics of Rate of Dissipation of Turbulent Energy ε

Depth, m	n	$\bar{\varepsilon}$, $\frac{cm^2}{sec^3}$	$S_{\bar{\varepsilon}}$, $\frac{cm^2}{sec^3}$	S, $\frac{cm^2}{sec^3}$	95% confidence interval for $\bar{\varepsilon}$	95% confidence interval for S	q
			Fifth polygon				
30	4	0,07	0,00	0,01	0,05—0,09	0,00—0,04	0,20
40	9	0,09	0,03	0,09	0,03—0,15	0,07—0,14	1,0
50	8	1,63	0,70	2,04	0,02—3,22	1,35—4,15	1,26
60	7	0,55	0,17	0,44	0,13—0,97	0,28—0,97	0,80
70	7	3,93	0,45	1,20	2,83—5,03	0,77—2,64	0,30
80	8	1,41	0,33	0,93	0,63—2,19	0,61—1,89	0,66
87	5	6,74	1,39	3,12	2,88—10,60	1,87—8,97	0,46
			Sixth polygon				
30	9	1,22	0,14	0,46	0,90—1,54	0,31—0,88	0,38
40	15	0,82	0,11	0,43	0,58—1,06	0,31—0,68	0,52
50	10	0,29	0,07	0,22	0,13—0,45	0,15—0,40	0,76
60	10	0,09	0,02	0,05	0,05—0,13	0,03—0,09	0,56
77	8	0,11	0,01	0,03	0,02—0,73	0,02—0,06	0,27
			Seventh polygon				
36	7	0,24	0,04	0,12	0,14—0,34	0,08—0,26	0,50
52	7	0,36	0,08	0,21	0,26—0,66	0,14—0,46	0,36
73	8	0,18	0,04	0,10	0,08—0,28	0,07—0,20	0,56
90	9	0,43	0,06	0,18	0,29—0,57	0,12—0,34	0,42
110	8	0,34	0,02	0,05	0,29—0,39	0,03—0,10	0,17
140	4	0,08	0,02	0,05	0,02—0,14	0,03—0,19	0,58

The ε values computed using formula (2) for each depth had a great scatter and thus it was necessary to check them for statistical homogeneity. In the checking use was made of the Grubbs test [6], computed using the formulas

$$v_{emp} = \frac{x_{max} - \bar{X}}{S} \quad \text{or} \quad v_{emp} = \frac{\bar{X} - x_{min}}{S}, \tag{5}$$

where v_{emp} is the empirical value of the test, $\bar{X}$ is the mean sample to be checked, x_{min}, x_{max} are the extremal terms of the sample, S is the evaluation of the standard deviation, determined using this sample.

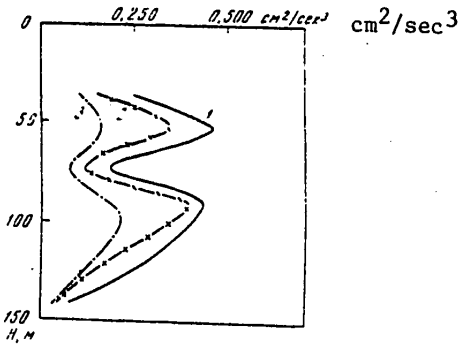

Fig. 5. Profiles of rate of dissipation of turbulent energy computed using formulas (2) and (4) and using universal curve.

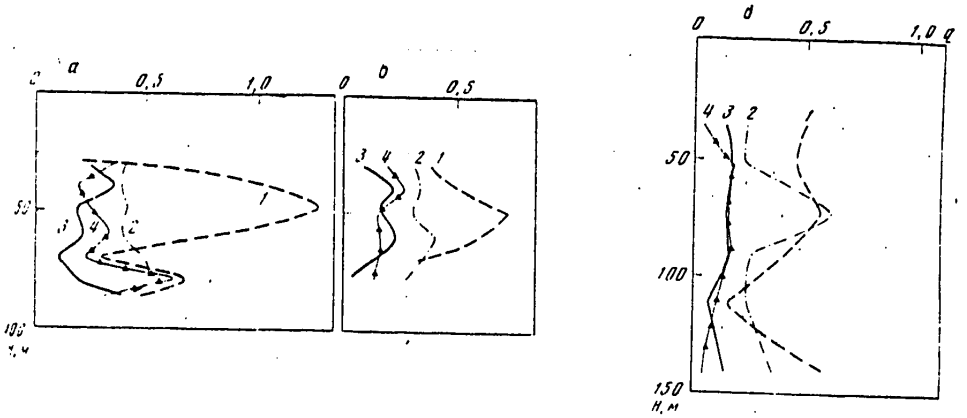

Fig. 6. Vertical profiles of coefficients of relative variability $r_{0.05}$, λ, $\overline{u'z'}$ and ε in fifth (a), sixth (b) and seventh (c) polygons.

Table 7

Results of Dispersion Analysis of Variability of ε Parameter

Polygon	Standard deviation, cm^2/sec^3	
	at one depth	between depths
5	1.33	2.13
6	0.44	0.12
7	0.14	0.12

The computed value of the test was compared with the tabulated v_T values corresponding to the significance level 0.01 and the number of terms in the sample. In the case of the inequality $v_{emp} > v_T$ the checked term of the sample was considered to belong to the other general set (to other conditions of the dissipation of turbulent energy) and excluded from consideration in this sample. However, despite expectations, only two ε values were excluded.

Table 6 gives the results of statistical processing of data on the rate of dissipation of turbulent energy in polygons.

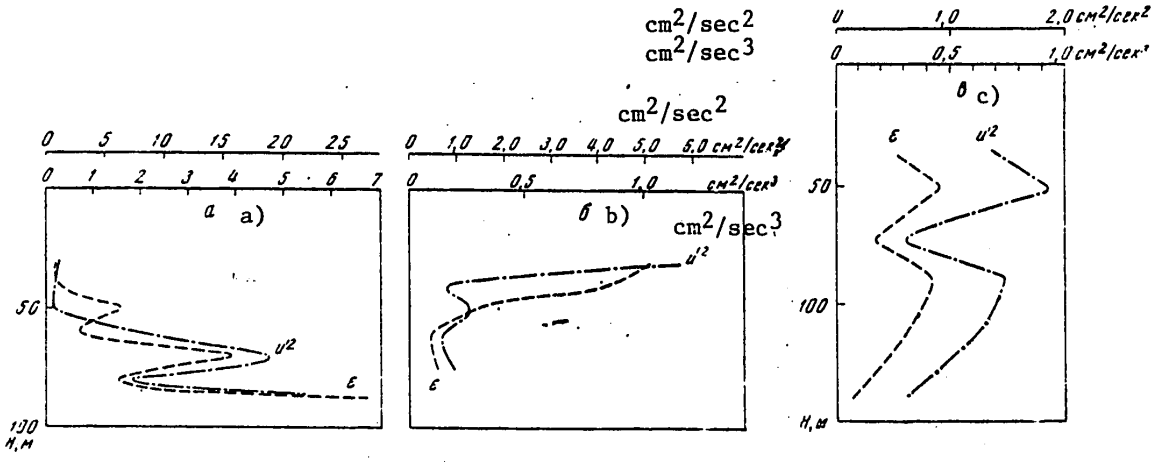

Fig. 7. Vertical profiles of $\overline{u'^2}$ and ε in fifth (a), sixth (b) and seventh (c) polygons.

It can be seen that the dissipation rates, even in the same polygon, varied with depth by an order of magnitude, and in one case, even two orders of magnitude (fifth polygon, depths 30, 87 m). With such a great vertical variability the statistical homogeneity of dissipation rates was observed only between individual layers, as, for example, at depths 30 and 40, 50 and 80 m in the fifth polygon, at depths of 60 and 77 m in the sixth polygon and at 52, 90 and 110 m in the seventh polygon. The variability of the dissipation rate at one and the same depth and between depths is characterized by the data in Table 7, in which we give evaluations of the corresponding standard deviations obtained by dispersion analysis.

The rate of dissipation of turbulent energy varied with depth differently in each polygon: in the fifth polygon it increased, in the sixth it decreased, in the seventh it varied, first increasing and then decreasing with depth.

A comparative analysis of the coefficients of relative variability $r_{0.05}$, λ_0, $\overline{u'^2}$ and ε revealed an interesting peculiarity in the structure of turbulence in the polygons: the relative variability of its energy parameters considerably exceeded the variability of its characteristic scales (assuming that the variability of the limiting correlation radius is identical with the variability of the external turbulence scale). Figure 6 shows the vertical profiles of the coefficients of relative variability in the fifth, sixth and seventh polygons. It can be seen from the relative positioning of these profiles that the greatest relative variability is for the dissipation rate (curve 1), then for the energy level (curve 2), and then

it is approximately identical for the microscale and the limiting correlation radius (curves 3 and 4). According to formula (2) the changes in the energy level and the turbulence microscale exert an identical (in absolute value) influence on changes in the dissipation rate. The absolute and relative variability of the microscale in the polygons was small: water layers with a thickness of tens of meters are characterized by the same microscale value but its relative variability in most cases did not exceed 20-30%. Thus, the change in the rate of dissipation was influenced to a considerable degree, apparently, by the energy level of turbulence due to its great spatial-temporal variability. A confirmation of this assumption may be the almost complete reproduction of the details of the vertical profile of the energy level of turbulence in the profile of the dissipation rate, especially in the fifth and seventh polygons (Fig. 7).

All the results of statistical processing cited above clarify the problem of the possible mean values of the individual characteristics of microscale turbulence in the ocean. However, the next step, a comparison of these data with the evaluations of hydrological factors obtained from measurements with existing standard instruments, once again has demonstrated the untenability of such attempts due to the extreme paucity of hydrological information. For example, the considerable spatial-temporal variability of turbulence characteristics observed in the fifth polygon found no explanation in the materials of background hydrological conditions obtained in the polygon using standard oceanological instruments.

Turbulence measurements relating to the equatorial current (seventh polygon) agree only partially with data on the hydrological conditions in this polygon, which were also determined using standard instruments. Thus, the insignificant spatial-temporal variability of the characteristics of turbulence along the flow can be attributed to the stability of current direction and velocity registered by BPV current meters installed on a buoy station in the polygon. But the absence of significant differences in turbulence levels, for example, at the depths 36, 90 m, was completely inexplicable.

According to hydrological data at a depth of 36 m there was a considerable vertical current gradient and a small vertical water density gradient, conditions favorable for the existence of a relatively high turbulence level. At a depth of 90 m, according to these same hydrological data, there was an opposite situation, and nevertheless in both cases the turbulence levels did not have statistically significant differences. Evidently some local details of the vertical structure of the density field could not be detected using the standard oceanological instruments employed.

In order to clarify such fine relationships and the dependences between the parameters of microscale turbulence, dynamic and thermal state of the investigated water layers it is necessary to have complexes of new oceanological instruments. Only with the availability of these instruments will the researcher be able to trace all the local changes in hydrological conditions from micro- to mesoscales inclusive.

BIBLIOGRAPHY

1. Dunin-Barkovskiy, I. V. and Smirnov, N. V., TEORIYA VEROYATNOSTEY I MATEMATICHESKAYA STATISTIKA V TEKHNIKE (Theory of Probabilities and Mathematical Statistics in Technology), Moscow, Gostekhizdat, 1955.

2. Khintse, I. O., TURBULENTNOST' (Turbulence), Moscow, Fizmatgiz, 1963.

3. Belyayev, V. S., Gezentsvey, A. N., Lyubimtsev, M. M., Ozmidov, R. V., Paka, V. T. and Pozdynin, V. D., "Some Results of an Experimental Investigation of Fluctuations of Hydrophysical Fields in the Upper Layer of the Ocean," ISSLEDOVANIYE OKEANICHESKOY TURBULENTNOSTI (Investigation of Oceanic Turbulence), Moscow, "Nauka," 1973.

4. Belyayev, V. S., Lyubimtsev, M. M. and Ozmidov, R. V., "Rate of Dissipation of Turbulent Energy and Rate of Evening-out of Temperature Nonuniformities in the Ocean," IZV. AN SSSR: FIZIKA ATMOSFERY I OKEANA (News of the USSR Academy of Sciences: Physics of the Atmosphere and Ocean), No 11, 1973.

5. Stewart, R. W. and Grant, H. L., "Determination of the Rate of Dissipation of Turbulent Energy Near the Sea Surface in the Presence of Waves," J. GEOPHYS. RES., 67, No 8, 1962.

6. Grubbs, --, "Sample Criteria for Testing Outlying Observations," ANN. MATH. STATISTICS, 21, No 1, 1950.

5303
CSO: 8144/1839

EXPERIENCE IN INVESTIGATING MICROSTRUCTURE OF OCEANIC CONDUCTIVITY FIELD BY SOUNDING METHOD

Moscow ISSLEDOVANIYE IZMENCHIVOSTI GIDROFIZICHESKIKH POLEY V OKEANE in Russian 1974 pp 61-65

[Article by V. P. Vorob'yev, N. N. Korchashkin and O. N. Nikolayev from monograph "Ocean Research on Hydrophysical Field Variability," edited by R. V. Ozmidov, doctor of physical and mathematical sciences, Izdatel'stvo "Nauka", 211 pages, number of copies printed unknown]

[Text] During recent years great interest has been manifested in study of the fine structure of hydrophysical fields in the ocean. Such investigations are being carried out using special sounding apparatus developed both in our country and abroad. The AIST probe, developed at the Institute of Oceanology imeni P. P. Shirshov, USSR Academy of Sciences [1], for example, as well as probes of the STD type [2], with a vertical resolution of about 1 m, have gained great reknown. The measurements which have been made using such instruments have substantially changed our ideas concerning the structure of hydrophysical fields in the ocean and the physical processes transpiring in it.

***

Numerous vertical sections of thermohaline fields which have been obtained by the use of sounding instruments have demonstrated that the vertical profiles of temperature and salinity in the ocean usually have a "stepped" structure which varies in time and in space. It was found that in the ocean there are thin interlayers of water with very great vertical changes in their properties, in turn separated by more extensive layers where the vertical gradients of the measured parameters change slightly.

On the seventh voyage of the scientific research ship "Dmitriy Mendeleyev" in the winter of 1972 in the neighborhood of the Comoro Islands in the Indian Ocean specialists carried out a series of sounding measurements of the vertical structure of the conductivity field using a new low-inertia sounding instrument with a resolution of less than 1 cm vertically. The sounding was carried out to a depth of 300 m with a rate of lowering of the instrument from 0.7 to 1.3 m/sec.

SE = sensing element
G = generator
PS = pressure sensor
OA = operational amplifier
A = amplifier
D = detector

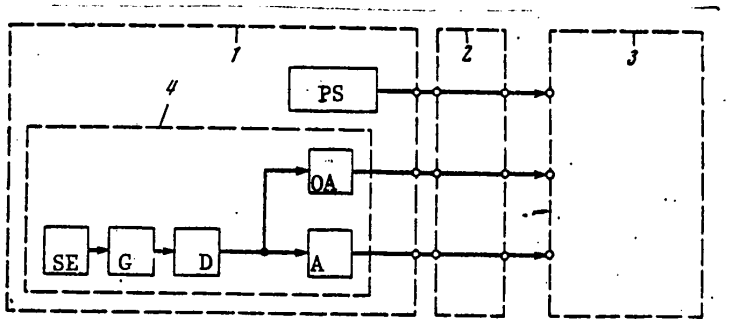

Fig. 1. Block diagram of measurement apparatus. 1) probe; 2) communication line (supporting-electrical cable); 3) recording apparatus carried on ship; 4) hydroresistor instrument for measuring conductivity.

The probe used in the experiments was created at the Special Design Bureau for Oceanological Equipment at the Institute of Oceanology imeni P. P. Shirshov. In different operating regimes the instrument can simultaneously measure up to five different parameters. The probe has a three-strand supporting and electrical cable for data transmission. In the described experiment the probe operated in a regime for measuring the conductivity of sea water with the simultaneous registry of the depth of instrument submergence. The conductivity of sea water was measured employing a so-called hydroresistor measuring instrument whose block diagram is shown in Fig. 1.

The sensing element of this instrument is the volume of sea water situated between the central and annular electrodes of this sensor. The electrodes were applied to a hemispherical surface. The central electrode has the form of a "point" with a diameter of 0.3 mm and the annular electrode is situated along the diameter of the hemisphere, equal to 9 mm. The electrodes were cut into the circuit of the generator G in such a way that with a change in the conductivity of the sea water between the electrodes there is a change in the amplitude of the signal produced by the generator. The generator frequency is about 5 MHz.

The effective volume of sea water, that is, the volume whose change of conductivity exerts an influence on amplitude of the signal received from the generator G, is equal to approximately 3 mm^3, which also determines the minimum dimension of the measured inhomogeneities. The equivalent resistance between the electrodes is approximately 170 ohms with a generator frequency equal to 5 MHz and a medium conductivity of about 50 mmho/cm.

The signal from the generator is fed to the detector D, from which it is fed through the supporting and electrical cable to the recording apparatus or through the amplifier A (in this case the signal is proportional to the mean conductivity value) or through an operational amplifier OA. In the latter case the recording apparatus receives a signal proportional to conductivity fluctuations. The d-c amplifier A has a voltage amplification factor 7, whereas the operational amplifier of fluctuations OA amplifies the voltage by a factor of 100 and has a bandpass at the 0.7 level from 1 to 5000 Hz. The level of electric noise in this instrument in conductivity units is $3.5 \cdot 10^{-4}$ mmho/cm, which corresponds to approximately $2.5 \cdot 10^{-4}$°C for temperature or $5 \cdot 10^{-4}$ o/oo for salinity.

The transconductance of the instrument for measuring conductivity of the instrument at the detector output was 1 mV/mmho/cm.

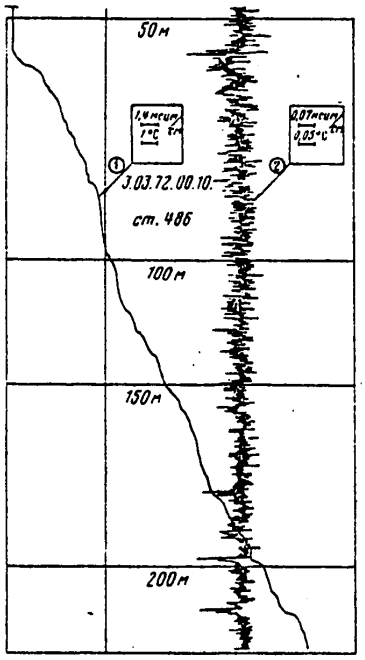

Fig. 2. Profiles of mean (1) and fluctuating (2) components of conductivity field obtained by vertical sounding.

Depth was measured using a pressure sensor PS. The probe signals were registered on a magnetic tape and also using an automatic pen recorder with depth marks being registered each 50 m (Fig. 2).

The information obtained during sounding was then subjected to statistical processing on a shipboard electronic computer; this made it possible to ascertain the correlation and spectral functions and also the reciprocal statistical characteristics of the signals.

In the course of the experiment a total of ten soundings were made at a single point in the ocean with intervals between soundings of 40-60 minutes. The repeated soundings made it possible to evaluate the temporal variability of the microscale vertical structure of the conductivity field. As an example, Fig. 2 shows the profiles of mean conductivity and fluctuations of conductivity obtained during the sounding. The scales of these curves are given both in conductivity units and scaled to temperature units. The figure shows that the rate of sounding varied somewhat with depth, which evidently is associated with flexure of the electrical and supporting cable due to nonuniformity of the ship's drift and the variability of the velocity of sea currents with depth. A distinguishing characteristic of all these profiles (as is clearly traced in Fig. 2) is an increase in the mean

conductivity values and a relatively weak change in conductivity fuctuations with depth. Such a regularity is also detected in the spectra of conductivity fluctuations computed for sections of records from different horizons: the total level of spectral density is virtually identical at depths from 50 to 250 m.

Figure 2 clearly shows that the curve of mean conductivity has a clearly expressed "steplike" character in virtually the entire investigated layer of the ocean. The thicker quasihomogeneous layers alternate with thin interlayers with large conductivity gradients. Strong "surges" in the fluctuations of conductivity are associated with such interlayers.

For statistical processing on an electronic computer we selected several equal segments of records from each sounding at depths corresponding to 50, 100, 150, 200 and 250 m. The length of the processed record corresponded to a vertical extent of the record of about 20 m. A continuous signal of the conductivity fluctuation (first registered on an analog magnetic recorder) was introduced into an electronic computer with a discreteness of 0.002 sec. Such a discreteness was selected in accordance with the frequency characteristic of the microsensor.

The statistical homogeneity of the records introduced into the electronic computer was achieved by the filters incorporated in the instrument circuit. The homogeneity was then checked from the curve of the current dispersion of the processed pieces. A reciprocal statistical analysis was carried out for pairs of records selected at identical horizons in two successive soundings. The wave number interval in the processing of records was in the range 0.07-10 cm^{-1}, which corresponded, as noted above, to vertical dimensions of inhomogeneities 0.6-90 cm.

A reciprocal statistical analysis of the records afforded a possibility for tracing the variability of vertical structure of the conductivity field during the time interval between successive soundings. The reciprocal spectral characteristics obtained using an electronic commputer indicated that the microstructure of the conductivity field changes considerably over the course of 40-60 minutes. For the considered range of wave numbers the values of the coherence functions for the records were extremely low (the maximum coherence did not exceed 0.4). Thus, it can be concluded that in this case the inhomogeneities of the conductivity field with a dimension to 1 m vertically existed in this region for less than one hour or that their dimension horizontally was sufficiently small that there was then an influence of the ship's drift, which in the course of the experiment was insignificant.

Figure 3 gives the normalized correlation functions determined from one conductivity fluctuation profile. The length of each processed record was equal to a depth change of 20 m and their beginning corresponded to the horizons 100, 150, 200 and 250 m. The correlation radius has the value r = 25-30 cm and varies little with depth. Similar graphs of the normalized correlation functions were obtained for all other soundings. A constant r value for all horizons and for all profiles is indicative of the fact of vertical homogeneity of microscale turbulence (in the ocean layer to 300 m) in the considered wave number range.

Figure 4 shows a "bundle" of spectral density curves obtained for these same horizons (50, 100, 150, 200 and 250 m) along one conductivity fluctuation profile. Since it can be assumed that the conductivity of sea water is linearly related to

temperature, the values of the spectral density functions are conveniently represented in temperature units, as has been done in Fig. 4. The values of the dissipation rate functions for the inhomogeneities were also computed in temperature units using the formula

$$\overline{N} = 2\chi \int_{k_1}^{k_2} k^2 E(k)\, dk,$$

where χ is the thermal conductivity coefficient, k_1, k_2 are the limiting values of the considered wave number interval.

The $\overline{N}$ value, computed for all horizons, other than the upper horizon, and for all the soundings, varied little and was close to $5 \cdot 10^{-5}$ degree$^2 \cdot$sec^{-1}.

The agreement in the behavior of curves 2-5 in Fig. 4 and in the considered range of wave numbers means that the vertical structure of the field of conductivity fluctuations in the layer 100-300 m was statistically homogeneous.

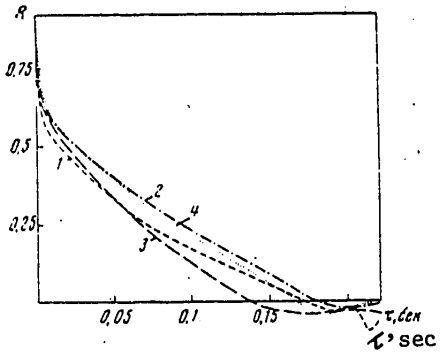

Fig. 3. Normalized correlation functions for conductivity fluctuations corresponding to horizons 100 (1), 150 (2), 200 (3), 250 m (4).

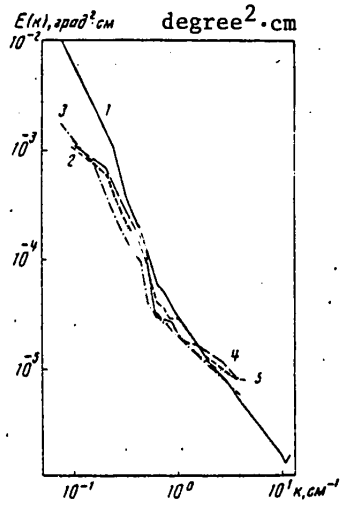

Fig. 4. "Bundle" of spectral density curves for conductivity fluctuations corresponding to the horizons 50 (1), 100 (2), 150 (3), 200 (4), 250 m (5).

In the spectral density functions in Fig. 4 it is possible to discriminate two characteristic segments with different curve slopes (at a logarithmic scale): the first in the range of wave numbers $k = 7 \cdot 10^{-2} - 7 \cdot 10^{-1}$ cm^{-1}, the second $k = 7 \cdot 10^{-1} - 7 \cdot 10^{0}$ cm^{-1}. The spectral curves in the first segment have a high energy density level and rapidly drop off with an increase in wave number. The slope of the curve in this segment is close to "-5/3." The spectral functions of the second segment are characterized by a slower dropoff with an increase in wave number and the slope of the curves here is close to "-1."

The spectral density function 1 (Fig. 4) was obtained on the basis of the results of the same measurement, but from the segment of the record in the upper region of the thermocline. Two segments can also be discriminated: one with the slope "-3" and a second with the slope "-7/5." The spectral curve 1 is also characterized by a higher density level for the energy of fluctuations in the zone of small values of the wave numbers and a sharper dropoff of the curve with an increase in k. Such a behavior of this function can indicate a somewhat different mechanism of the formation of microstructure of the conductivity field in the upper-layer thermocline in comparison with deeper layers of the ocean. For example, it is not impossible that in layers with sharp drops in density there are very high-frequency internal waves for which steep dropoffs of spectral densities with an increase in wave number values are characteristic [3].

In conclusion, the authors express appreciation to R. V. Ozmidov for advice and attention given in all stages of the work and to Ye. I. Kuznetsov and V. I. Fedonov who participated in developing the probe.

BIBLIOGRAPHY

1. Borkovskiy, M. M., Volochkov, A. G., Prokhorov, V. I., Pudov, V. D., Sorokhtin, O. G. and Shekhvatov, V. V., "The AIST Digital Hydrophysical Probe," 4-y VSESOYUZNYY SIMPOZIUM PO AVTOMATIZATSII NAUCHNYKH ISSLEDOVANIY MOREY I OKEANOV (Fourth All-Union Symposium on Automation of Scientific Research in the Seas and Oceans), Sevastopol', Izd-vo MGI, 1972.

2. Tait, R. J. and Howe, M. R., "Some Observations of Thermohaline Stratifications in Deep Ocean," DEEP-SEA RES., 15, 1968.

3. Ozmidov, R. V., "Experimental Investigations of Microscale Oceanic Turbulence. Ninth Voyage of the Scientific Research Ship 'Akademik Kurchatov'," VESTNIK AN SSSR (Herald of the USSR Academy of Sciences), No 7, 1971.

5303
CSO: 8144/1839

APPROVED FOR RELEASE: 2007/02/09: CIA-RDP82-00850R000500040036-3

INERTIAL INTERVAL IN TURBULENCE SPECTRA IN STRATIFIED FLUID (HEISENBERG-MONIN MODEL)

Moscow ISSLEDOVANIYE IZMENCHIVOSTI GIDROFIZICHESKIKH POLEY V OKEANE in Russian 1974 pp 83-91

[Article by A. Yu. Benilov and I. D. Lozovatskiy from monograph "Ocean Research on Hydrophysical Field Variability," edited by R. V. Ozmidov, doctor of physical and mathematical sciences, Izdatel'stvo "Nauka", 211 pages, number of copies printed unknown]

[Text] Turbulence plays a major role in many processes in the ocean. For this reason the investigation of oceanic turbulence is of great practical interest. Since the ocean is usually stably stratified, the turbulence which is observed there must have characteristics associated with the influence of Archimedes forces and distinguishing it from the turbulence in a density-stratified fluid.

Experimental data are now available indicating some characteristics typical for the oceanic turbulence phenomenon. Observations which have been made by Canadian researchers [1] and by specialists of the Institute of Oceanology [2] have shown that in the spectra of oceanic turbulence there is often an absence of an inertial interval of scales and in many cases the measured spectra agreed well with the Bolgiano-Obukhov "-11/5 law"[3, 4], which is correct under conditions of a strong stable stratification. In the opinion of the authors of [1], the influence of stratification leads to a decrease in the characteristic turbulence scale, that is, the Reynolds number becomes small and the inertial interval can be very narrow. On the other hand, with a strong stable stratification the Archimedes forces can exert an influence on the turbulence regime up to scales where viscosity is important and this can also lead to the disappearance of an inertial interval. This article is devoted to a discussion of these peculiarities.

***

1. According to the theory of locally isotropic turbulence in a density-homogeneous fluid [5], the separation of the inertial interval, where the "-5/3 law" is correct and the "dissipation interval" in the spectrum is observed for a sufficiently great

Reynolds turbulence number. If L_u is the characteristic scale of change in the field of mean velocity $\vec{u}(\vec{x}, t)$, $\eta = (\nu^3/\varepsilon)^{1/4}$ is the Kolmogorov scale, coinciding in order of magnitude with the scales of the maximum of those disturbances on which molecular viscosity ν exerts a substantial influence, ε is the rate of dissipation of turbulent energy, the width of the inertial interval can be characterized by the value of the η/L_u ratio. The following evaluation [5] is correct for this value in the approximation of locally isotropic turbulence

$$n/L_u \sim Re^{-3/4}, \quad Re = \Delta \bar{u} L_u/\nu, \tag{1}$$

where $\Delta \bar{u}$ is the characteristic change in the field of mean velocity at the scale L_u. It can be seen from this evaluation that with a decrease in the Re number there is a narrowing of the inertial interval. In a study by Gibson and Schwarz [6] there is a comparison of the longitudinal one-dimensional normalized spectra obtained in a flow of water in a pipe beyond a grid at different Re numbers with the data from other authors. It was found that the width of the inertial interval is the lesser the lesser the Re number. In the Stewart-Townsend data [7], obtained with relatively very small Re ($Re \approx 2.6 \cdot 10^3$), the inertial interval is virtually absent. Similar effects can also be observed in the turbulence spectra in a stratified fluid.

As is well known [5], turbulence in a stratified fluid differs from the turbulence in a homogeneous medium in that fluid particles are in the field of action of the Archimedes forces. The minimum scale of the inhomogeneities, beginning from which the influence of Archimedes forces becomes substantial, is determined by the scale L_*, introduced by A. M. Obukhov [3] and Boldgiano [4], which is equal to

$$L_* = \frac{\varepsilon^{3/4}}{N^{3/2}\beta^{3/2}}, \tag{2}$$

where N is the rate of evening-out of temperature inhomogeneities, β is the buoyancy parameter. If $L_0 = \min(L_u, L_T)$ is the characteristic scale of the mean velocity fields $\vec{u}(\vec{x}, t)$ and temperature fields $T(\vec{x}, y)$, L_T is the characteristic scale of the mean temperature field and the following inequality is correct

$$L_0 \gg L_* \gg L_\eta = \max(\eta, \eta\, Pr^{-3/4}), \quad Pr = \nu/\chi, \tag{3}$$

inhomogeneities with scales $l \ll L_0$ belong to the equilibrium interval of scales in which the fields of turbulent fluctuations of hydrodynamic fields must be considered locally homogeneous and unambiguously determined by the parameters ε, N, β, ν and χ (χ is the coefficient of molecular thermal conductivity [3, 4]. Inhomogeneities with the scales l from the interval

$$L_0 \gg l \gg L_* \tag{4}$$

are under the influence of Archimedes forces. Inhomogeneities with scales from the interval

$$L_* \gg l \gg L_\eta \tag{5}$$

belong to the inertial interval. Inhomogeneities with the scales

$$l \lesssim L_\eta \tag{6}$$

belong to the "dissipation interval." Thus, the equilibrium interval, determined by inequality (3), breaks down into three subintervals, the limits of which are stipulated by the inequalities (4)-(6).

Our reasonings make it possible to adopt the value of the ratio η/L_* as an evaluation of the width of the inertial interval in the turbulence spectra in a stratified fluid under the condition that $L_0 \gg L_*$. It follows from the inequalities (3)-(6) that in this case the criterion of existence of a quite broad inertial interval is the condition $\eta/L_* \ll 1$.

In the simplest case of statistically stationary and horizontally homogeneous turbulence, using the equation for the balance of turbulent energy and the intensity of temperature inhomogeneities in the form [5]:

$$\varepsilon = K\left(\frac{\partial \bar{u}}{\partial z}\right)^2 (1 - \sigma \mathrm{Rf}), \tag{7}$$

$$N = K_T \left(\frac{\partial \bar{T}}{\partial z}\right)^2, \quad \mathrm{Rf} = \beta K_T \frac{\partial \bar{T}}{\partial z} \Big/ K\left(\frac{\partial \bar{u}}{\partial z}\right)^2, \tag{8}$$

where K is the coefficient of turbulent viscosity, K_T is the coefficient of turbulent thermal conductivity, Rf is the dynamic Richardson number, σ is a parameter which in the case of an unstable stratification takes into account the diffusion of turbulent energy, and in the case of stable stratification $\sigma = R^{-1}$ (R is the critical Richardson number), for the η/L_* value we obtain the formula

$$\frac{\eta}{L_*} = \frac{1}{(\sigma^3 \mathrm{Re}_T)^{1/4}} \left(\frac{\sigma |\mathrm{Rf}|}{1 - \sigma \mathrm{Rf}}\right)^{3/4}, \tag{9}$$

where $\mathrm{Re}_T = K_T/\nu$ is the Reynolds turbulence number. The dependence on the Reynolds number here is similar to formula (1), but by virtue of the dependence on Rf, even with a finite adequately large Re_T number in the case of a strong stable stratification, the inertial interval in the turbulence spectra can be absent. When the L_* scale becomes greater than L_0 and no longer belongs to the equilibrium interval of scales, formula (9) does not determine the width of the inertial interval. In this situation the width of the inertial interval can be evaluated by the η/L_0 ratio.

It can be seen from what has been stated above that the turbulence spectra can have a different form in dependence on the relationship of scales limiting the width of each of the subintervals of the equilibrium interval of scales.

II. In order to explain the specific form of the spectral densities in a stratified turbulent flow with different Re numbers and stratification regimes we will examine the spectral equations for the balance of turbulent energy and the intensity of temperature inhomogeneities in the form [5]

$$\varepsilon - 2\nu \int_{k_0}^{k} p^2 E(p)\, dp = S(k) \pm \beta \int_{k}^{\infty} E_{T\mathrm{W}}(p')\, dp', \tag{10}$$

$$N - 2\chi \int_{k_0}^{k} p^2 E_T(p)\, dp = R(k), \tag{11}$$

where E(k), $E_T(k)$, $E_{TW}(k)$ are the spectral densities of turbulent energy, temperature fluctuations and the turbulent heat flux (with an accuracy to the factor $c_p\rho_0$), S(k) and R(k) describe energy transfer and the measures of inhomogeneities of the temperature field from the macroscale turbulence components (with wave numbers less than k) to microscale (with wave numbers greater than k). As the hypothesis for closure of this system of equations we will use a generalization of the Heisenberg closure proposed by A. S. Monin [8] for the case of a turbulent flow with mean velocity and temperature gradients:

$$S(k) = K(k)\left[\left(\frac{\partial \bar{u}}{\partial z}\right)^2 + 2\int_{k_0}^{k} p^2 E(p)\,dp\right], \tag{12}$$

$$R(k) = \alpha K(k)\left[\left(\frac{\partial \bar{T}}{\partial z}\right)^2 + \int_{k_0}^{k} p^2 E_T(p)\,dp\right], \tag{13}$$

$$\int_{k}^{\infty} E_{TW}(p')\,dp' = \alpha K(k)\left[\left(\frac{\partial \bar{T}}{\partial z}\right)^2 + \int_{k_0}^{k} p^2 E_T(p)\,dp\right]^{1/2}, \tag{14}$$

where K(k) is the coefficient of turbulent viscosity, α is the ratio of the coefficient of turbulent viscosity to the coefficient of turbulent thermal conductivity, in general, dependent on Rf. Adhering to [8], for K(k) we will use the formula

$$K(k) = \gamma\left[\int_{k}^{\infty} p'^{-2} E(p')\,dp'\right]^{1/2}, \tag{15}$$

where γ is a numerical constant. With $k = k_0$ (10)-(15) are transformed into a system of macroscopic equations (7)-(8) with $\sigma = 1$. Proceeding in (10)-(15) to a dimensionless form using the formulas

$$x = c_1 L_* k, \tag{16}$$

$$\psi_E(x) = [c_2 N^{3/4}\varepsilon^{-11/4}\beta^{3/2}]\,E(k), \tag{17}$$

$$\psi_T(x) = [c_3 N^{1/4}\varepsilon^{-7/4}\beta^{3/2}]\,E_T(k), \tag{18}$$

$$c_1 = 2^2\alpha^{-3/4}\gamma^{-1/2}, \quad c_2 = 2^{-6}\alpha^{3/4}\gamma^{3/2}, \quad c_3 = 2^{-7}\alpha^{3/4}\gamma^{3/2}, \tag{19}$$

for determining the functions ψ_E and ψ_T we obtain the two equations:

$$1 - \Gamma_3\int_{x_0}^{x} \xi^2\psi_E(\xi)\,d\xi = 2^3F^2\left[\Gamma_1 + \int_{x_0}^{x} \xi^2\psi_E(\xi)\,d\xi\right] \pm 2^{4.5}F^2\left[\Gamma_2 + \int_{x_0}^{x} \xi^2\psi_T(\xi)\,d\xi\right]^{1/2} \tag{20}$$

where

$$1 - \Gamma_4\int_{x_0}^{x} \xi^2\psi_T(\xi)\,d\xi = 2^3F^2\left[\Gamma_2 + \int_{x_0}^{x} \xi^2\psi_T(\xi)\,d\xi\right], \tag{21}$$

$$F(x) = 2\left[\int_{x}^{\infty} \xi'^{-2}\psi_E(\xi')\,d\xi'\right]^{1/4}. \tag{22}$$

The solution of system (20), (21) in the case $\Gamma_3 = \Gamma_4 = 0$ was investigated in detail by A. S. Monin in [8].

The parameters Γ_1, Γ_2, Γ_3 and Γ_4 are dependent on the relationship between the scales which can be formed from the dimensionless parameters entering into (10)-(14). These dependences have the form:

$$\Gamma_1 = \frac{1}{2\alpha}\left[\frac{L_*}{L_u}\right]^{4/3}, \quad \Gamma_2 = \frac{1}{2}\left[\frac{L_*}{L_T}\right]^{4/3}, \tag{23}$$

$$\Gamma_3 = 2\alpha\left[\frac{\eta}{L_*}\right]^{4/3}, \quad \Gamma_4 = \frac{4}{\mathrm{Pr}}\left[\frac{\eta}{L_*}\right]^{4/3}, \tag{24}$$

where L_u and L_T are scales dependent on the gradients of the mean fields of velocity and temperature and accordingly are equal to

$$L_u = \varepsilon^{1/3}\left(\frac{\partial \bar{u}}{\partial z}\right)^{-3/2}, \tag{25}$$

$$L_T = N^{3/4}\varepsilon^{-1/4}\left(\frac{\partial \bar{T}}{\partial z}\right)^{-3/2}. \tag{26}$$

Since the scales (25), (26) are determined through the mean velocity and temperature fields, they can be adopted within the framework of this model as the characteristic scales of these mean fields.

The solution of equations (20)-(21) can be obtained in parameteric form much as was done in [8]. Assuming F as a new independent variable, for x, ψ_E and ψ_T we obtain the formulas:

$$x = 2^{11/3}F^{-11/4}A^{-1/2}B^{-1/3}[2^{1/3}CB^{1/3} \mp (2^3PF^3AB^{-1} + 2^3PF^2 - PA)]^{1/4}, \tag{27}$$

$$\psi_E = 2^{-13/3}F^6A^3B^{1/3}Q^{-1}x^5, \tag{28}$$

$$\psi_T = 2^{-1/3}P^2F^3A^3B^{-2/3}Q^{-1}x, \tag{29}$$

where A, B, Q are some functions of the argument F, equal to

$$A = 2^3F^2 + \Gamma_3, \quad B = 2^3F^2 + \Gamma_4, \tag{30}$$

$$Q = 2^{1/3}CB^{1/3}A(1 + 2^4F^2A^{-1}) \mp [2^5PF^4AB^{-1}(1 + 3\cdot 2^{-1}AB^{-1}) + 2^7PF^4(1 + 2^{-2}AB^{-1}) - PA^2(1 + 2^3F^2A^{-1} + 2^2F^2B^{-1})], \tag{31}$$

and the parameters C and P are expressed through the parameters of the problem (23)-(24) in accordance with the formulas:

$$C = 1 + \Gamma_1\Gamma_3, \quad P = (1 + \Gamma_2\Gamma_4)^{4/3}. \tag{32}$$

The functions ψ_E and ψ_T, determined by the formulas (28), (29), are solutions of the equations (20)-(21) only when $x > x_0$, where the x_0 value, in accordance with [8], determines the maximum scale of the disturbances allowed by the geometry of the flow. The x_0 value is found from (27) with $F = F_0$. In turn the F_0 value can be obtained from system (20)-(21), assuming $x = x_0$. Using (20)-(21), (23), (25), (26), we express F_0 and the parameters Γ_1 and Γ_2 through Rf. After

simple transformations we obtain the formulas:

$$\Gamma_1 = \frac{1-\mathrm{Rf}}{2\mathrm{Rf}^2}, \qquad \Gamma_2 = \frac{(1-\mathrm{Rf})^2}{2\mathrm{Rf}^2}, \qquad F_0 = \frac{1}{2}\frac{|\mathrm{Rf}|}{1-\mathrm{Rf}}, \tag{33)-(35)}$$

which makes it possible to indicate the relationships between the scales under different stratification conditions:

1) in the region of Rf values such that $\mathrm{Rf} < 1 - \alpha$, the scale $L_T < L_u$, hence $L_0 = L_T$;
2) with $\mathrm{Rf} > 1 - \alpha$ we will have $L_u < L_T$, hen .e $L_0 = L_u$;
3) with $\mathrm{Rf} < 1 - \alpha$ we will have $L_* \geqslant L_0$ (the equation is satisfied in the case of limiting instability when $\mathrm{Rf} \to -\infty$); the L_* scale with such Rf values belongs to the equilibrium interval of scales (interval (4) is absent);
4) with

$$1 - \alpha < \mathrm{Rf} < \sqrt{\frac{\alpha^2}{4} + \alpha} - \frac{\alpha}{2}$$

we will have $L_* < L_0$ (slight stability, interval (4) is absent), with

$$\sqrt{\frac{\alpha^2}{4} + \alpha} - \frac{\alpha}{2} < \mathrm{Rf} \leqslant 1$$

we will have $L_* \leqslant L_0$ (strong stability, interval (4) exists);
5) the value $F_0 \to 1/2$ with $\mathrm{Rf} \to -\infty$ and for values $\mathrm{Rf} < 0$ we will have $0 \leqslant F_0 \leqslant 1/2$; with $\mathrm{Rf} > 0$ the F_0 value increases with an increase in stability and tends to infinity with $\mathrm{Rf} \to 1$; as noted in [8], the corresponding F_0-x_0 values in the case of an unstable stratification are always finite and different from zero (essentially an influence of the limiting surface); with an increase in stability ($\mathrm{Rf} \to 1$) $x_0 \to 0$ (turbulence has a primarily local character). The solution of equations (20)-(21), determined by formulas (27)-(29), (35), has the following asymptotic peculiarities.

1. With $\Gamma_3 = \Gamma_4 = 0$ ($\nu = \chi = 0$) the derived solution coincides with the solution in [8]. When $x \to \infty$ the ψ_E, ψ_T functions are proportional to $x^{-5/3}$. In the case of a strong stable stratification (in the interval of scales (4))

$$\psi_E \sim x^{-11/3}, \qquad \psi_T \sim x^{-7/3} \qquad (x_0 < x \ll 1). \tag{36}$$

2. With $\Gamma_3 \neq 0$, $\Gamma_4 \neq 0$ and $\mathrm{Pr} \approx 1$ the ψ_E and ψ_T functions are proportional to x^{-7} with $x \to \infty$, which is a consequence of closing of the initial equations using the Heisenberg hypothesis. In the case of a stable stratification this asymptotic behavior exists if the parameters of the problem (23)-(24) satisfy the inequality

$$(1 + \Gamma_0)^2 > \Gamma_0 (a + b\Gamma_0),$$
$$\Gamma_0 = \Gamma_1\Gamma_3 = \left(\frac{\eta}{L_u}\right)^{4/3}, \quad a = \frac{\alpha\,\mathrm{Pr}}{2}\frac{\mathrm{Rf}^2}{1-\mathrm{Rf}}, \quad b = \mathrm{Rf}^2, \tag{37}$$

which is derived from formulas (27)-(31), (33), (34) after a limiting transition with $F \to 0$, by virtue of the positive certainty of the ψ_T function. When Γ_0 is such that (37) is transformed into the equation

$$(1 + \Gamma_0)^2 = \Gamma_0 (a + b\Gamma_0), \tag{38}$$

the ψ_E and ψ_T functions become equal to zero with some final x value equal to $x = x_m > x_0$. For the x_m value from (27), with (38) taken into account, after a limiting transition with $F \to 0$ we obtain the formula

$$x_m = 2\alpha^{1/4}\,\mathrm{Pr}^{1/4}\Gamma_0^{-3/4}\,\mathrm{Rf}^{-3/4}(1 - \mathrm{Rf})^{3/4}R_1^{1/4}, \tag{39}$$
$$R_1 = (1 + \Gamma_0)(1 - \mathrm{Rf})^{1/3} + \mathrm{Rf}\,[2^{-1}\alpha\,\mathrm{Pr} + (1 - \mathrm{Rf})\Gamma_0]^{1/3}\Gamma_0^{1/3},$$

from which it can be seen that with an increase in stability (Rf$\to$1) $x_m \to 0$, that is, in this limiting situation the turbulence spectra will degenerate with an increase in the Richardson number; with a tendency of Rf to zero (a stratification close to neutral) $x_m \to \infty$; within the framework of the model employed this limiting case corresponds to the asymptotic equation

$$\Gamma_1 + \int_{x_0}^{x_m} \xi^2 \psi_E(\xi)\, d\xi = 2^{-1/2}\left[\Gamma_2 + \int_{x_0}^{x_m} \xi^2 \psi_T(\xi)\, d\xi\right]^{1/2}, \qquad (40)$$

equivalent to the condition (38).

3. In the case $Pr \ll 1$ the temperature spectrum reveals an inertial-heat conducting interval of the scales $Pr^{3/4}\eta \gg l \gg \eta$ in which the temperature inhomogeneities begin to disappear due to the influence of molecular thermal conductivity and viscosity still does not exert an influence on velocity fluctuations. According to the theory of Batchelor, Howells and Townsend [9] (neutral stratification), in this interval of scales the energy spectrum is proportional to $k^{-5/3}$ and the temperature spectrum is proportional to $k^{-17/3}$. With an adequately small value of the Γ_0 parameter an inertial-heat conducting interval exists in the considered model under different stratification conditions, but the temperature spectrum in this interval has the form:

$$E_T(k) \sim k^{-11/3}, \quad Pr^{3/4}\eta^{-1} \ll k \ll \eta^{-1}, \qquad (41)$$

that is, decreases with an increase in the wave number by k times more slowly than follows from the theory of Batchelor, Howells and Townsend [9].

4. In the case $Pr \gg 1$ in the spectra of turbulence in a density-homogeneous fluid there is a viscoconvective interval of scales in which the velocity fluctuations are already acted upon by molecular viscosity (the E(k) spectrum decreases proportionally to k^{-7} in the Heisenberg theory or as the exponent in the Batchelor theory [10]), whereas temperature inhomogeneities still are not subjected to molecular thermal conductivity. The temperature spectrum $E_T(k)$ in the range of scales $\eta \gg l \gg Pr^{-3/4}\eta$, according to the Batchelor theory [10], decreases proportionally to k^{-1}. From the resulting solutions under conditions close to neutral stratification for the range of scales (η , $\eta\, Pr^{-3/4}$), we obtain power laws in the form

$$E(k) \sim k^{-7}, \quad E_T(k) \sim k, \quad Rf \to 0, \quad \eta^{-1} \ll k \ll Pr^{3/4}\eta^{-1}. \qquad (42)$$

The noted differences in the asymptotic behavior of the temperature spectrum in this model and in the Batchelor theory can be explained in the following way. In the Batchelor theory the formulas for spectral densities are obtained from linearized equations; the turbulence described by these equations must be considered weak, as is correct for the region of scales $k \gg \eta^{-1}$. The Heisenberg closure is essentially nonlinear; mixing in this model occurs more intensively than in the Batchelor model; by virtue of this circumstance the spectral densities obtained in the Heisenberg approximation decrease with an increase in the wave number considerably more slowly than in the Batchelor theory.

In the case of unstable stratification

$$E(k) \sim k^{-11/3}, \quad E_T(k) \sim k^{-1/3}, \quad Rf < 0, \quad \eta^{-1} \ll k \ll Pr^{3/4}\eta^{-1}. \qquad (43)$$

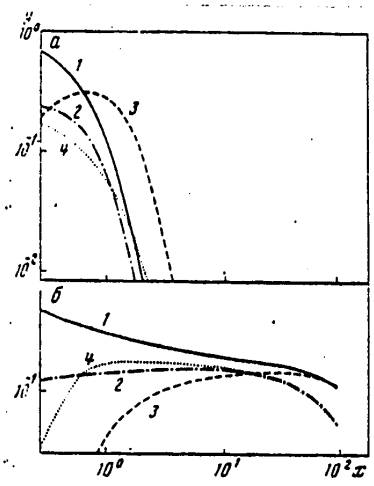

Fig. 1. Dependence of the products $x^{5/3}\psi_E$ and $x^{5/3}\psi_T$ on the dimensionless wave number for different stratification conditions.

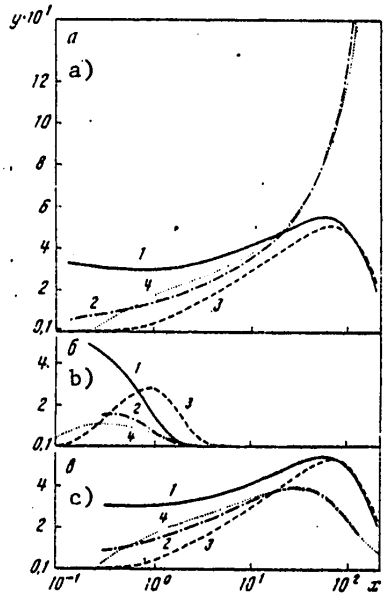

Fig. 2. Dependence of the products $x^2\psi_E$ and $x^2\psi_T$ on dimensionless wave number for different stratification conditions and Pr numbers. Notations are the same as in Fig. 1.

The result is related to the fact that with $Rf<0$ the temperature fluctuations induce fluctuations of buoyancy forces which maintain velocity fluctuations in the viscous interval. As a result, the E(k) spectrum decreases with an increase in the wave number more slowly than k^{-7} and since some of the energy of the buoyancy forces was expended on overcoming viscous forces, the $E_T(k)$ spectrum becomes decreasing in comparison with the case (42). Analysis of equations (20)-(21) shows that in this situation the parameters determining the turbulent regime in the interval of scales ($\eta, \eta Pr^{-3/4}$) are the values ν, N and β.

In the case of a stable stratification ($Rf>0$) the system (20)-(21) does not have asymptotic solutions ($Pr \gg 1$), since the inequality (37) in this case loses sense; however, the viscoconvective interval with large but finite Pr numbers, when (37) is still correct, can exist. Under the condition (38) the functions ψ_E and ψ_T are different from zero only for x values in the interval $[x_0, x_m]$, where x_m is given by formula (39).

It follows from what has been stated above that the turbulence spectra in a stratified fluid can have a different form in dependence on stratification conditions, Pr number and width of the equilibrium interval, which can be determined by the value of the Γ_0 parameter. The inertial interval, as was demonstrated, in a number of cases can be absent. In the case of a strong stable stratification and a quite small width of the equilibrium interval (large values of the Γ_0) the turbulence spectra degenerate, that is, are different from zero in a finite interval of values of the wave numbers, which is narrowed with an increase in stability.

III. On the basis of the derived formulas we carried out computations illustrating the noted characteristics (Figures 1, 2). Figure 1 shows the functions ψ_E and ψ_T multiplied by $x^{5/3}$. These values in the inertial interval, if it exists, become constant. The computations were made for cases of large Γ_0 (Fig. 1,a) and small Γ_0 (Fig. 1,a) and small Γ_0 (Fig. 1,b). In the first case the relationships among the scales are such that the following inequalities are correct:

$$L_T < L_u < L_* < \eta, \quad Rf < 0, \tag{44}$$

$$L_* \lesssim L_u < \eta \lesssim L_T, \quad Rf > 0. \tag{45}$$

With $Rf<0$, as indicated in Fig. 1,a and inequality (44), viscosity is operative in the entire region of values $x \geqslant x_0$; the inertial interval is absent. In the case of a stable stratification viscosity is also operative in the entire region $x \geqslant x_0$; the inertial interval is absent.

In the second case the relationships between the scales have the form:

$$\eta \ll L_T < L_u < L_*, \quad Rf < 0, \tag{46}$$

$$\eta \ll L_* \lesssim L_u < L_T, \quad Rf > 0. \tag{47}$$

In the case of an unstable stratification the interval (4), by virtue of (46), is absent. There is an appreciable interval of the argument x in which the ψ_E function (curve 3) adheres to the "$x^{-5/3}$ law." There is no such interval for the ψ_T function

and for all $x > x_0$ it decreases more rapidly than $x^{-5/3}$. This is attributable to the fact that the Reynolds number, stipulated by the Γ_0 value and the Rf number, is inadequately large. Thus, molecular thermal conductivity begins to act on turbulent fluctuations whose scales in order of magnitude are comparable to the scales L_T and L_u.

In the case of a stable stratification the functions ψ_E (curve 1) and ψ_T (curve 2) are solutions of equations (20)-(21) in a broader range of values of the argument $x \geqslant 1.04$. As indicated in Fig. 1,b the product $x^{5/3}\psi_E$ for all $x > x_0$ decreases. In the region of scales where the influence of viscosity is negligible ($x < 50$), the decrease occurs more slowly than follows from the asymptotic formulas (36). It can be assumed that in the considered case there is a slightly expressed inertial interval, since the Reynolds number is inadequately great. For the ψ_T function there is a region of values of the argument x ($3 \leqslant x \leqslant 10$), where $\psi_T \sim x^{-5/3}$. It is easy to see that the resulting difference in the behavior of the ψ_E and ψ_T functions in the region of scales belonging to the inertial-convective interval of scales is related to an insignificant deviation of the exponent on the function ψ_T in interval (4) (in comparison with ψ_E) from 5/3. Accordingly, the transition from the interval (4) to the inertial convective interval is not so drawn out as for the function ψ_E.

Figure 2 shows the dissipation spectra (product of $x^2\psi_E$ and $x^2\psi_T$). The curves in Figure 2,b,c correspond to the same values of the Γ_0 and Rf parameters as in Fig. 1. When the Re number is small (Fig. 2,b, $\Gamma_0 = 3.2$), the dissipation spectra for the velocity and temperature fields do not have maxima with $x \geqslant x_0$, since the functions ψ_E and ψ_T decrease rapidly with an increase in the x argument under the influence of molecular forces. For greater Re (Fig. 2,c, $\Gamma_0 = 3.2 \cdot 10^{-3}$) the dissipation spectra have maxima; with an increase in the Re number the maxima in the dissipation spectra are displaced into the region of greater x values. As an example, Fig. 2,a shows dissipation spectra with the same values of the parameters as in Fig. 2,c, but with a Pr number 10. In this case the maximum in the temperature dissipation spectrum is displaced relative to the maximum in the velocity dissipation spectrum into the region of relatively greater values of the x argument. The greatest contribution to the temperature dissipation spectrum is from scales less than η. With $x > 60$ the temperature dissipation spectrum increases sharply (curves 2, 4 in Fig. 2,a), that is, in the region of small scales the local gradients can be significant. This peculiarity in the behavior of the turbulence spectra with large Pr numbers was noted earlier in [5].

This analysis and the numerical examples presented in Fig. 1 and Fig. 2 show that in a stratified fluid the turbulence spectra have a nonuniversal form. The behavior of the spectral densities in a broad range of wave numbers is determined by the Re number (or the Γ_0 value), the Rf number and the Pr number. The inertial interval of scales exists with a sufficiently large Re number and not excessively great Rf (in the case of stable stratification).

These qualitative conclusions agree well with observations [1, 2]. However, for the time being it is difficult to put the measured spectra [1, 11] and the formulas derived above in unambiguous correspondence [1, 11]. The nonuniversal form of the turbulence spectra, as was demonstrated, is related to the properties of the mean velocity and temperature fields, that is, for comparison of theory and experiment

it is necessary to have information not only on the regime of fluctuations of the velocity and temperature fields, but also data on the mean gradients of these fields at the measurement point. At present there are still no such measurements.

BIBLIOGRAPHY

1. Grant, H. L., Hughes, V. A., Vogel, W. M. and Moilliet, A., "The Spectrum of Temperature Fluctuations in Turbulent Flow," J. FLUID MECH., 34, No 3, 1968.

2. Ozmidov, R. V., "Second Voyage of the Scientific Research Ship 'Dmitriy Mendeleyev'," OKEANOLOGIYA (Oceanology), 11, No 1, 1971.

3. Obukhov, A. M., "Influence of Archimedes Forces on the Structure of the Temperature Field in a Turbulent Flow," DOKL. AN SSSR (Reports of the USSR Academy of Sciences), 125, No 6, 1959.

4. Boldgiano, R., "Turbulent Spectra in a Stably Stratified Atmosphere," JOURNAL OF GEOPHYS. RES., 64, No 4, 1959.

5. Monin, A. S. and Yaglom, A. M., STATISTICHESKAYA GIDROMEKHANIKA (Statistical Hydromechanics), Part 1, Moscow, "Nauka," 1965; Part 2, 1967.

6. Gibson, C. M. and Schwarz, W. H., "The Universal Equilibrium Spectra of Turbulent Velocity and Scalar Field," J. FLUID MECH., No 3, 16, 1963.

7. Stewart, R. W. and Townsend, A. A., "Similarity and Self-Preservation in Isotropic Turbulence," PHILOS. TRANS. ROY SOC., A243, No 867, 1951.

8. Monin, A. S., "Spectrum of Turbulence in a Temperature-Inhomogeneous Atmosphere," IZV. AN SSSR: SERIYA GEOFIZ. (News of the USSR Academy of Sciences: Geophysical Series), No 3, 1962.

9. Batchelor, G. K., Howells, I. D. and Townsend, A. A., "Small-Scale Variation of Convected Quantities Like Temperature in Turbulent Fluid," J. FLUID MECH., No 1, 5, 1959.

10. Batchelor, G. K., "Small-Scale Variation of Convected Quantities Like Temperature in Turbulent Fluid," J. FLUID MECH., No 1, 5, 1959.

11. Belyayev, V. S., Lyubimtsev, M. M. and Ozmidov, R. V., "Rate of Dissipation of Turbulent Energy and Rate of Evening-out of Temperature Inhomogeneities in the Ocean," IZV. AN SSSR: FIZIKA ATMOSFERY I OKEANA (News of the USSR Academy of Sciences: Physics of the Atmosphere and Ocean), 9, No 11, 1973.

5303
CSO: 8144/1839

INTERNAL GRAVITATIONAL WAVES IN OCEAN

Moscow ISSLEDOVANIYE IZMENCHIVOSTI GIDROFIZICHESKIKH POLEY V OKEANE in Russian 1974 pp 91-98

[Article by Yu. A. Ivanov, Ye. G. Morozov and A. S. Samodurov from monograph "Ocean Research on Hydrophysical Field Variability, edited by R. V. Ozmidov, doctor of physical and mathematical sciences, Izdatel'stvo "Nauka", 211 pages, number of copies printed unknown]

[Text] Intensive experimental investigations in the ocean carried out during recent years have made it possible to study a number of important characteristics of internal gravitational waves in the real ocean.

We will examine the principal results of these investigations. On the basis of an analysis of long series of measurements of fluctuations of temperature and currents in the Atlantic polygon [1] information was obtained on the distribution of the energy of fluctuations in a wide frequency range. Figure 1 shows the spectrum of temperature fluctuations, from which it can be seen that the energy-bearing bursts of spectral density are in tidal (semidiurnal and diurnal) and inertial periods. The spectral density decreases sharply in the direction of high frequencies and its values here are one or two orders of magnitude less.

As indicated by an analysis of the measurements [2], the fluctuations of hydrological fields with a tidal period are determined by the propagation of internal waves of a tidal period. As an illustration, below we give the coherence and phase shift of fluctuations of a semidiurnal period as a function of distance:

L, miles	5	20	30	50	70	80
H (12 hours)	0.88	0.85	0.83	0.85	0.77	0.73
$\Delta\varphi$ (12 hours) degrees	18	56	100	156	264	320

These data were obtained from temperature measurements in the Atlantic polygon for eight points at the 1,000-m horizon. The monotonic increase in phase with distance and the high coherence give basis for assuming that the observed fluctuations are a result of the propagation of an internal gravitational wave.

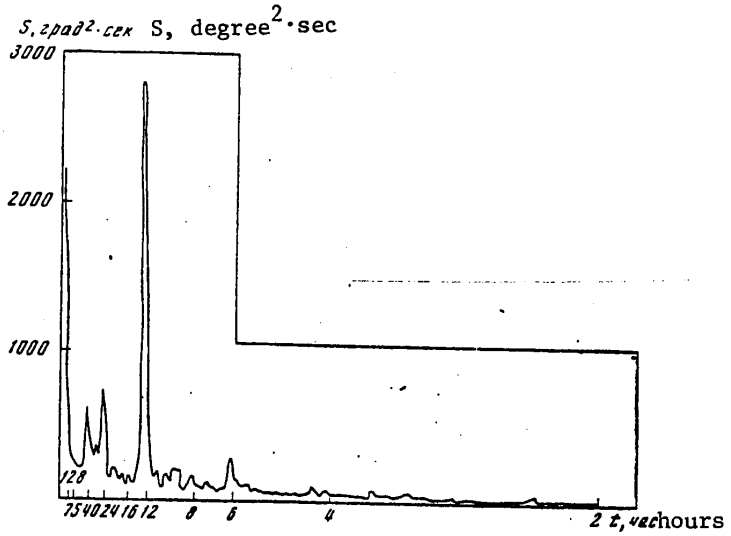

Fig. 1. Spectral density of temperature fluctuations at the 200-m horizon (Atlantic polygon, 1970). The length of the series is 5 months, the discreteness of the measurements is 30 minutes.

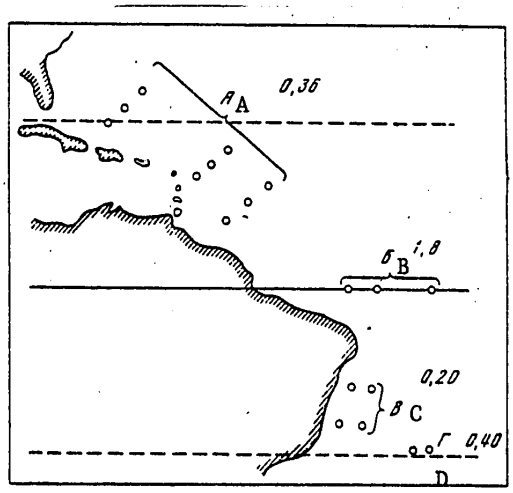

Fig. 2. Diagram of location of research regions. The figures represent the maximum dispersion values; the letters indicate the research regions.

The phase diagrams constructed on the basis of measurements of temperatures and currents in the polygon confirm this conclusion. The lengths of the waves determined from the diagrams for the measurements made during different periods were virtually

identical and equal to 110-120 km. The direction of wave propagation was maintained. The length of the semidiurnal internal wave of the first mode, computed from the dispersion expression with a close approximation of the vertical density distribution, gives virtually the same value*. Waves of such a type, as indicated in [3, 4], are generated during the interaction of a barotropic tide with bottom relief nonuniformities. Experiments on the shelf [5, 6] confirm this result.

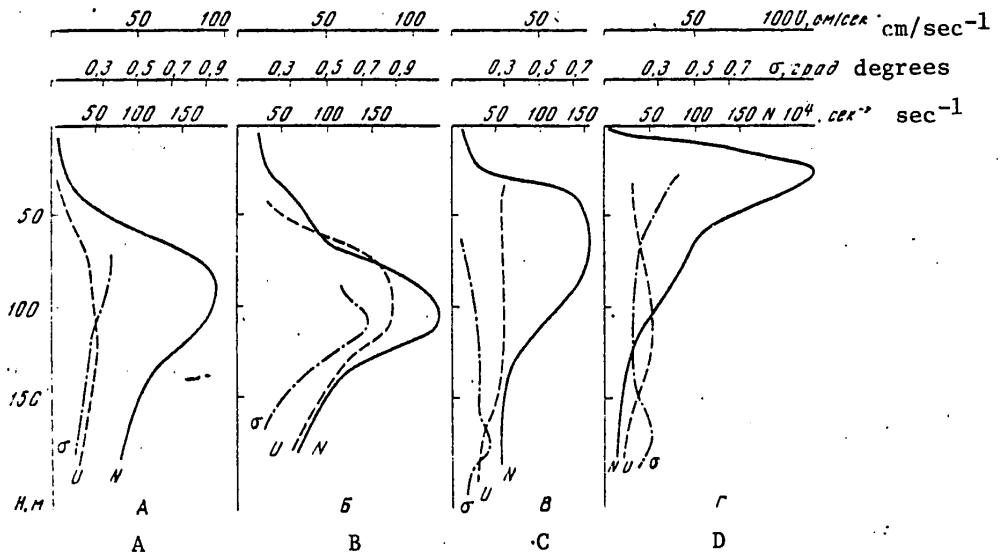

Fig. 3. Profiles of Väisälä-Brent period, current velocities and standard deviation of temperature fluctuations with depth for different research regions. The letters denote the research regions.

Considerable fluctuations of hydrological fields at frequencies close to inertial are also discovered in the experimental spectra. There is always some frequency shift of the burst of the spectral density function relative to the inertial frequency. Cross-statistical analysis of the measurements indicates a relatively rapid attenuation of coherence horizontally. In the Atlantic polygon on the basis of temperature measurements at three points situated at a distance of 15 miles from one another it was possible to determine the wavelength and direction of propagation of disturbances with a frequency close to inertial [2]. It can be seen from the computations that these disturbances may correspond to the propagation of waves whose length is 25 miles to the south-southeast. Measurements [7] show that the spectrum of temperature fluctuations near the inertial frequency has a sawtooth-like character (somewhat separated by frequency of the peaks). On the other hand, in [8], on the basis of measurements at points situated along the meridian it was found that the energy of the fluctuations at the inertial frequency at the first point also has bursts at more southerly points. These experimental results are in agreement with the Munk-Phillips theoretical model. In this model it was possible

* Thus, measurements in the Atlantic polygon indicate the existence of stationary systems of internal tidal waves.

to obtain an asymptotic form of solutions for internal waves at frequencies close to inertial periods. The dependence of the solutions on latitude is expressed through the Airy functions. An evaluation of the Airy scale gives a value 25 miles. The problem of the generation of internal inertial waves for the time being has not had either an experimental or theoretical solution.

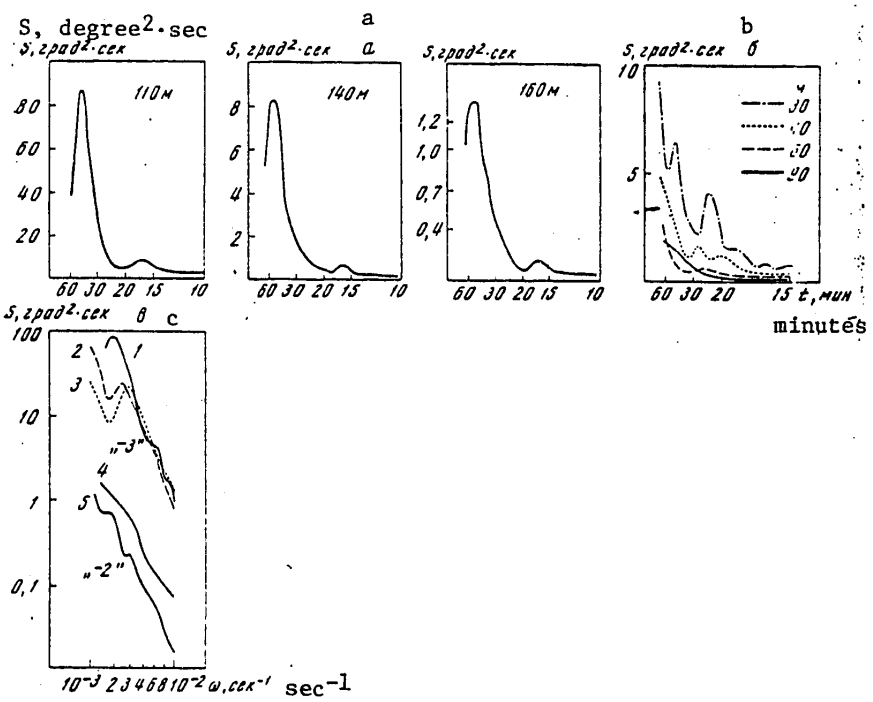

Fig. 4. Graphs of spectral densities of temperature fluctuations. a) equatorial region; b) region of northern tropic; c) 1, 2, 3 -- fluctuations at the equator at the horizon 110 m at different times of investigation; 4) region Γ , horizon 110 m; 5) region A, horizon 120 m.

Fluctuations of the characteristics in the higher frequency range, corresponding to an interval of periods less than 12 hours and more than 10 minutes (average discreteness of standard instruments), were studied in many characteristic regions of the ocean under different mean conditions (vertical density stratification, vertical velocity shear) [10]. First of all it should be noted that the dispersion of fluctuations in this frequency range changes substantially in time and space. Figure 2 shows the maximum dispersion values in the upper thermocline, determined from 24-hour series, for some regions of the Atlantic Ocean. A comparative analysis of the stated dispersion values with the mean vertical density and current velocity profiles shows that the dispersion increases with an increase in the mean velocity shear. The greatest dispersion is observed in the equatorial region, where the vertical velocity shear is maximum. The observed stratification differences do not introduce a significant contribution to the change in dispersion. With virtually coinciding density and temperature profiles the dispersions can differ substantially. The form of the distribution of dispersion with depth in most cases corresponds

to the vertical profile of the Väisälä-Brent frequency. However, there are cases when the maximum dispersion values are discovered in the layer where the vertical density gradients are less than in the density jump layer (Fig. 3).

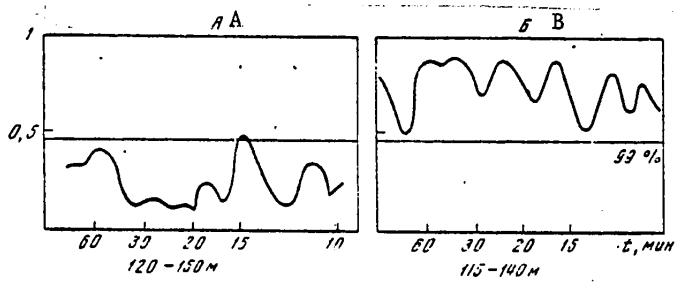

Fig. 5. Graphs of coherence functions between records at different horizons. A, B) investigated regions.

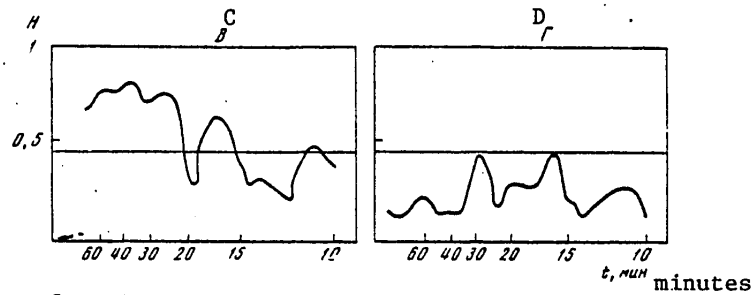

Fig. 6. Coherence functions between temperature fluctuations and current velocity modulus for horizon 110 m. C, D) investigated regions.

The form of the spectra, as indicated by computations, is dependent on the dispersion of the oscillations. The dropoff of the spectral density functions for regions with a small dispersion approaches the "-2 law"; at the equatorial stations, where the dispersion is maximum, the dropoff is close to "-3" (Fig. 4,c). In the layer of the upper thermocline with small values of the total dispersion the spectra are considerably deformed with depth and the spectral density peaks move along the frequency axis. In the case of great dispersions there are virtually no distortions of the spectra (Fig. 4,a,c).

A cross-analysis of temperature fluctuations in the vertical section also indicates a difference in the statistical properties of the two mentioned types of fluctuations (maximum and minimum of the total dispersion) (Fig. 5). A common characteristic is the appearance of maximum coherence in the layer where the dispersions are maximum. The fluctuations of characteristics above and below this layer are displaced in phase. For equatorial stations (maximum dispersion) a high coherence in a broad frequency range is discovered in the entire layer of the upper thermocline. At stations occupied beyond the equator coherence values above the confidence level are discovered in thin layers in a narrow frequency range. At some stations the coherence in the entire layer is below the confidence level.

The results of a cross-analysis between temperature fluctuations and the current velocity modulus (the instruments were spaced 1-2 m vertically) are of interest. Figure 6 shows examples of the results of a cross-analysis. In the equatorial region the coherence is great in most of the studied frequency range; in other regions it is almost everywhere below the confidence level.

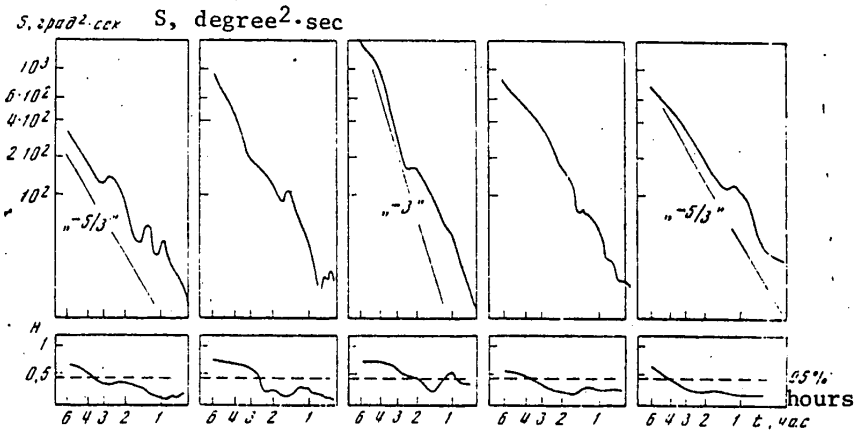

Fig. 7. Spectral densities of temperature fluctuations for horizon 125 m and coherence between fluctuations at 125 and 150 m.

Thus, the most intensive fluctuations of the hydrological fields in the considered frequency range, observed in the equatorial region and probably characteristic of other regions of boundary currents with a great vertical shear, are characterized by statistical properties which indicate a wave nature of these fluctuations. In the ocean area where there are small mean velocity shears and small dispersion values the fluctuations of the hydrological characteristics are determined by unsteady internal waves and turbulent fluctuations.

In an analysis of long series of measurements there is found to be an intermittence of the energy of fluctuations with time. Such results were obtained in measurements in polygons in the Black Sea, Atlantic and Indian Oceans, that is, this phenomenon has a general character. Figure 7, based on temperature measurement data for the polygon in the northwestern part of the Indian Ocean, shows spectral density curves constructed with a three-day shift. With an increase in the total dispersion there is an increase in the slope of the spectrum from "-5/3" to "-3" and an increase in vertical coherence; then, when the dispersion decreases, the slope of the spectrum becomes, as before, "-5/3" and the coherence decreases. Such patterns to one degree or another are manifested in an analysis of all long measurement series.

It can be concluded from the results of experimental investigations that internal gravitational waves are generated as a result of the instability of motion of a stratified fluid with a vertical velocity shear. It was demonstrated in [11] that instability arises when the Richardson number is less than one-quarter and the coefficients of wave growth increase with a further decrease in this number. At least qualitatively the experiments correspond to the theoretical conclusions. As a rule it is impossible to carry out quantitative evaluations on the basis of available measurements since there is no detailed information concerning the vertical

structure of density and currents.

Investigation of microscale turbulence is closely related to the problem of the destruction of internal gravitational waves. This process is probably one of the principal sources of generation of turbulence in a density-stratified ocean [12]. There has been virtually no experimental study of the process of destruction of internal gravitational waves in the ocean. In [13] an attempt was made to describe the manifestation of this process by computing the changes in potential energy in the layer 50-250 m during the propagation of a train of waves. Computations show that an increase in potential energy is about 10% of the change in energy with total mixing of this layer. The potential energy was computed by the averaging of data from bathometric series registered before and after propagation of the train. Accordingly, the evaluation can contain an error, but such an approach with the availability of special measurements can be promising.

A theoretical study of the processes of destruction of internal gravitational waves is being carried out in two principal directions. The first direction is an investigation of the stability of small disturbances imposed on the mean state; the second is a study of the nonlinear interaction of waves. The stationary distribution of the field of currents and density is used as the mean state. In [11, 13-15] the mean state (current density and velocity) is a function only of the vertical coordinate, that is, a study is made of the stability of disturbances relative to velocity shear in a vertically stratified fluid. As a result of these investigations it has been demonstrated that if the Väisälä-Brunt frequency and the velocity gradient are dependent on the vertical coordinate, the characteristic values of the problem will be complex with $Ri < 1/4$. This indicates an instability of small fluctuations. Naturally, these complex characteristic values still do not indicate a process of wave destruction, but give basis for assuming that if the receipt of energy from mean motion is equal to the dissipation in the wave, neutral waves of a finite amplitude are formed; however, if the receipt of energy exceeds the rate of dissipation, the wave amplitude will increase, which can also lead to its destruction. Here intelligible results can be obtained only in a nonlinear formulation. In [16] a study was made of the behavior of disturbances in a fluid with a horizontally variable Väisälä-Brunt frequency. As a result it was found that with an approach to the point $N(x_0) = \omega$ (ω is wave frequency, $N(x_0)$ is the Väisälä-Brunt frequency at the point x_0) the wave amplitude increases and the wave length decreases. The wave deformation can cause its destruction, which, however, has a different nature than that described above (receipt of energy from mean movement). Like surface waves internal waves can be destroyed when they encounter the shore slope. This effect was investigated by Woods [17] in a model of a corner region. It was demonstrated for the case N-const that waves lose stability under the condition

$$\operatorname{tg}\theta < \sqrt{\omega^2/(N^2 - \omega^2)},$$

where θ is the angle between the horizontal wall and a sloping bottom, ω is angular frequency. The amplitude increases with approach to the corner point approximately inversely proportionally to the distance to it. This inequality was also obtained by Munk and Winbush [18].

The conclusions from the theory of stability of plane-parallel movement of a stratified fluid with a velocity gradient were applied by Phillips [19] and Munk and Garrett [20] to wave movement. In these studies the local instability

criterion is determined in the wave process by analogy, that is, with such an approach it is assumed that the critical Richardson number is formed as a result of disturbance of the mean state, which in itself is stable. In the latter study these considerations are applied to an examination of the superposing of waves, which can consist of the entire spectrum of the internal gravitational waves. It is assumed that the criterion can be realized sporadically at individual points in space and time (coincidence of phases) in the wave process, and accordingly, lead to the local destruction of waves. However, if the wave process already is developing against a background of considerable quasimean current gradients, the total critical Richardson number (of mean state and the wave process) no longer requires unrealistically great slopes of individual waves (h/λ is the amplitude-length ratio), as was necessary in [19]. It appears that the qualitative mechanism of destruction of internal waves described in [20] can be of great importance in the energy supply of the ultrashort-wave part of the spectrum of fluctuations of physical fields in the ocean.

The criterion of destruction of waves $Ri < 1/4$ for real conditions may be too strong, since it was obtained in linear theories in which no allowance is made for the finite nature of amplitude in the wave. A study by Orlanski and Bryan [21] described a numerical experiment for study of the nonlinear interaction of waves. The authors ascertained the condition for the overturning of a nonlinear internal wave as a result of an increase in amplitude in the absence of a mean current

$$u > c.$$

Here u is the horizontal component of the orbital velocity of particles in the wave, c is the phase velocity of the wave.

It is of interest to examine the interaction of a nonlinear wave with a quasimean state in the presence of current velocity. It can be surmised that allowance for currents leads to a weakening of the determined criterion.

Thus, the destruction of internal gravitational waves, on the one hand, is determined by the total energy of the characteristic wave process, and on the other hand, inhomogeneities of the medium (velocity shear, horizontal nonuniformity of the density field) in which the wave is propagated.

We note in conclusion that virtually all the problems considered in this study are only in the initial stage of their solution. The problem of the stability of internal waves, their destruction and the generation of microscale turbulence has only a hypothetically qualitative solution and therefore requires the carrying out of specialized experiments.

BIBLIOGRAPHY

1. Brekhovskikh, L. M., Ivanov-Frantskevich, G. N., Koshlyakov, M. I., Fedorov, K. N. and Yampol'skiy, A. D., "Some Results of a Hydrophysical Experiment in the Tropical Atlantic," IZV. AN SSSR: FIZIKA ATMOSFERY I OKEANA (News of the USSR Academy of Sciences: Physics of the Atmosphere and Ocean), No 5, 1971.

2. Ivanov, Yu. A. and Morozov, Ye. G., "Investigation of Fluctuations of Temperature in the Tidal and Inertial Periods," TRUDY IN-TA OKEANOLOGII. GIDROFIZICHESKIY POLIGON 70 (Transactions of the Institute of Oceanology. Hydrophysical Polygon 70), Moscow, "Nauka," 1974.

3. Cox, C. S. and Sandstrom, H., "Coupling of Internal and Surface Waves in Water of Variable Depth," J. OCEANOGR. SOC. JAPAN, 1962, 20th ANNIV. VOLUME.

4. Pammpu, M., "Development of Internal Tides in the Coastal Zone," VNUTRENNIYE VOLNY (Internal Waves), Moscow, "Mir," 1964.

5. Reid, J. L., "Observations of Internal Tides in October 1950," TRANS. AMER. GEOPHYS. UNION, 37 (3), 1956.

6. Summers, H. J. and Emery, K. O., "Internal Tides of Tidal Period Off Southern California," J. GEOPHYS. RES., 68(3), 1963.

7. Webster, F. and Fofonoff, N., "A Compilation of Moored Current Meter Observations," WOODS HOLE OCEANOGR. INST. TECHN. REPT., No 3, pp 61-66, 1967.

8. Hendershott, Myrl C., "Inertial Oscillations of Tidal Period," Ph. D. Thesis, Harvard Univ., 1964.

9. Munk, W. and Phillips, N., "Coherence and Band Structure of Inertial Motion in the Sea," RES. GEOPH., 6(4), 1968.

10. Ivanov, Yu. A. and Morozov, Ye. G., "Analysis of Water Temperature Fluctuations in the Upper Layer of the Ocean," IZV. AN SSSR: FIZIKA ATMOSFERY I OKEANA, 9, No 10, 1973.

11. Miles, J. W., "On the Stability of a Heterogeneous Shear Flow," J. FLUID MECH., 10(4), 1961.

12. Monin, A. S. and Yaglom, A. M., STATISTICHESKAYA GIDROMEKHANIKA (Statistical Hydromechanics), Part 1, Moscow, "Nauka," 1965, Part 2, 1967.

13. Morozov, Ye. G., "Destruction of Internal Waves," OKEANOLOGIYA (in press).

14. Thorpe, S. A., "Experiments on the Instability of Stratified Shear Flow: Miscible Fluids," J. FLUID MECH., 46(2), 1971.

15. Wunch, C., "On the Propagation of Internal Waves Up a Slope," DEEP SEA RES., 15(3), 1968.

16. Samodurov, A. S., "Internal Waves in a Medium With a Väisälä-Brunt Frequency Varying Horizontally," IZV. AN SSSR: FIZIKA ATMOSFERY I OKEANA (in press).

17. Woods, J., "Investigation of Some Physical Processes Associated With a Vertical Heat Flow Through the Upper Layer of the Ocean," FORMIROVANIYE STRUKTURY I FLUKTUATSII VERKHNEGO TERMOKLINA V OKEANE (Formation of Structure and Fluctuations of the Upper Thermocline in the Ocean), Moscow, Gidrometeoizdat, 1971.

18. Munk, W. and Wimbush, M., "Simple Criterion for the Destruction of Waves on a Shore Slope," OKEANOLOGIYA (Oceanology), No 1, 1969.

19. Phillips, O. M., DINAMIKA VERKHNEGO SLOYA OKEANA (Dynamics of the Upper Layer of the Ocean," Moscow, "Mir," 1969.

20. Garrett, C. and Munk, W.,"Oceanic Mixing by Breaking Internal Waves," DEEP SEA RES., 19 (12), 1972.

21. Orlanski, J. and Bryan, K., "Formation of the Thermocline Step Structure by Large Internal Gravity Waves," J. GEOPHYS. RES., 74(28), 1969.

5303
CSO: 8144/1839

CONSTRUCTION OF RECORDING COMPLEX FOR INVESTIGATING FINE OCEAN STRUCTURE

Moscow ISSLEDOVANIYE IZMENCHIVOSTI GIDROFIZICHESKIKH POLEY V OKEANE in Russian 1974 pp 155-162

[Article by V. P. Vorob'yev and L. G. Palevich from monograph "Ocean Research on Hydrophysical Field Variability," edited by R. V. Ozmidov, doctor of physical and mathematical sciences, Izdatel'stvo "Nauka", 211 pages, number of copies printed unknown]

[Text] Towed measurement complexes, including those for measuring mean and fluctuating values of various parameters, are used extensively by the Institute of Oceanology imeni P. P. Shirshov of the USSR Academy of Sciences in experimental studies of microscale hydrophysical processes. There is a clear tendency to these complexes becoming more complicated due to the need for increasing the number of measured parameters. Whereas in experiments carried out by the Institute of Oceanology in 1968 [2] the towed line carried only one instrument for measuring velocity fluctuations in water masses, in subsequent work by the institute's research ships the towed line was transformed into a diversified measurement complex. In particular, on the 7th voyage of the research ship "Dmitriy Mendeleyev" in 1971-1972 use was made of towed complexes with instruments for simultaneous measurement of the fluctuating and mean velocity, conductivity and temperature values in the ocean medium, instrumentation for measuring submergence depth and instrument carrier vibrations and a number of other auxiliary devices. Measurements of some parameters were made synchronously at several horizons

The towed complexes usually consist of experimental models of measurement instruments whose reliability is not always adequately high; sometimes, for comparative purposes, use is made of measurement instruments designed on different physical principles for measuring the same parameter (for example, thermoanemometric, hydroresistor, electromagnetic instrumentation for measuring velocity fluctuations, etc.). Accordingly, the task of monitoring the performance of measurement complex components is assuming great importance in different types of experimental work so that the experimenter can, in case of need, without interrupting the experiment, adjust the measurement complex or even restructure it in order to ensure continuation of a maximum information yield when individual components of the complex malfunction. The conditions prevailing on long oceanic expeditions impose additional requirements on the measurement complex as a whole with respect to reliability and performance since an oceanic experiment is very costly, is limited in time and usually there is no possibility of repeating measurements. Repetition of an experiment usually involves the organization of a new expedition. Accordingly, in implementing a physical experiment in the ocean the design of a complex simultaneously performing instrument monitoring functions and graphic visualization of results

of the measurements for the purpose of controlling the towed complex is transformed, as the latter becomes more complicated, into an independent task, in many cases more complex than the construction of the measurement complex itself.

Work on formulating the principles for constructing the registry complex were initiated at the institute, including by the authors, immediately after implementation of the first specialized hydrophysical voyage in 1968. On the 9th voyage of the scientific research vessel "Akademik Kurchatov" this problem was dealt with by a specialized detachment which successfully carried out the registry and speedy processing of experimental data. On the 7th voyage of the scientific research vessel "Dmitriy Mendeleyev" use was made of several extremely complex towed complexes, there was an increase in the number of measured parameters and more perfect recording apparatus was used for data registry. On this voyage much work was done for improving the recording complex, directed primarily to improvement in the system for functional monitoring of the measurement complex and methods for preparing for an experiment and carrying it out.

The authors carried out this work applicable to a towed measurement complex consisting of instrumentation developed at the Special Design Bureau of Oceanological Apparatus of the Institute of Oceanology of the USSR Academy of Sciences (OKB OT complex).

In determining the principal hydrophysical parameters -- fluctuating and mean values of velocity, temperature and conductivity -- use was made for the most part of new experimental models of measurement instruments. The technical specifications of these instruments are given in the table. Standard-produced industrial instruments were used for measuring the depth h of submergence and vibrations of the carrier α_x, α_y, α_z: vibration pressure sensor of the DDV type and accelerometric ceramic vibration sensors.

Highly reliable standard-produced instruments were used in constructing the recording complex. The Soviet-produced apparatus used included EPP-09 automatic recorders, N-700 loop oscillograph with registry on ultraviolet photopaper, pen five-channel N-327-5 automatic recorder, Ch-3-30 frequuency meters, SICh-1 low-frequency spectrum analyzer (parallel-action type) with photoattachment, standard controlling amplifiers from electronic modeling units, digital voltmeters, one- and two-ray oscillographs.

Among foreign instrumentation use was made of: Japanese four-channel magnetic recorder, type R-400, of the TEAS Company. This magnetic recorder, with a registry rate of 3 inches/sec, has a bandwidth 0-1000 Hz, with a rate 20 inches/sec -- 0-20 KHz, allowing for a transformation of signal frequencies during reregistry or when working with a spectrum analyzer; the dynamic range is 40-43 db; the error is not greater than 1%; the input resistance is 100 kilohm and the output resistance about 10 ohm. A "Rikadenki" three-channel automatic pen recorder with a bandwidth up to 20 Hz; DISA amplifiers with an amplification factor 10 db, supplied with low- and high-frequency filters (attenuation 6 db/octave); DISA quadratic voltmeters with an averaging time from 0.1 to 30 sec.

When working with the OKB OT towed measurement complex in the first polygons use was made of traditional placement of measurement and recording instruments [3], as shown in Figures 1 and 2. In particular, in polygon 3 (Timor Sea, 21-22 January

1972), the principal parameters in the experiment were the mean and fluctuating values of velocity and salinity which were fed to four channels of one of the magnetic recorders through decoupling amplifiers. The working band of the amplifier of fluctuating parameters began from 1.5 Hz, whereas the amplifiers of mean values had a working band beginning from 0 Hz.

In order to evaluate the influence of vibrations of the carrier on measurement of fluctuations of velocity in the immediate neighborhood of the IPS sensors there were vibration sensors. The components of vibrations α_x, α_y and α_z are registered on a second magnetic recorder together with the signal u'. The repeated registry of the u' parameter on the second magnetic recorder was caused by the necessity of synchronization with the introduction into the electronic computer of signals from different magnetic recorders for the purpose of eliminating discrepancies in the rates of movement of the magnetic recorder carrier. Taking this into account, it is also necessary to register on the common carrier groups of signals which it is proposed be processed jointly thereafter. In addition, the presence of a common signal considerably facilitates comparison of the results from different magnetic recorders when visualizing data on photopaper.

Technical Specifications of OKB OT Complex Instruments

Type of measurement instrument	Measured parameter	Notation	Measurement range	Frequency range
Thermoanemometric instrument for measuring velocity fluctuations (IPS)	Mean velocity	u	1-5 m/sec	0-0.3 Hz
	Velocity fluctuations	u'	±25 cm/sec	1.5-150 Hz
Hydroresistor instrument for measuring velocity fluctuations (GIPS)	Mean velocity	$\overline{u}$	1-10 m/sec	0-0.3 Hz
	Velocity fluctuations	u'	±25 cm/sec	1.5-1000 Hz
Hydroresistor instrument for measuring conductivity fluctuations (GIPE)	Mean conductivity	$\overline{\sigma}$	3000-6000 mmho/m	0.1 Hz
	Conductivity fluctuations	σ'	±100 mmho/m	1.5-1000 Hz
Thermistor instrument for measuring mean temperature (TIST)	Temperature	$\overline{T}$	-2+30°C	0-1 Hz
Film instrument for measuring temperature fluctuations (IPT)	Temperature fluctuations	T'	±1°C	1.5-150 Hz

In order to form some idea concerning the nature of hydrophysical processes in the polygon the principal parameters u', σ' and the mean temperature T_3 at the horizon for measuring these parameters (and sometimes also α_x, α_y and α_z) were visualized at the time of the experiment using an N-700 loop oscillograph. Thereafter this oscillogram served as a basis for choosing records for input into the electronic

computer. Monitoring of instrument performance and an approximate rejection of signals caused by grid induction or distortions associated with limitations in the amplifiers were both accomplished using electronic oscillographs.

Temperature sensors, attached on a towed line and catamaran, had a time constant of about 1 sec and therefore temperature data were visualized on EPP-09 automatic recorders and a five-pen N-327-5 automatic recorder for creating a general picture of temperature changes at the horizons.

In accordance with the method employed by the institute on preceding voyages [4-6], the carrying out of experiments with a towed complex was preceded by a study of materials from a hydrological investigation of the polygon, and, in particular, bathythermograms. In order to clarify the general pattern of small-scale processes we selected both the horizons with minimum and maximum vertical temperature gradients and the horizons where there was a sharp bend on the bathythermogram; we also took into account the characteristics of currents at different horizons. Figure 3 shows a bathythermogram of one of the polygons on the 7th voyage (fifth polygon, equator in the neighborhood of the Maldive Islands (13-14 February 1972)), with the noted towing horizons. From the point of view of the experimenter, one should expect difficulties (which in the course of the experiment was also confirmed when carrying out measurements at the horizons 55, 105, 120, 129 m), characterized by a sharp temperature change in a relatively thin layer, which is associated with the need for a very rigorous monitoring of the depth of submergence of the carrier. An investigation of the neighborhood of horizon 129 m indicated that a change in the depth of submergence of the towed measurement complex by even 0.5 m gives a substantially different picture of small-scale hydrophysical processes [7]. Using visualization of the temperature gradients in the measurement zone (Fig. 4), the authors succeeded in considerably expanding the possibilities of the experiment. According to Monin [1, 7], the data obtained in instrumental investigations of small-scale processes contain information on the small-scale turbulence, on microstructure and on internal waves.

In this light the visualization of gradient measurements in the course of an experiment is especially important.

The data from vertical soundings, traditionally carried out at the beginning of the polygon, are points of departure in the first stage of the experiment with a towed complex. Later, after several hours of work and increasing distance from the sounding point -- tens of miles -- the features of vertical structure of interest to the researcher are usually displaced in depth due to the spatial and temporal variability of hydrophysical fields in the thickness of the ocean. Naturally, the initial choice of the measurement horizons prior to an experiment is of a preliminary character and there is need for correction in the course of the experiment. The use of so-called "losable probes" is extremely promising for this purpose. Such probes have already come into rather extensive use in the United States (for example, see [8]) for the most part for military purposes and fishing. The introduction of "losable probes" in the practice of the large-scale hydrophysical experiments developed and conducted by the Institute of Oceanology, it seems, would substantially increase the effectiveness of this method.

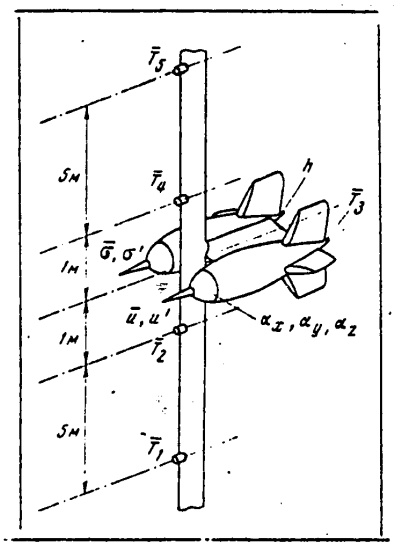

Fig. 1. Diagram of placement of sensors in towed "fish" and on towed line.

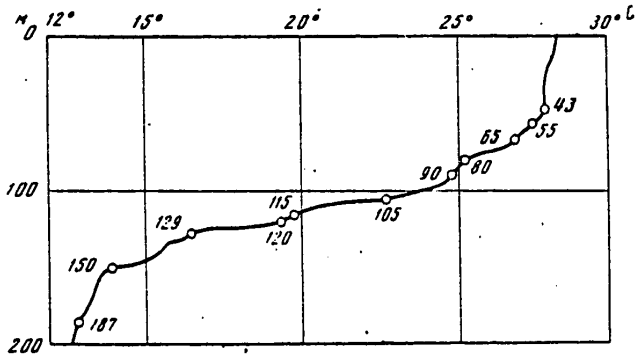

Fig. 3. Bathythermogram with noted towing horizons (in m).

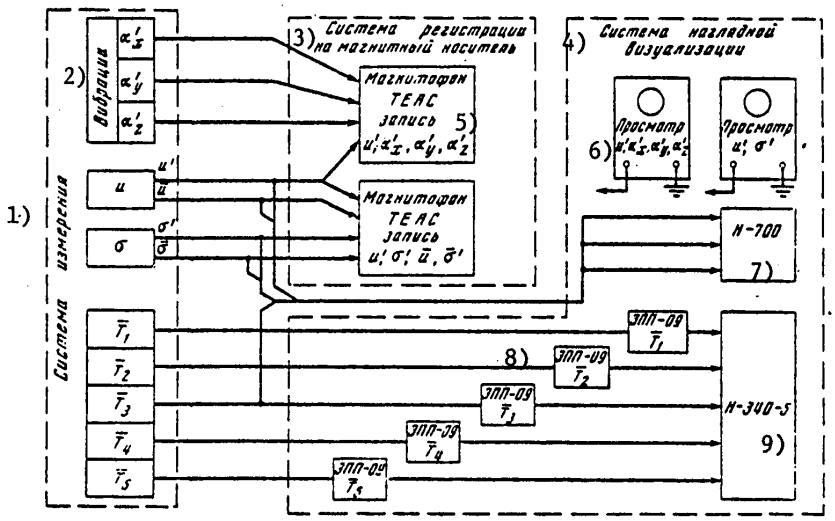

Fig. 2. Diagram of recording complex (in polygon 3).

KEY:

1. Measurement system
2. Vibrations
3. System for registry in magnetic cassette
4. Graphic visualization system
5. TEAS magnetic recorder, registry of
6. Examination of
7. N-700
8. EPP-09
9. N-340-5

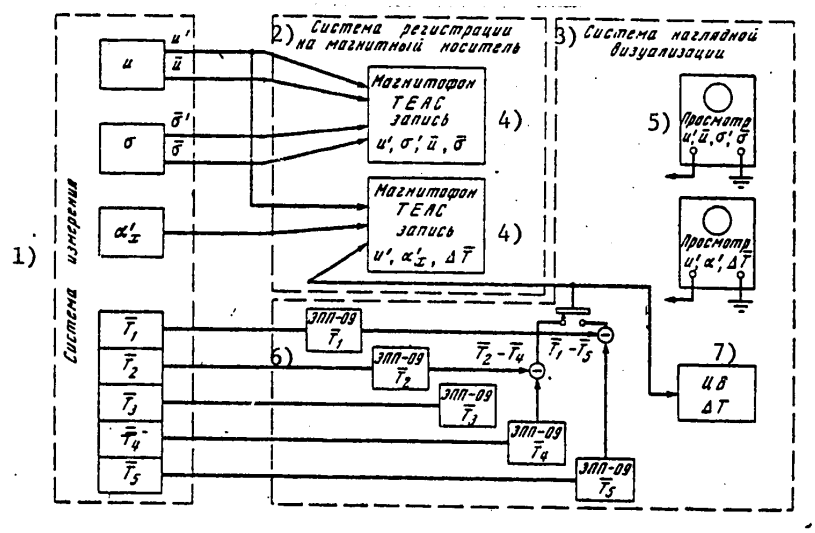

Fig. 4. Diagram of recording complex with gradient measurements (polygon 5).

KEY:

1) Measurement system
2) System for registry on magnetic carrier
3) Graphic visualization system
4) TEAS magnetic recorder
5) Examination of
6) EPP-09
7) Digital voltmeter

On the 7th voyage of the scientific research ship "Dmitriy Mendeleyev" there was also a further improvement in the recording complex associated with the introduction of a number of devices for operational control of the experiment. One of the last schemes is shown in Fig. 5 (station 510, equatorial zone of the Indian Ocean, 1 April 1972).

The first magnetic recorder was used in registry of the three fluctuating parameters u', σ', T' and the depth of submergence h. The T' and u' fluctuations are measured at a single point by a sensor with two sensitive film elements. The second magnetic recorder is used in registry of the mean values of these same parameters and the third is used in registry of longitudinal vibrations of the "fish" (α_x) and the vertical temperature gradient relative to the measurement point -- ΔT_0. The parameter u' was a common linking parameter for all the magnetic carriers, as in the preceding variant. The investigation of vibrations of the carrier of these instruments was not the objective of this experiment and therefore for monitoring purposes we registered only one component of vibrations α_x, which, it was established, can exert a maximum influence on the readings of the fluctuation sensors. The remaining vibration components were observed periodically during the measurements using an electronic oscillograph. The mean temperatures, as before, were registered on EPP-09 magnetic recorders.

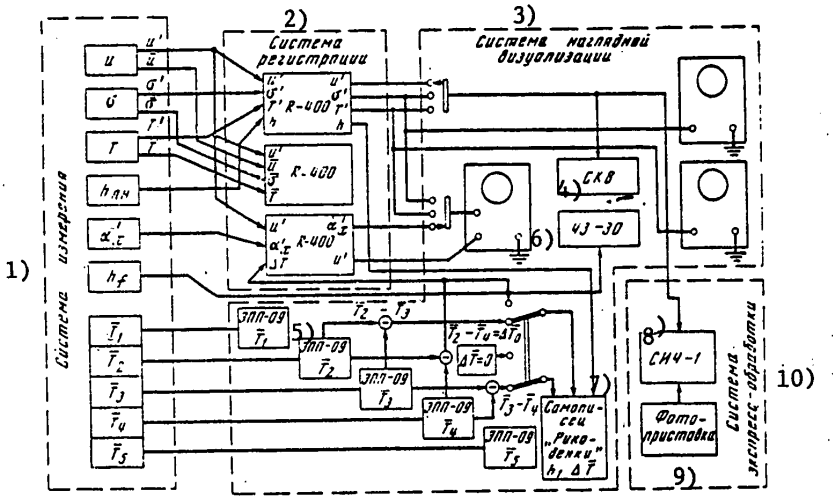

Fig. 5. Diagram of recording complex with gradient measurements.

KEY:

1) Measurement system
2) Registry system
3) Graphic visualization system
4) Mean square voltmeter
5) EPP-09
6) Ch-3-30 frequency meter
7) Rikadenki automatic recorder
8) SICh-1 spectrum analyzer
9) Photoattachment
10) Speedy processing system

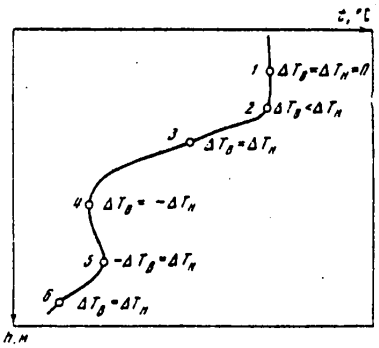

B = above
H = below

Fig. 6. Symbolic bathythermogram with discrimination of sectors on basis of gradient criteria.

The difference $\overline{T}_2 - \overline{T}_4$ was determined for measuring the temperature gradient in the zone of the towed instrument carrier. In addition, the vertical temperature gradients above and below the instrument "fish" $\Delta T_B = \overline{T}_2 - \overline{T}_3$ and $T_H = \overline{T}_3 - \overline{T}_4$ were determined, which together with the depth h were registered using a "Rikadenki" three-pen automatic recorder. For a more precise determination of the temperature

at extremal points use was made of digital voltmeters. It must be remembered that the gradients ΔT_B and ΔT_H may not be registered; they are auxiliary parameters rather than the main parameters and enable the experimenter to seek routinely and with the necessary accuracy the required measurement horizon or correct the towing depth if this is deemed necessary because the method for investigating the selected horizon may be different; there may also be an effort for precise tracing of a selected layer, even if it changes its depth, for example, due to internal waves, meandering relative this layer, and some other maneuvers with the measurement complex. An additional depth measurement element with an output to a Ch-3-30 frequency meter, by means of which the instrument carrier with great accuracy can be sited at the necessary measurement horizon, is also of substantial assistance in such maneuvering.

The introduction of new instrumental methods for checking the microstructure of the pycnocline substantially simplified control of the towed complex in the investigation of small-scale processes. In the example of a symbolic bathythermogram, represented in Fig. 6, whose appearance is extremely typical, it can be seen that by stipulating a definite value of the difference $\Delta T_B - \Delta T_H$ the experimenter can carry out towing in the stipulated layer, in case of necessity correcting the depth. For example, for investigating segment 4 it is possible to select the condition $\Delta T_B = -\Delta T_H$. For the extremal point 5 in the temperature inversion zone it is possible to select the condition $-\Delta T_B = \Delta T_H$. In an investigation of layers with a constant gradient (segments 3, 6) it is convenient to exercise control using the expression $\Delta T_B = \Delta T_H$ or even using the expression $\Delta T_B = \Delta T_H = 0$. The cited considerations can serve as a point of departure for creating an automated measurement complex in which the relationship $|\Delta T_B - \Delta T_H|$ is used as the adjustable parameter of a closed control system acting on the rudder device of the instrument carrier. [B = upper; H = lower]

With respect to use of the SICh-1 spectrum analyzer and the mean square voltmeter (in Fig. 4 denoted SKB), which were intended for the most part for analog speedy processing during the time of the experiment, it must be noted that a parallel-action spectrum analyzer can be used as a good indicator of the quality of the results from the point of view of the influence of the noise introduced by the shipboard net and also for rejecting unsuitable data in the experimental stage. The appearance of noise from the shipboard net is attributable to the fact that four generators operate on shipboard simultaneously in a synchronized regime. When there are peak loads created by powerful motors (motors of the active rudders, winches, etc.) the synchronization of the generators can change and the noise can attain appreciable levels. This noise freely passes through the power rectifiers of the measurement instruments and introduces noise into the units containing amplifiers capable of amplifying these low frequencies, that is, into all the instruments for measuring fluctuations and into the recording apparatus. This interference as a rule cannot be determined using an oscillograph, other than in the most conspicuous cases, and since it is virtually impossible to predict with what combination of operating shipboard motors this interference may appear, a spectrum analyzer must be an indispensable part of the recording complex as the only effective means making it possible to suspend in time the carrying out of experiments whose results will obviously be incorrect.

The results of operation of the improved towed complex on the 7th voyage of the scientific research ship "Dmitriy Mendeleyev" confirmed the usefulness and possibility of carrying out a controllable experiment, as is extremely important in an investigation of small-scale processes in the ocean. For a more operational control of the measurement complex and improvement in control it appears desirable to introduce some new improvements, enumerated below.

1. Introduction into the complex of apparatus for measuring the temperature gradients above and below the instrument "fish." The use of gradient meters not only will increase measurement accuracy and the information yield of the records, but also will make it possible to discriminate a parameter which is extremely important for control -- the derivative of the time gradient. A change of this derivative is needed by the operator for more precise holding of the instrument container in the selected temperature layer. With the creation of a self-controllable instrument container such a method will make it possible to make an attempt at a separate study of small-scale turbulence, the fine microstructure and internal waves, whereas the data now registered usually represent a superpositioning of these phenomena.

2. Introduction of additional spectrum analyzers for simultaneous monitoring of signals of fluctuating parameters for the purpose of determining noise. In addition, in the measurement of the spectra of several parameters in the experimental stage it is already possible to establish interrelationships with changes in different parameters.

3. For a continuing analysis of hydrological conditions during the time of towing it is necessary to give attention to the development of sounding apparatus operating while the ship is proceeding on course, in particular, simplified, inexpensive probes for one-time use which should be included in the makeup of the towed complexes.

BIBLIOGRAPHY

1. Monin, A. S., "Principal Features of Marine Turbulence," OKEANOLOGIYA (Oceanology), 10, No 2, 1970.

2. Ozmidov, R. V., "Second Voyage of the Scientific Research Ship 'Dmitriy Mendeleyev'," OKEANOLOGIYA, 11, No 1, 1971.

3. Ozmidov, R. V., "Experimental Investigation of Small-Scale Oceanic Turbulence on the 9th Voyage of the Scientific Research Ship 'Akademik Kurchatov'," VESTNIK AN SSSR (Herald of the USSR Academy of Sciences), No 7, 1971.

4. "Report on the Second Voyage of the Scientific Research Ship 'Dmitriy Mendeleyev'," Archives of the Institute of Oceanology, USSR Academy of Sciences.

5. "Report on the Fifth Voyage of the Scientific Research Ship 'Dmitriy Mendeleyev'," Archives of the Institute of Oceanology, USSR Academy of Sciences.

6. "Report on the Ninth Voyage of the Scientific Research Ship 'Akademik Kurchatov'," Archives of the Institute of Oceanology, USSR Academy of Sciences.

7. "Report on the Seventh Voyage of the Scientific Research Ship 'Dmitriy Mendeleyev'," Archives of the Institute of Oceanology, USSR Academy of Sciences.

8. Brown, N. L., Diehl, R. J., Marmin, H. B. and Stahl, P. S., MARINE SCI. INSTRUMENTATION, Vol 3, pp 91-97, 1965.

5303
CSO: 8144/1839

ABSTRACTS OF PAPERS IN 'ISSLEDOVANIYE IZMENCHIVOSTI GIDROFIZICHESKIKH POLEY V OKEANE'

Moscow ISSLEDOVANIYE IZMENCHIVOSTI GIDROFIZICHESKIKH POLEY V OKEANE in Russian 1974 pp 208-211

[Text] UDC 551.465.15

INVESTIGATION OF VARIABILITY OF HYDROPHYSICAL FIELDS IN OCEAN POLYGON

[Abstract of article by Ozmidov, R. V., Belyayev, V. S., Lyubimtsev, M. M. and Paka, V. T.]

[Text] The article describes a method for complex measurements of fluctuations of hydrophysical fields in a wide range of spatial-temporal scales. The authors give the results of measurements in the seventh polygon on the 7th voyage of the scientific research vessel "Dmitriy Mendeleyev." There was found to be a complex spatial-temporal structure of macro- and microscale background conditions on the basis of data from standard hydrological measurements using the AIST hydrophysical sonde, an acoustic current velocity sonde, radiotemperature buoy and temperature "trawl." There is a dependence between the intensity of microscale turbulence and local background conditions. Also given are the results of deep-water (up to 1200 m) measurements of conductivity fluctuations in a sounding regime. The strong variability of hydrophysical fields in the entire investigated range of scales is attributable to the interrelationship of different processes transpiring in the ocean. Figures 28, references 10. (p 3)

UDC 551.465.15

INTENSITY SPECTRA OF MICROPULSATIONS OF CURRENT VELOCITY AND DISSIPATION OF KINETIC ENERGY IN OCEAN

[Abstract of article by Belyayev, V. S., Gezentsvey, A. N. and Ozmidov, R. V.]

[Text] On the basis of measurement data for a number of ocean stations it was possible to obtain the intensity spectra of current velocity fluctuations and dissipation of turbulent energy in the upper 200-m layer of the ocean. The curves of distribution of the intensity of current velocity fluctuations in the spectrum of wave numbers in most cases have a tendency to saturation in the region of small wave numbers. In some cases the spectra of dissipation of turbulent energy attain

maxima in the investigated range of scales, which is evidence of an important influence of viscosity forces on pulsating movements. Figures 12, references 5. (p 31)

UDC 551.465.15

SPECTRAL CHARACTERISTICS OF FLUCTUATIONS OF CONDUCTIVITY FIELD IN OCEAN

[Abstract of article by Belyayev, V. S., Gezentsvey, A. N. and Ozmidov, R. V.]

[Text] The article gives the spectra of microscale fluctuations of the conductivity field $E_1(k)$, the spectra $kE_1(k)$ and $k^2E_1(k)$, where k is the wave number, in a series of polygons in the Indian and Pacific Oceans. The $E_1(k)$ spectral curves at a logarithmic scale can be approximated by straight lines with slopes changing in a relatively wide range. In some cases the $kE_1(k)$ spectral curves are saturated with small k. Figures 11, references 4. (p 42)

UDC 551.465.15

STATISTICAL EVALUATIONS OF PARAMETERS OF MICROSCALE TURBULENCE

[Abstract of article by Pozdynin, V. D.]

[Text] The author gives the results of a statistical processing of measurements of microscale turbulence in three polygons in the Atlantic Ocean. The measurements were made by the method of horizontal towing of instruments in the layer with a depth of 30-200 m. Estimates of the mean values, standard deviations and their 95% confidence intervals are given for the energy levels of turbulence, limiting horizontal correlation radii, Taylor microscales and the rates of dissipation of turbulent energy. Figures 7, tables 7, references 6. (p 50)

UDC 551.465.15

EXPERIENCE IN INVESTIGATING MICROSTRUCTURE OF CONDUCTIVITY FIELD IN OCEAN BY SOUNDING METHOD

[Abstract of article by Vorob'yev, V. P., Korchashkin, N. N. and Nikolayev, O. N.]

[Text] This paper is devoted to a study of the vertical microstructure of the conductivity field using a low-inertia sonde on a connecting electrical and supporting cable. A block diagram of a hydroresistor instrument for measuring sonde conductivity is given. On the basis of correlation functions and spectral curves obtained using an electronic computer there is a discussion of this experiment. Figures 4, references 3. (p 61)

UDC 551.501

METEOROLOGICAL SUPPORT FOR EXPERIMENTAL INVESTIGATIONS OF OCEAN TURBULENCE

[Abstract of article by Shishkov, Yu. A.]

[Text] The possible influence of macroscale atmospheric disturbances on the variability of the microscale structure of physical fields in the ocean is examined.

The author gives some methodological recommendations on the implementation of meteorological measurements. Figures 1, tables 1, references 8. (p 66)

UDC 551.465.15

BALANCE OF TURBULENT ENERGY IN OCEAN

[Abstract of article by Lozovatskiy, I. D.]

[Text] On the basis of data on current velocities obtained in 1970 in a polygon in the Atlantic Ocean it was possible to estimate the values in the equation for the balance of the mean density of kinetic energy of turbulent fluctuations in the ocean. Also examined is the spatial and temporal change in characteristics of the field of turbulent velocity fluctuations E_t. It was found that in the course of individual time intervals with a duration of 5-10 days the E_t function can be considered quasistationary. In the polygon there is a predominance of transfer of turbulent energy by "turbulent viscosity" and at the considered turbulence scales is homogeneous. Figures 1, tables 2, references 7. (p 71)

UDC 551.46.062

STATISTICAL CHARACTERISTICS OF CURRENTS BASED ON OBSERVATIONAL DATA FOR ATLANTIC POLYGON

[Abstract of article by Vasilenko, V. M. and Krivelevich, L. M.]

[Text] The article gives the results of a statistical analysis of time series of velocity components on the basis of data from polygon investigations by the scientific research ships of the USSR Academy of Sciences in the Atlantic Ocean. The energy spectrum of current velocity was obtained in the range of scales from 720 to 7 hours. A study was made of the spectral characteristics of second-order moments of the velocity field. Figures 7, references 7. (p 76)

UDC 551.465.15

INERTIAL INTERVAL IN TURBULENCE SPECTRA IN STRATIFIED FLUID (HEISENBERG-MONIN MODEL)

[Abstract of article by Venilov, A. Yu. and Lozovatskiy, I. D.]

[Text] A solution was obtained for a system of spectral equations in a stratified fluid in a wide range of wave numbers. The analysis made and the numerical examples given show that the turbulence spectra have a nonuniversal form. The behavior of the spectral densities is determined by the Re number (or by the Γ_0 value), the Rf number and the Pr number. The inertial interval of scales exists with an adequately high Re number and not excessively large Rf (in the case of a stable stratification). Figures 2, references 11. (p 83)

UDC 551.46.062.6

INTERNAL GRAVITATIONAL WAVES IN OCEAN

[Abstract of article by Ivanov, Yu. A., Morozov, Ye. G. and Samodurov, A. S.]

[Text] The results of statistical processing of measurements of fluctuations of temperature and current velocity in different regions of the ocean in the range of frequencies of internal gravitational waves are described and an analysis is given of theoretical investigations related to the problems of wave generation. Figures 7, references 21. (p 91)

UDC 551.46.662.6

GENERATION OF TRAINS OF INTERNAL WAVES IN OCEAN

[Abstract of article by Samodurov, A. S.]

[Text] The author has solved the problem for disturbances in the neighborhood of the critical point ($u = c_0$) by some internal wave of a finite amplitude which is assumed to be known. It was found that disturbances in this region have the form of packets of waves. The characteristics of these packets are analyzed. Numerical estimates are given for the real ocean which make it possible to conclude that the most probable generator of the trains of internal waves of the indicated type in the ocean is internal tides. Figures 2, references 11. (p 99)

UDC 551.46.062.6

OBSERVATION OF INTERNAL WAVES IN CENTRAL ATLANTIC

[Abstract of article by Karabasheva, E. I. and Paka, V. T.]

[Text] The article presents the results of observations of internal waves in the range of wave numbers from 10^{-3} to 10^{-2} m^{-1} in the layer of the seasonal thermocline. The measurements were made using a temperature "trawl" towed in different directions. The results are presented in the form of temperature sections, dispersions and spectra of fluctuations of isotherms, and also in the form of the dispersions and spectra of temperature fluctuations, averaged in the entire layer of the thermocline. There is a stationarity and isotropicity of the field of internal waves. The averaged one-dimensional spectrum of displacements drops off in conformity to the law k^{-3} and does not have peaks. Figures 6, references 16. (p 108)

UDC 551.465.15

SPECTRUM OF REYNOLDS STRESS

[Abstract of article by Benilov, A. Yu.]

[Text] A solution of the spectral equation for turbulence in a flow with a shear of mean velocity is cited. Velocity spectra and Reynolds stresses are obtained. These agree sufficiently well with the experimental data. Figures 2, references 14. (p 115)

UDC 551.465.15

MEASUREMENT OF PARAMETERS OF WAVE-COVERED SEA LAYER AS METHOD FOR REMOTE STUDY OF SURFACE VERTICAL TURBULENCE

[Abstract of article by Aleksandrov, A. P. and Vayndruk, E. S.]

[Text] An acoustic method is proposed for investigating some properties of surface turbulence unrelated to the need for surface-layer placement of unwieldy floating carriers and sensors for measuring the velocity of water movement. The method makes it possible, on the basis of measurements of the parameters of the aerated (bubble) layer, closely associated with the hydrophysical characteristics of the water medium, to carry out investigations of vertical turbulence remotely from beneath the water under stationary conditions. Figures 10, references 4. (p 122)

UDC 551.465.15

SOME PROBLEMS IN USE OF STRUCTURAL FUNCTIONS FOR DETERMINING GEOMETRIC PARAMETERS OF ANISOTROPY OF TURBULENT FIELD

[Abstract of article by Konovalov, Ye. A. and Yasenskiy, V. N.]

[Text] A model of a two-dimensional turbulent field with an anisotropy close to elliptical is considered. An expression is derived for a section of a two-dimensional structural function related to the adopted anisotropy index β. The results of an experiment with an anisotropic field of conductivity of a submerged jet are given. Figures 2, references 3. (p 129)

UDC 551.465.15

ONE APPROXIMATE METHOD FOR COMPUTING EVALUATION OF DISPERSION OF TURBULENT SIGNALS

[Abstract of article by Konovalov, Ye. A., Matytsin, V. D. and Yassiskiy, V. N.]

[Text] A method for computing an evaluation of the current dispersion is examined for a random signal with a normal distribution law. This involves the squaring of the smoothed values of the modulus of a random signal. A dependence is found for the dispersion of the scatters of the evaluation on the duration of the averaging interval and the interval for correlation of the initial signal. Experimental curves of the current dispersion of fluctuations of conductivity of a submerged jet, computed by two methods, are given. Figures 1, references 2. (p 131)

UDC 553.72

INVESTIGATION OF DIFFUSION OF IMPURITY IN SEA USING LUMINESCENT INDICATORS AND TOWED SENSOR

[Abstract of article by Karabashev, G. S. and Ozmidov, R. V.]

[Text] The authors generalize experience in investigating diffusion processes in the sea using artificially introduced fluorescent dyes. The article describes a

towed instrument, a fluorometer making it possible to measure small concentrations of dye in water. Methods are given for experiments with instantaneous and continuous dye point sources. The results of experiments in the Black and Baltic Seas are given. These demonstrated a marked anisotropy of the diffusion process in horizontal and vertical directions. The drawing out and deformation of dye spots is attributable to the joint influence of the gradients of mean velocity and turbulent diffusion. The values of the coefficients of turbulent diffusion are estimated and computations of the statistical characteristics of impurity fields in the sea are presented. Figures 8, references 8. (p 135)

UDC 553.72

TURBULENT DIFFUSION OF IMPURITY IN SEA COASTAL ZONE

[Abstract of article by Goroshko, V. N.]

[Text] The field of concentration of an impurity generated by a point stationary source in the coastal zone of the sea is computed. The change in the averaged velocity of a coastal current is taken into account, as well as the coefficients of vertical turbulent diffusion and the changes with increasing distance from the shore. The results of numerical computations are analyzed on the basis of an expression derived in the study for the field of concentration of an impurity. Figures 2, references 3. (p 145)

UDC 551.465.15

EXAMPLE OF COMPUTATION OF VERTICAL CURRENT VELOCITY AND VERTICAL COEFFICIENT OF TURBULENT VISCOSITY IN OCEAN BY INDIRECT METHODS

[Abstract of article by Dobroklonskiy, S. V. and Pyzhevich, M. L.]

[Text] Solutions of the stationary equations of motion of a viscous fluid and the continuity equation made it possible to derive expressions for the vertical velocity of movement of water masses w and the kinematic coefficient of vertical turbulent viscosity ν in the ocean. Computations of these parameters are given for an equatorial point in the Pacific Ocean for the upper 500 m. In the Cromwell Current $\nu < 0$ and the characteristic values $w = 10^{-2}$-10^{-1} cm/sec. Figures 4, references 5. (p 150)

UDC 551.46.08

CONSTRUCTION OF RECORDING COMPLEX IN INVESTIGATION OF FINE STRUCTURE OF OCEAN

[Abstract of article by Vorob'yev, V. P. and Palevich, L. G.]

[Text] The recording complex as a component part of a measurement complex is among the principal means for experimental investigation of macroscale physical processes in the ocean. In addition to recording the measurement data, the recording complex performs the functions of monitoring and functional checking of the measurement apparatus and also for graphic visualization of measurements in the experimental process for a prelimary evaluation of the results for the purpose of

choosing the most informative records. The article gives recommendations on improvement of the recording complex and the method for working with it for operational control of an experiment in the course of its implementation for increasing the reliability of measurements and for increasing the information yield of the records. Figures 6, tables 1, references 8. (p 155)

UDC 551.46.08

USE OF A THERMOANEMOMETER IN A FLOW WITH TEMPERATURE FLUCTUATIONS

[Abstract of article by Nabatov, V. N., Paka, V. T. and Skurenko, V. I.]

[Text] The authors analyze the influence of temperature inhomogeneities of the turbulent flow of a fluid on the readings of instruments of the thermoanemometric and hydroresistor type for measuring velocity fluctuations. Under conditions of a stationary turbulent flow created in a hydraulic apparatus the authors made measurements of its fluctuating components in the presence and absence of temperature fluctuations. The measurements were made by the "three heatings" method. Processing of the thermoanemometer readings indicated that the influence of temperature fluctuations in the velocity spectra is manifested to frequencies not exceeding 100 Hz. The "three heatings" method is recommended for checking the thermoanemometer and its characteristics used in the data processing procedure. In investigations of oceanic turbulence it is better to employ an instrument with a hydroresistor-type sensor. Figures 8, tables 1, references 10. (p 162)

UDC 551.46.08

FREQUENCY-TYPE PRESSURE-SENSITIVE DEPTH DETECTORS FOR OCEANOLOGICAL RESEARCH

[Abstract of article by Plushnikov, V. M. and Khlystunov, M. S.]

[Text] The article deals with the problem of metrology and designing of frequency-type depth (pressure) detectors constructed on the basis of AT-type tensocontrollable resonators employed as a sensing element. The authors give computation expressions, technical parameters and characteristics of a discretely constructed and monolithic sensor and it is shown that it is superior in comparison with the parameters of the depth (pressure) sensors used at the present time. Figures 11, tables 1, references 4. (p 175)

UDC 551.46.08

AMERICAN 'BREAKAWAY' TEMPERATURE PROBES

[Abstract of article by Vorob'yev, V. P., Kuznetsov, Ye. I., Obukhova, L. V. and Palevich, L. G.]

[Text] On the basis of materials in foreign publications the article gives an analysis of the design, circuitry and operational features of "breakaway" temperature probes produced by different companies in the United States. A comparative table of the technical specifications of different types of "breakaway" temperature probes is included. Figures 2, tables 1, references 39. (p 185)

UDC 681.3

IMPROVEMENT OF SYSTEM FOR CURVE PLOTTING FOR 'MINSK-22' COMPUTER

[Abstract of article by Arvan, B. M.]

[Text] The article describes an output device for the "Minsk-22" computer making it possible to construct curves of spectral densities, correlation functions, histograms, isolines of hydrological sections, etc. The authors set forth the sequence of operations and work regimes for the unit in dependence on the nature of the information fed out to the curve plotter. Figures 4, references 3. (p 197)

UDC 518.5

ERROR IN RECONSTRUCTING PROCESS FROM SIGNIFICANT READINGS

[Abstract of article by Sorokin, A. A.]

[Text] Three algorithms for reconstructing a telemetric process on the basis of significant readings obtained as a result of processing of a flow of readings following with some initial time quantization interval, with a zero-order predictor with a floating aperture, are analyzed. Comparison of the restoration algorithms with one another is accomplished using the maximum values of the dispersion of the interpolation error in the interval between successive significant readings. Figures 2, references 7. (p 201)

5303
CSO: 8144/1839

- END -